Quantum chromodynamics at high energy and noisy traveling waves

Stéphane Munier

Université Pierre et Marie Curie

Mémoire d'habilitation à diriger des recherches

"Quantum chromodynamics at high energy and noisy traveling waves"

Stéphane Munier

présenté le 30 novembre 2011 devant la Commission composée de

Nestor Armesto	rapporteur
Yuri Dokshitzer	membre
François Gélis	rapporteur
Cécile Monthus	rapporteur
Lech Szymanowski	membre
Jean-Bernard Zuber	président

Abstract

When hadrons scatter at high energies, strong color fields, whose dynamics is described by quantum chromodynamics (QCD), are generated at the interaction point. If one represents these fields in terms of partons (quarks and gluons), the average number densities of the latter saturate at ultrahigh energies. At that point, nonlinear effects become predominant in the dynamical equations. The hadronic states that one gets in this regime of QCD are generically called "color glass condensates".

Our understanding of scattering in QCD has benefited from recent progress in statistical and mathematical physics. The evolution of hadronic scattering amplitudes at fixed impact parameter in the regime where nonlinear parton saturation effects become sizable was shown to be similar to the time evolution of a system of classical particles undergoing reaction-diffusion processes. The dynamics of such a system is essentially governed by equations in the universality class of the stochastic Fisher-Kolmogorov-Petrovsky-Piscounov equation, which is a stochastic nonlinear partial differential equation. Realizations of that kind of equations (that is, "events" in a particle physics language) have the form of noisy traveling waves. Universal properties of the latter can be taken over to scattering amplitudes in QCD.

This review provides an introduction to the basic methods of statistical physics useful in QCD, and summarizes the correspondence between these two fields and its theoretical and phenomenological implications.

Résumé

Lors de la diffusion de hadrons à haute énergie, d'intenses champs de couleur, dont la dynamique est décrite par la chromodynamique quantique (QCD), sont créés au point d'interaction. Si on représente ces champs en termes de partons (quarks et gluons), la densité de ces derniers sature à très haute énergie. Les effets non-linéaires deviennent alors dominants dans les équations dynamiques. Les états hadroniques que l'on obtient dans ce régime de la QCD sont génériquement appelés "condensat de verre de couleur".

Notre compréhension de la diffusion en QCD a bénéficié de progrès récents en physique statistique et en physique mathématique. On a montré que l'évolution des amplitudes de diffusion hadronique à paramètre d'impact fixé dans le régime dans lequel les effets non-linéaires de saturation des densités de partons deviennent importants est semblable à l'évolution temporelle d'un système de particules classiques soumis à des processus de type réaction-diffusion. La dynamique d'un tel système est essentiellement gouvernée par des équations dans la classe d'universalité de l'équation de Fisher-Kolmogorov-Petrovsky-Piscounov stochastique, qui est une équation aux dérivées partielles stochastique et non-linéaire. Les réalisations de telles équations (c'est-à-dire les événements, dans un langage de physique des particules) ont la forme d'ondes voyageuses bruitées. Les propriétés universelles de celles-ci peuvent être transposées aux amplitudes d'interactions en QCD.

Ce mémoire est une introduction aux méthodes de physique statistique utiles en QCD, et résume la correspondance entre ces deux domaines ainsi que ses implications théoriques et phénoménologiques.

Preface

The present memoir is based on the review paper of Ref. [1] published as a Physics Report in 2009. The general structure has not changed, but large parts of the text have been rewritten in order to propose different perspectives, and to incorporate the latest developments. Most notably, recent studies on the density correlations in impact-parameter space have been added as a new chapter (Chap. 5), and a better derivation of the model for the front fluctuations is given in Chap. 4. Many other more minor modifications have been implemented in the present version of the review: For example, Sec. 3.3 was simplified. This thesis was presented on November 30, 2011 to receive the habilitation degree from the Pierre et Marie Curie University in Paris.

The work reported here was completed over a period of about 8 years starting in 2003. It was inspired in an essential way by A.H. Mueller and Bernard Derrida, both by their writings, about the dipole model for the former and traveling waves for the latter, and by direct collaboration. Both of them are leading researchers in their respective fields, and it has been a honor to be involved in such a collaboration: My first acknowledgements naturally go to them.

I would like to thank all my collaborators during these years and especially the once PhD students and postdocs with whom I had the pleasure to work, the collegues who kindly shared their views with me, as well as the members of my group, led by Bernard Pire, and all my labmates at CPHT.

I warmly thank the members of the Committee, namely Jean-Bernard Zuber (chair), Nestor Armesto, François Gélis and Cécile Monthus (referees), and Yuri Dokshitzer and Lech Szymanowski.

Finally, my work from 2006 to 2010 was funded by the Agence Nationale de la Recherche (France), contract ANR-06-JCJC-0084-02, a grant received together with Samuel Wallon.

Stéphane Munier
Centre de physique théorique, École polytechnique, CNRS
June 2012

Contents

Chapter 1

Introduction to high energy scattering in QCD

What is the origin of the mass of ordinary matter? How are the nucleons "glued" together to form stable nuclei? How can we understand the "zoo" of the particles (hadrons) which are sensitive to the "strong" force?

The modern theory of strong interactions, quantum chromodynamics (abreviated QCD; For a comprehensive textbook, see Ref. [2]), discovered about 40 years ago, seems to have the ability to help all these problems and many others in a most compact and elegant way. This theory is parallel in its formulation to the more well-known theory of electromagnetic interactions, quantum electrodynamics, and, with some caveats still to be understood, to the theory of weak interactions, consistently with the idea of a (partial) unification of the elementary forces. However, QCD poses outstanding mathematical problems, and it became soon clear that its various regimes had to be explored by dedicated experiments and specialized theoretical tools. While "simple" fixed-order perturbation theory has proved extremely successful to investigate electrodynamics due to the intrinsic weakness of the force acting between charged leptons (the characteristic coupling is $\alpha_{\text{em}} \simeq \frac{1}{137}$), chromodynamics has to deal with strong coupling instead (the coupling α_s is of order 0.1 in the most favorable cases and up to 1 in general), and with more subtle nonlinearities which severely limits the use of fixed-order perturbation theory. Perturbative expansions have to be handled with care, and dedicated tools have to be invented for QCD.

It has happened that methods were borrowed from other fields of physics: For example the computation of low-energy properties of the hadrons (masses, decay rates...) are investigated using lattice field theory, like in solid state physics. More recently, tools developed by string theorists have proved useful to address the calculation of specific processes involving very high-order terms in a perturbative expansion.

This review, which is a revised version of the author's publication [1], summarizes some recent investigations in a specific regime of quantum chromodynamics, the so-called high-energy or, more technically, "small-x" regime. We focus on how this regime is formally related to some models which appear in statistical physics and show how this correspondence may be used. We shall first go over the recent history of high-energy QCD in order to better expose the context of this research.

Short history of the field. The study of quantum chromodynamics in the high-energy regime has undergone a rapid development in the last 15 years with the wealth of experimental data that have been collected, first at the electron-proton collider DESY-HERA, and then at the heavy-ion collider RHIC. More energy in the collision enables the production of objects of higher mass in the final state, and thus the discovery of new particles. But higher energies make it also possible to observe more quantum fluctuations of the incoming objects, that is to say, to study more deeply the structure of the vacuum.

Analytical approaches to QCD in this regime are based on a sophisticated handling of per-

turbative expansions of observables in powers of the strong coupling constant α_s which, thanks to asymptotic freedom, is justified for carefully chosen observables in special kinematical regimes. Some sophistication is needed because in the evaluation of Feynman graphs, the coupling constant always comes with "infrared" and "collinear" logarithms that are related to the phase space that is available to the reaction, that is to say, to kinematics, and may easily push the effective coupling to large values. Resumming part of these logarithms is mandatory. Resumming all of them is too difficult. The question is to carefully select the dominant ones, and this is not at all easy.

An experimental facility able to investigate the high-energy regime of QCD was the HERA collider, where electrons or positrons scattered off protons at the center-of-mass energy $\sqrt{s}$, exchanging a photon of virtuality Q. Through the scattering, one could probe partonic fluctuations of the proton (made of quarks and gluons) of transverse momenta $k \sim Q$, and longitudinal momentum fractions $x \sim Q^2/(Q^2+s)$.

For a long time, the dominant paradigm had been that the *collinear logarithms* $\ln Q^2$, that become large when Q^2 is large compared to the QCD confinement scale Λ^2, were the most important ones. As a matter of fact, searches for new particles or for exotic physics require to scrutinize matter at very small distances, and hence very large Q^2 have to be considered. Perturbative series of powers of $\alpha_s \ln Q^2$ have to be fully resummed. The equation that performs this resummation is the celebrated Dokshitzer-Gribov-Lipatov-Altarelli-Parisi (DGLAP) equation [3–5].

However, once HERA had revealed its ability to get extremely good statistics in a regime in which Q^2 is moderate (from 1 to 100 GeV^2) and x very small (down to 10^{-5}) it became clear that *infrared logarithms* ($\ln 1/x$) could show up and even dominate the measured observables. The resummation of the series of infrared logs is performed by the Balitsky-Fadin-Kuraev-Lipatov (BFKL) equation [6–8]. The series $\sum(\alpha_s \ln 1/x)^k$ (with appropriate coefficients) is the leading order (LO), while the series $\sum \alpha_s(\alpha_s \ln 1/x)^k$ is the next-to-leading order (NLO), which has also been computed [9, 10]. The BFKL equation is a linear integro-differential equation.

At ultrahigh energy, the bare BFKL equation seems to violate the Froissart bound, that states that total hadronic cross-sections cannot rise faster than $(\ln^2 s)/m_\pi^2$. The latter is a consequence of the unitarity of the probability of scattering. The BFKL equation predicts a power rise with the energy of the form s^ε, where ε is positive and quite large (0.3 to 0.5 according to the effective value of α_s that is chosen). The point at which the BFKL equation breaks down depends on the value of the typical transverse momentum which characterizes the observable (It is the photon virtuality Q in the case of deep-inelastic scattering). One may define the energy-dependent *saturation scale* $Q_s(x)$ in such a way that the BFKL equation holds for $Q > Q_s(x)$. For $Q \sim Q_s(x)$, the probability for scattering to take place is of order 1, and for $Q < Q_s(x)$, it would be larger than 1 if one trusted the BFKL equation. The saturation scale is a central observable, which we shall keep discussing in this review: It signs the point at which the linear (BFKL) formalism has to be corrected for nonlinear effects. The regime in which nonlinearities manifest themselves is a regime of strong color fields, sometimes called the *color glass condensate* (For the etymology of this term, see e.g. the lectures of Ref. [11]; for a review, see Ref. [12]).

The fact that unitarity is violated is not only due to the lack of a hadronic scale in the BFKL equation, which is a perturbative equation; Introducing confinement in the form of a cutoff would not help this particular problem: The violation of unitarity which we are talking about occur at small distances. It is just that still higher orders are needed. The NLO corrections to the BFKL kernel indeed correct this behavior in such a way that the description of the HERA data in the small-x regime is possible by the BFKL equation. However, these corrections are not enough to tame the power-like growth of cross-sections as predicted by the LO BFKL equation. It seems that a resummation of contributions of arbitrary order would be needed.

New equations were proposed well before the advent of colliders able to reach this regime. Gribov-Levin-Ryskin wrote down a model for the evolution of the hadronic scattering cross-sections in the early 80's [13, 14], and Mueller and Qiu derived a similar equation from QCD a bit later [15]. These equations are integral evolution equations with a nonlinear term, which basically takes into account parton saturation effects, that is to say, recombination or rescattering. The latter cannot be described in a linear framework such as the BFKL formalism. Subsequently, more involved QCD evolution equations were derived from different points of view. In the 90's,

McLerran and Venugopalan [16–18] proposed a first model, mainly designed to approach heavy-ion collisions. Later, Balitsky [19], Jalilian-Marian, Iancu, McLerran, Weigert, Leonidov and Kovner (B-JIMWLK) [20–24] worked out QCD corrections to this model, and got equations that reduce to the BFKL equation in the appropriate limit. Technically, these equations actually have the form of an infinite hierarchy of coupled integro-differential equations (in Balitsky's formulation [19]), of a functional renormalization group equation, or alternatively, of a Langevin equation (in Weigert's formulation [24]). A much simpler equation was derived in 1996 by Balitsky [19] and rederived by Kovchegov in 1999 [25, 26] in a very elegant way within a different formalism. The obtained equation is called the Balitsky-Kovchegov equation (BK). The latter derivation was based on Mueller's color dipole model [27], which proves particularly suited to represent QCD in the high-energy limit.

The exciting feature of this kinematical regime of hadronic interaction from a theoretical point of view is that the color fields are strong, although, at sufficiently high energies, the QCD coupling is weak, authorizing a perturbative approach, and thus some of the analytical calculations outlined above. In such strong field regime, nonlinear effects become crucial. But the conditions of applicability of the different equations that had been found had never been quite clear. Anyway, these equations are extremely difficult to solve, which had probably been the main obstacle to more rapid theoretical developments in the field until recently.

Furthermore, for a long time, the phenomenological need for such a sophisticated formalism was not obvious, since linear evolution equations such as the DGLAP equation were able to account for almost all available data. But Golec-Biernat and Wüsthoff showed that unitarization effects may have already been seen at HERA [28, 29]. Their model predicted, in particular, that the virtual photon-proton cross-section should only depend on one single variable τ, made of a combination of the transverse momentum scale (fixed by the virtuality of the photon Q) and x. This phenomenon was called "geometric scaling" [30]. It was found in the HERA data (see Fig. 1.1): This is maybe one of the most spectacular experimental result from HERA in the small-x regime.

This observation has triggered many phenomenological and theoretical works. Soon after its discovery in the data, geometric scaling was shown to be a feature of some solutions of the Balitsky-Kovchegov (BK) equation, essentially numerically, with some analytical arguments (see e.g. [32–35]). The energy dependence of the saturation scale was eventually precisely computed by Mueller and Triantafyllopoulos [36]. Later, it was shown that the BK equation is actually in the universality class of the Fisher-Kolmogorov-Petrovsky-Piscounov (FKPP) equation [37, 38], and geometric scaling was found to be implied by the fact that the latter equation admits *traveling-wave* solutions [39].

A first step beyond the BK equation, in the direction of a full solution to high energy QCD, was taken by Mueller and Shoshi in 2004 [40]. Actually, they did not solve the B-JIMWLK equations, which would be the natural candidate for a complete theory. Instead, they solved the linear BFKL equation with two absorptive boundary conditions, which they argued to be appropriate to represent the expected nonlinearities. Geometric scaling *violations* were found from their calculation, which should show up at any energies.

Subsequently, it was shown that high-energy QCD at fixed coupling is actually in the universality class of *reaction-diffusion processes*, studied in statistical physics, whose dynamics may be encoded in equations similar to the *stochastic* FKPP equation [41]. The Mueller-Shoshi solution was shown to be consistent with solutions to the latter equation. So high-energy QCD seems to be in correspondence with disordered systems studied in statistical physics. This correspondence has provided a new understanding of QCD in the high-energy regime, and it has proven very useful to find more features of high-energy scattering.

Outline of this memoir. The next chapter is devoted to describing scattering in QCD from a s-channel point of view, relying essentially on the parton model or, rather, on a realization useful in the high-energy limit, the color dipole model. Once this picture is introduced, it is not difficult to understand the correspondence with reaction-diffusion processes occuring in one spatial dimension, whose dynamics is captured by equations in the universality class of the Fisher-

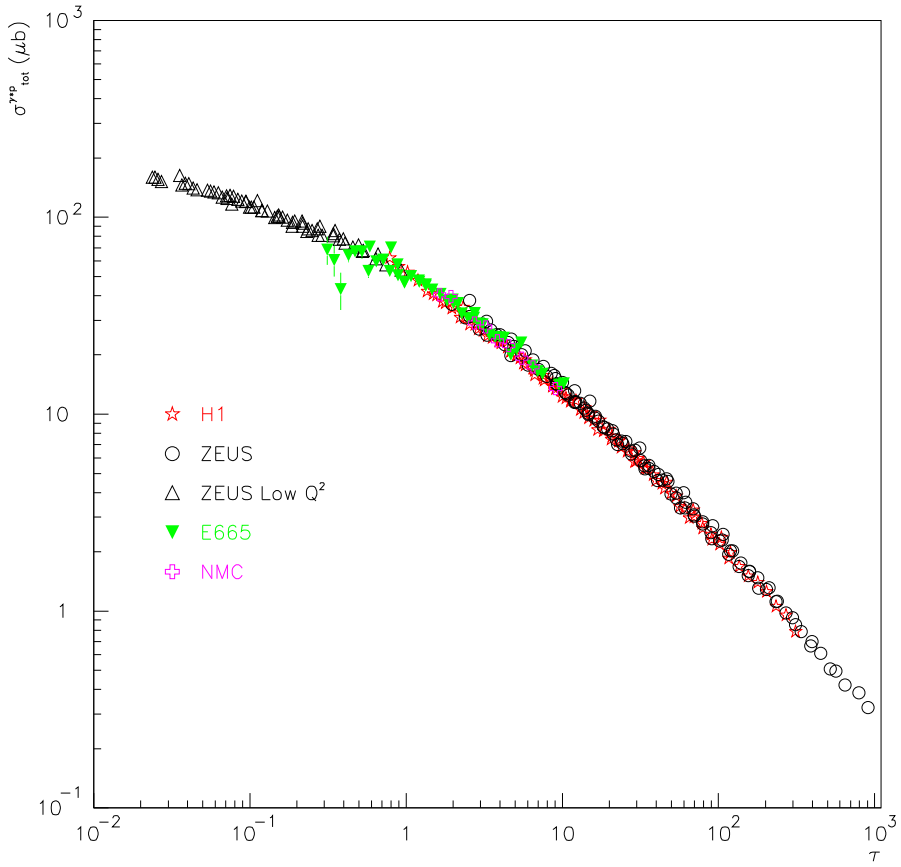

Figure 1.1: [From Ref. [31]] Photon-proton total cross-section from the most recent set of deep-inelastic scattering data in the low-x regime plotted as a function of a single scaling-variable $\tau = Q^2/Q_s^2(x)$, where Q is the virtuality of the photon and $Q_s^2(x) \sim \Lambda^2 x^{-0.3}$ is the so-called saturation scale. Although the cross-section is a priori a function of two variables, all data fall on the same curve. This phenomenon is called *geometric scaling* and was discovered in Ref. [30].

Kolmogorov-Petrovsky-Piscounov (FKPP) equation. We then explain how traveling waves appear in this context. In Chap. 3, we study in greater detail a toy model for which many technics (field theory, statistical methods) may be worked out completely. This model however ignores spatial dimensions, and thus, does not account for traveling waves. We summarize the state-of-the-art research on equations in the universality class of the FKPP equation in Chap. 4. We then come back to QCD, discussing the issue of the impact parameter. This will lead us to introduce new models beyond the simple one-dimensional reaction-diffusion type models (Chapter 5). Finally, we will show how noisy traveling waves may show up in the actual data.

Over the last few years, several hundreds of papers have appeared related to this subject, mainly issued from a very active though restricted community. Obviously, this memoir cannot give a complete account of this abundant literature. As a matter of fact, some important recent developments had to be left out. Concerning the correspondence itself, we do not attempt to establish a definite stochastic nonlinear evolution equation for QCD amplitudes, for to our judgement, this research line is not mature enough yet: A better understanding of the very saturation mechanism at work in QCD is definitely needed before one may come to this issue. Furthermore, it is not clear to us that a stochastic formulation would be a technical progress, since there are not many known methods to handle complicated stochastic equations. We feel that the same is true for the search for effective actions that would include so-called Pomeron loops. We also do not address the developments based on the boost-invariance symmetry that scattering amplitudes should have: This would drive us too far off the main focus of this review. As for more phenomenological aspects, we only discuss the basic features of total cross-sections without attempting to address other observables such as diffraction. We do also not address the issue of next-to-leading effects such as the running of the QCD coupling. This discussion, though crucial if one wants to make predictions for actual colliders, would probably only be technical in its nature: There is no conceptual difference between the fixed coupling and the running coupling cases. Here, only basic phenomenological facts brought about by this new understanding of high-energy QCD are addressed, namely geometric scaling and diffusive scaling.

Chapter 2

Hadronic interactions and reaction-diffusion processes

We shall introduce here the physical picture of high-energy scattering in the parton model. In the first section, the color dipole model [27] is described since it is particularly suited to address high-energy scattering, especially close to the regime in which nonlinear effects are expected to play a significant role. In a second section, we shall argue that high-energy scattering is a peculiar reaction-diffusion process.

Contents

2.1 Parton model and dipoles

2.1.1 General picture

For definiteness, let us consider the scattering of a hadronic probe off some given target, in the restframe of the probe and at a fixed impact parameter, that is to say, at a fixed distance between the probe and the center of the target in the two-dimensional plane transverse to the collision axis. In the parton model, the target interacts through one of its quantum fluctuations, made of a high-occupancy Fock state if the energy of the reaction is sufficiently high (see Fig. 2.1a). As will be understood below, the probe effectively "counts" the partons in the Fock state of the target whose transverse momenta k (or sizes $r \sim 1/k$) are of the order of the momentum that characterizes the probe: The amplitude for the scattering off this particular partonic configuration is proportional to the number of such partons.

The observable that is maybe the most sensitive to quantum fluctuations of a hadron is the cross-section for the interaction of a virtual photon with a hadronic target such as a proton or a

nucleus. The virtual photon is emitted by an electron (or a positron). What is interesting with this process, called "deep-inelastic scattering", is that the kinematics of the photon is fully controlled by the measurement of the scattered electron. The photon can be considered a hadronic object since it interacts through its fluctuations into a quark-antiquark state. The latter form a color dipole since although both the quark and the antiquark carry color charge, the overall object is color neutral due to the color neutrality of the photon. The probability distribution of these fluctuations may be computed in quantum electrodynamics (QED). Subsequently, the dipole interacts with the target by exchanging gluons. The dipole-target cross-section factorizes at high energy. One typical event is depicted in Fig. 2.1a.

Dipole models [42, 43] have become more and more popular among phenomenologists since knowing the dipole cross-section enables one to compute different kinds of observables. Like parton densities, the latter is a universal quantity, that may be extracted from one process and used to predict other observables. Different phenomenological models may be tried for the dipole cross-section. QCD evolution equations may even be derived, as we shall explain below. A critical recent study of the foundations of dipole models may be found in Ref. [44, 45].

In QCD, the state of a hadronic object, encoded in a set of wave functions, is built up from successive splittings of partons starting from the valence structure. This is visible in the example of Fig. 2.1a: The quark and the antiquark that build up, in this example, the target in its asymptotic state each emit a gluon, which themselves emit, later on in the evolution, other gluons. As one increases the rapidity y by boosting the target, the opening of the phase space for parton splittings makes the probability for high occupation numbers larger. Indeed, the probability to find a gluon that carries a fraction z (up to dz) of the momentum of its parent parton (which may be a quark or a gluon) is of order $\alpha_s N_c dz/z$ for small z (N_c is the number of colors; $N_c = 3$ in real-life QCD). As we see, there is a logarithmic singularity in z, meaning that emissions of very soft gluons (small z) are favored if they are allowed by the kinematics. The splitting probability is of order 1 when the total rapidity of the scattering $y = \ln 1/x$ is increased by roughly $1/\bar{\alpha}$ (the convenient notation $\bar{\alpha} = \alpha_s N_c/\pi$ has been introduced). Only splittings of a quark or of a gluon into a gluon exhibit the $1/z$ singularity. Therefore, at large rapidities, gluons eventually dominate the partonic content of the hadrons.

The parton model in its basic form, where the fundamental objects of the theory (quarks and gluons) are directly considered, is not so easy to handle in the high-energy regime. One may considerably simplify the problem by going to the limit of a large number of colors ($N_c \gg 1$), in which a gluon may be seen as a zero-size quark-antiquark pair. Then, color-neutral objects become collections of color dipoles, whose endpoints consist in "half gluons" (see Fig. 2.1b). There is only one type of objects in the theory, dipoles, which simplifies very much the picture. Furthermore, going to *transverse coordinate space* (instead of momentum space, usually used in the DGLAP formalism) by trading the transverse momenta of the gluons for the sizes of the dipoles (through an appropriate Fourier transform) brings another considerable simplification. Indeed, the splittings that contribute to the amplitudes in the high-energy limit are the soft ones, for which the emitted gluons take only a small fraction of the momentum of their parent, the latter being very large. Therefore, the positions of the gluons, and thus of the edges of the dipoles, in the plane transverse to the collision axis are not modified by subsequent evolution once the gluons have been created. Thus, the evolution of each dipole proceeds through completely *independent* splittings to new dipoles.

We will now see how this picture translates into a QCD evolution equation for scattering amplitudes, first in the regime in which there are no nonlinear effects. In a second step, we will try and understand how to incorporate the latter.

2.1.2 BFKL equation from the dipole model

The building up of the states of each hadron is specified by providing the rate at which a dipole whose endpoints have transverse coordinates (x_0, x_1) splits into two dipoles (x_0, x_2) and (x_2, x_1) as the result of a gluon emission at position x_2 when the rapidity of the initial dipole is increased.

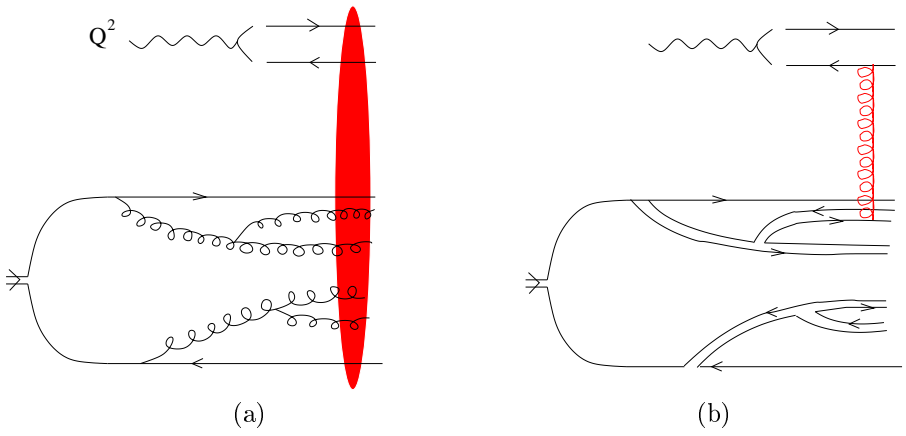

Figure 2.1: *(a)* The scattering of a virtual photon probe off a particular fluctuation of an evolved target made of a quark and an antiquark in its bare state. The photon necessarily goes through a quark-antiquark pair at high enough energies, when the target is dominated by dense gluon states. (What is represented in this figure is actually the inelastic amplitude, which is a cut of the total cross-section or of the forward elastic amplitude). *(b)* In the dipole model, the probe and the target may be represented by sets of color dipoles, and the interaction proceeds through gluon exchanges. It is now the elastic amplitude that is represented. The curly vertical lines represent 2-gluon exchanges between pairs of dipoles.

It is computed in perturbative QCD and reads [27]

$$\frac{dP}{d(\bar{\alpha}y)}(x_{01} \to x_{02}, x_{12}) = \frac{|x_0 - x_1|^2}{|x_0 - x_2|^2 |x_1 - x_2|^2} \frac{d^2x_2}{2\pi}. \tag{2.1}$$

Thanks in particular to the large-N_c limit, dipole splittings are independent. After some rapidity evolution starting from a primordial dipole, one gets a chain of dipoles such as the one depicted in Fig. 2.2.

The elementary scattering amplitude for one projectile dipole (x_0, x_1) off a target dipole (z_0, z_1) is independent of the rapidity and reads [27]

$$T^{\rm el}((x_0, x_1), (z_0, z_1)) = \frac{\pi^2 \alpha_s^2}{2} \ln^2 \frac{|x_0 - z_1|^2 |x_1 - z_0|^2}{|x_0 - z_0|^2 |x_1 - z_1|^2}. \tag{2.2}$$

If the target is an evolved state at rapidity y, then it consists instead in a distribution $n(y, (z_0, z_1))$ of dipoles. The (forward elastic) scattering amplitude $A(y, (x_0, x_1))$ is just given by the convolution of n and $T^{\rm el}$, namely

$$A(y, (x_0, x_1)) = \int \frac{d^2z_0}{2\pi} \frac{d^2z_1}{2\pi} T^{\rm el}((x_0, x_1), (z_0, z_1)) n(y, (z_0, z_1)). \tag{2.3}$$

Let us examine the properties of $T^{\rm el}$. To this aim, it is useful to decompose the coordinates of the dipoles in their size vector $r_a = x_0 - x_1$ (resp. $r_b = z_0 - z_1$) and impact parameter $b_a = \frac{x_0 + x_1}{2}$ (resp. $b_b = \frac{z_0 + z_1}{2}$). In the limit in which the relative impact parameters of the dipoles $b = b_a - b_b$ is very large compared to their sizes, we get the simplified expression

$$T^{\rm el}(r_a, r_b, b) \underset{|r_a|, |r_b| \ll |b|}{\sim} \alpha_s^2 \frac{r_a^2 r_b^2}{b^4}, \tag{2.4}$$

and thus the scattering amplitude decays fast as a function of the relative impact parameter. If instead the relative impact parameter is small (of the order of the size of the smallest dipole), we

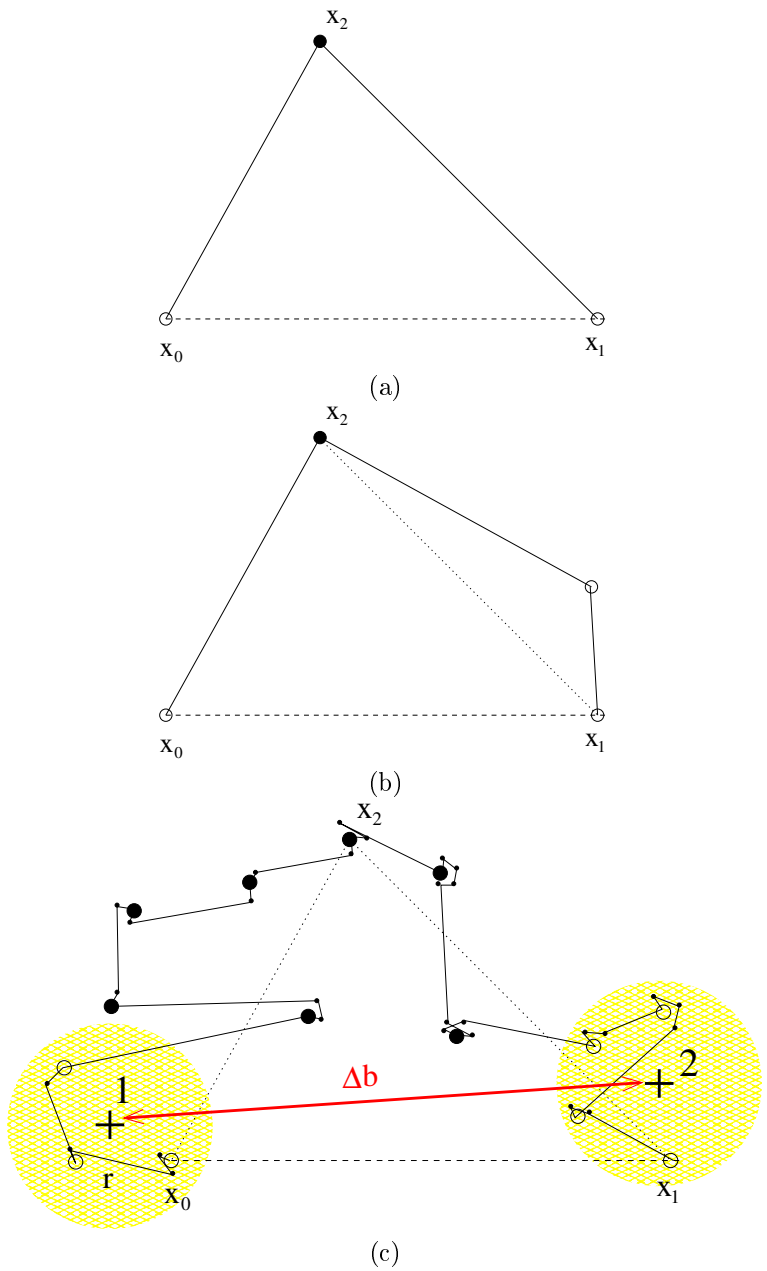

Figure 2.2: Schematic picture of a realization of the dipole evolution after the first two steps of the evolution ((a) and (b)), and after some larger rapidity evolution (c). In the first step (a), the initial dipole (x_0, x_1) (denoted by a dashed line) splits to the new dipoles (x_0, x_2) and (x_2, x_1) (full lines). The points represent the edges of each dipole, that is to say, the position of the gluons. In the next step (b), the dipole (x_2, x_1) itself splits in two new dipoles. The splitting process proceeds (c) until the maximum rapidity is reached. Many very small dipoles are produced in the vicinity of each of these endpoints, due to the infrared singularity visible in Eq. (2.1) (Only a fraction of them is represented). The zones 1 and 2 in (c), separated by the transverse distance Δb, would evolve quasi-independently after the stage depicted in this figure when saturation effects are included (See Sec. 5.1 for the corresponding discussion).

get for disymmetric sizes

$$T^{\rm el}(r_a, r_b, b) \underset{|r_a|,|r_b|\sim|b|}{\sim} \alpha_s^2 \frac{r_<^2}{r_>^2}, \tag{2.5}$$

where $r_< = \min(|r_a|, |r_b|)$, $r_> = \max(|r_a|, |r_b|)$, and where the integration over the angles has been performed.

Equation (2.4) means that the dipole interaction is local in impact parameter: It vanishes as soon as the relative distance of the dipoles is a few steps in units of their size. Eq. (2.5) shows that only dipoles whose sizes are of the same order of magnitude interact. These properties are natural in quantum mechanics. Thus the amplitude A in Eq. (2.3) effectively "counts" the dipoles of size of the order of $|x_{01}|$ at the impact parameter $\frac{x_0+x_1}{2}$ (up to $|x_{01}| = |x_0 - x_1|$), with a weight factor α_s^2.

An evolution equation for the amplitude A with the rapidity of the scattering can be established. It is enough to know how the dipole density in the target evolves when rapidity is increased, since all the rapidity dependence is contained in n in the factorization (2.3), and such an equation may easily be worked out with the help of the splitting rate distribution (2.1). It reads [27]

$$\frac{\partial n(y,(x_0,x_1))}{\partial(\bar\alpha y)} = \int \frac{d^2x_2}{2\pi} \frac{|x_{01}|^2}{|x_{02}|^2|x_{12}|^2} [n(y,(x_0,x_2)) + n(y,(x_2,x_1)) - n(y,(x_0,x_1))], \tag{2.6}$$

where $x_{ab} \equiv x_a - x_b$. The very same equation holds for A. The elementary scattering amplitude $T^{\rm el}$ only appears in the initial condition at $y = 0$, which is not shown in Eq. (2.6).

In a nutshell, the integral kernel encodes the branching diffusion of the dipoles. The total number of dipoles at a given impact parameter grows exponentially, and their sizes diffuse. The appropriate variable in which diffusion takes place is $\ln(1/|x_{01}|^2)$. (This is due to the collinear singularities in Eq. (2.1).) Equation (2.6) is nothing but the BFKL equation. A complete solution to this equation, including the impact-parameter dependence, is known [46].

An important property of the amplitude A is that it is boost-invariant. This property is preserved in the BFKL formulation. We could have put the evolution in the projectile instead of the target, or shared it between the projectile and the target: The result for the scattering amplitude would have been the same. In a frame in which the target carries y' units of rapidity and the projectile $y - y'$, the amplitude A reads

$$A(y,(x_0,x_1)) = \int \frac{d^2z_0}{2\pi}\frac{d^2z_1}{2\pi}\frac{d^2z_0'}{2\pi}\frac{d^2z_1'}{2\pi} n^{\rm projectile}(y-y',(z_0,z_1)|(x_0,x_1)) \times T^{\rm el}((z_0,z_1),(z_0',z_1')) n^{\rm target}(y',(z_0',z_1')). \tag{2.7}$$

$n^{\rm projectile}(y-y',(z_0,z_1)|(x_0,x_1))$ is the density of dipoles (z_0,z_1) found in a dipole of initial size (x_0,x_1) after evolution over $y-y'$ steps in rapidity. If $y' = y$, one recovers Eq. (2.3). If $y' = 0$, then all the evolution is in the projectile instead.

The amplitude A is related to an interaction probability, and thus, it must be bounded: In appropriate normalizations, A has to range between 0 and 1. But as stated above, the BFKL equation predicts an exponential rise of A with the rapidity for any dipole size, which at large rapidities eventually violates unitarity. Hence the BFKL equation is not the ultimate representation of high-energy scattering in QCD.

2.1.3 Unitarity and the Balitsky-Kovchegov equation

It is clear that one important ingredient that has been left out in the derivation of the BFKL equation is the possibility of *multiple scatterings* between the probe and the target. Several among the $n^{\rm projectile}$ dipoles in Eq. (2.7) may actually interact with the $n^{\rm target}$ dipoles in the other hadron simultaneously. The only reason why such interactions may not take place is that $T^{\rm el} \sim \alpha_s^2$ (see Eq. (2.2)), and thus the probability for two simultaneous scatterings is of order α_s^4, which is parametrically suppressed. But this argument holds only as long as the dipole number densities

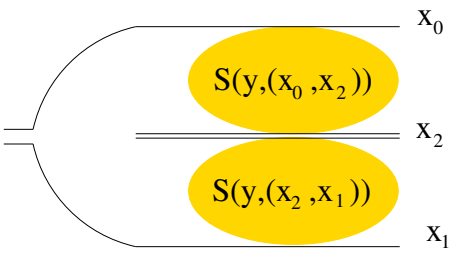

Figure 2.3: Derivation of the Balitsky-Kovchegov equation.

are of order 1. If $n \sim 1/\alpha_s^2$ (which is also the point above which the unitarity of A is no longer preserved in the BFKL approach), then it is clear that multiple scatterings should occur.

In order to try and implement these multiple scatterings, we introduce the probability that there be no scattering between a dipole (x_0, x_1) and a given realization of the target in a scattering with total rapidity y, that we shall denote by $S(y, (x_0, x_1))$. Let us start with a system in which the evolution is fully contained in the target. We increase the total rapidity by boosting the *projectile* (initially at rest) by a small amount dy. Then there are two cases to distinguish, depending on whether the dipole (x_0, x_1) splits in the rapidity interval dy. In case it splits into two dipoles (x_0, x_2) and (x_2, x_1), the probability that the projectile does not interact is just the product of the probabilities that each of these new dipoles do not interact. This is because once created, dipoles are assumed to be independent. In summary:

$$S(y+dy,(x_0,x_1)) = \begin{cases} S(y,(x_0,x_1)) \text{ with proba } 1-\bar{\alpha}dy\int_{x_2}\frac{dP}{d(\bar{\alpha}y)}(x_{01}\to x_{02},x_{12}) \\ S(y,(x_0,x_2))S(y,(x_2,x_1)) \text{ with proba } \bar{\alpha}dy\frac{dP}{d(\bar{\alpha}y)}(x_{01}\to x_{02},x_{12}) \end{cases} \tag{2.8}$$

Taking the average over the realizations of the target and the limit $dy \to 0$, we get

$$\frac{\partial}{\partial y}\langle S(y,(x_0,x_1))\rangle = \bar{\alpha}\int\frac{d^2x_2}{2\pi}\frac{x_{01}^2}{x_{02}^2x_{21}^2}[\langle S(y,(x_0,x_2))S(y,(x_2,x_1))\rangle - \langle S(y,(x_0,x_1))\rangle] \tag{2.9}$$

(See Fig. 2.3 for a graphical representation.) We see that this equation is not closed: An evolution equation for the correlator $\langle S(y,(x_0,x_2))S(y,(x_2,x_1))\rangle$ is required. However, we may assume that such correlators factorize in the following sense:

$$\langle S(y,(x_0,x_2))S(y,(x_2,x_1))\rangle = \langle S(y,(x_0,x_2))\rangle\langle S(y,(x_2,x_1))\rangle. \tag{2.10}$$

This assumption is justified if the dipoles scatter off uncorrelated targets, for example, off different nucleons of a very large nucleus. Writing $A = 1 - \langle S\rangle$, we get the following closed equation for A:

$$\frac{\partial}{\partial y}A(y,(x_0,x_1)) = \bar{\alpha}\int\frac{d^2x_2}{2\pi}\frac{x_{01}^2}{x_{02}^2x_{21}^2}[A(y,(x_0,x_2)) + A(y,(x_2,x_1)) - A(y,(x_0,x_1)) - A(y,(x_0,x_2))A(y,(x_2,x_1))], \tag{2.11}$$

which is the Balitsky-Kovchegov (BK) equation [25, 26]. Note that if one neglects the nonlinear term, one gets back the BFKL equation (2.6) (written for A instead of n). A graphical representation of this equation is given in Fig. 2.4.

It is not difficult to see analytically that the BK equation preserves the unitarity of A: When A becomes of the order of 1, then the nonlinear term gets comparable to the linear terms in magnitude, and slows down the evolution of A with y, which otherwise would be exponential. Hence the solution of the BK equation will exhibit essentially two regimes: A BFKL regime of low density in which $A \ll 1$ and in which the evolution proceeds linearly, and a high-density regime $A \sim 1$. At fixed y, the transition between these two regimes is controlled by the so-called

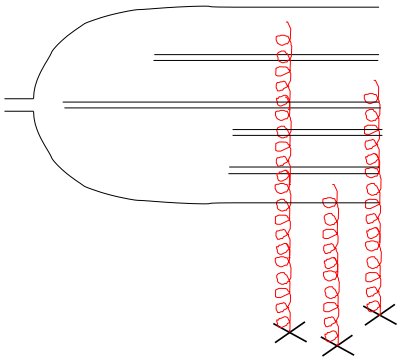

Figure 2.4: Picture of the BK equation. All the QCD evolution is put in the probe, which carries the total rapidity. It develops a high occupancy state of dipoles, which scatter independently off the target.

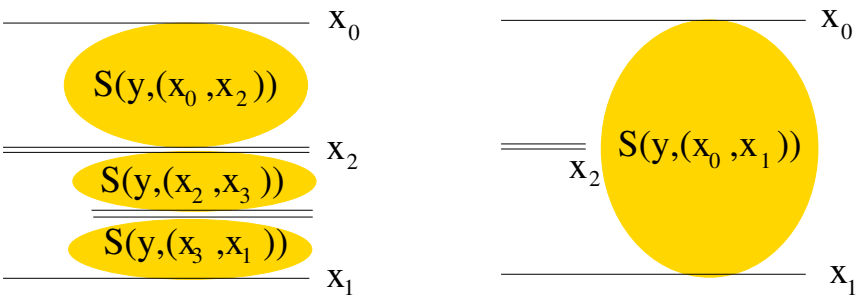

Figure 2.5: (a) Contribution to the B-JIMWLK equation for the 2-point correlator restricted to dipoles (x_2' is taken equal to x_2 in this figure). (b) A graph that would also contribute to the 2-point correlator and that is missing in the B-JIMWLK formalism.

saturation scale $Q_s(y)$, which is the inverse size of the dipoles which scatter with an amplitude A equal to some fixed number of order 1, for example $\frac{1}{2}$. (Q_s also depends a priori on the impact parameter, as will be discussed in Chap. 5).

Let us go back to Eqs. (2.8),(2.9) and instead of assuming the factorization of the correlators (2.10), work out an equation for the two-point correlator $\langle SS\rangle$. From the same calculation as before, we get

$$\frac{\partial}{\partial y}\langle S_{02}S_{2'1}\rangle = \bar{\alpha}\int\frac{d^2x_3}{2\pi}\frac{x_{02}^2}{x_{03}^2x_{32}^2}\left(\langle S_{03}S_{32}S_{2'1}\rangle - \langle S_{02}S_{2'1}\rangle\right) + \bar{\alpha}\int\frac{d^2x_3}{2\pi}\frac{x_{12'}^2}{x_{13}^2x_{32'}^2}\left(\langle S_{2'3}S_{31}S_{02}\rangle - \langle S_{02}S_{2'1}\rangle\right), \quad (2.12)$$

where we have introduced the notation $S_{ab}\equiv S(y,(x_a,x_b))$. (See Fig. 2.5a for the corresponding graphical representation.)

This equation calls for a new equation for the 3-point correlators, and so on. The obtained hierarchy is nothing but the Balitsky hierarchy [19] (see also Ref. [47–49]) restricted to dipoles.

2.1.4 The B-JIMWLK formalism

For completeness, let us briefly mention the Balitsky-Jalilian Marian-Iancu-McLerran-Weigert-Leonidov-Kovner (B-JIMWLK) formalism. It is a systematic approach beyond the large-N_c limit,

initially supposed to completely describe high-energy scattering under appropriate well-defined approximations. (Nowadays, the status of this approach is less clear, as we shall discuss later on). Instead of evolving dipole or parton number densities, B-JIMWLK evolves observables constructed with the help of Wilson operators

$$U(x) = P \exp\left(ig_s \int dx^\mu A^a_\mu(x) t^a \right) \tag{2.13}$$

where A^a_μ is the color 4-potential over which one eventually averages to arrive at observables, t^a the standard color matrics (fundamental representation), and $g_s = \sqrt{4\pi\alpha_s}$ the coupling of the line to the color field. The integration in the exponent goes along the trajectory of the quark whose interactions are described by U, which is essentially a straight lightlike line at very high energies.

There are several equivalent ways to present this physics. Let us exhibit the so-called "Balitsky hierarchy", which is an infinite system of coupled integro-differential equations for the correlators of U. In terms of the U's, the S-matrix for dipole scattering off a particular field configuration reads

$$S_{ab} = \frac{1}{N_c} \mathrm{Tr} U(x_a) U^\dagger(x_b). \tag{2.14}$$

The observables are the associated correlators: For example the dipole amplitude is obtained from S by averaging over the color fields.

The first equation of the Balitsky hierarchy for the observable $\langle S_{01} \rangle$ is identical to Eq. (2.9). The second equation, needed to solve the first one, reads

$$\begin{aligned}
\frac{\partial}{\partial y} \langle S_{02} S_{21} \rangle = \bar{\alpha} \int \frac{d^2 x_3}{2\pi} \Bigg\{ & \left[\frac{x_{02}^2}{x_{03}^2 x_{32}^2} \langle (S_{03} S_{32} - S_{02}) S_{21} \rangle + \frac{x_{01}^2}{x_{03}^2 x_{31}^2} \langle S_{02} (S_{03} S_{31} - S_{01}) \rangle \right] \\
& + \frac{1}{N_c^2} \left[- \frac{(x_0 - x_3) \cdot (x_1 - x_3)}{(x_0 - x_3)^2 (x_1 - x_3)^2} - \frac{1}{(x_2 - x_3)^2} + \frac{(x_0 - x_3) \cdot (x_2 - x_3)}{(x_0 - x_3)^2 (x_2 - x_3)^2} + \frac{(x_2 - x_3) \cdot (x_1 - x_3)}{(x_2 - x_3)^2 (x_1 - x_3)^2} \right] \\
& \times \left[\frac{1}{N_c} \left\langle \mathrm{Tr} \left(U_{x_0} U^\dagger_{x_2} U_{x_3} U^\dagger_{x_1} U_{x_2} U^\dagger_{x_3} \right) \right\rangle + \frac{1}{N_c} \left\langle \mathrm{Tr} \left(U_{x_0} U^\dagger_{x_3} U_{x_2} U^\dagger_{x_1} U_{x_3} U^\dagger_{x_2} \right) \right\rangle - 2 S_{01} \right] \Bigg\}
\end{aligned} \tag{2.15}$$

The first line is the same as Eq. (2.12). The other terms involve sextupoles and are suppressed at large-N_c. Hence in the dipole approximation, we recover Eq. (2.12).

The factorized correlators (2.10) is a solution of the whole dipole hierarchy, and turn actually out to be a good approximation to the solution of the full B-JIMWLK equations. This statement was first made after the numerical solution to a version of the B-JIMWLK formalism was worked out in Ref. [50]. We note however that the latter simulations did not cover a very large range in rapidity, and therefore, they may have missed physical effects that would differentiate the full B-JIMWLK equation from its approximate forms.

We may wonder why there are no terms involving one-point functions in the right-hand side of the previous equation. Actually, such terms would correspond to graphs like the one of Fig. 2.5b, in which, for example, two dipoles merge. They are expected to occur if saturation is properly taken into account. While the restriction of the Balitsky equation to dipoles does a priori not drastically change the solution for the scattering amplitudes, such terms would instead have a large effect, as we shall discover in the next section. To simplify the discussion, we will stick to the dipole approximation, which leads to the evolution equations (2.9),(2.12).

2.1.5 Saturation

The BK equation may be well-suited for the ideal case in which the target is a nucleus made of an infinity of independent nucleons. But it is not quite relevant to describe the scattering of more elementary objects such as two dipoles (or two virtual photons, to be more physical).

Indeed, following Chen and Mueller [51] (see also Ref. [52]), let us consider dipole-dipole scattering in the center-of-mass frame, where the rapidity evolution is equally shared between the projectile and the target (see Fig. 2.6a). Then at the time of the interaction, the targets are

dipoles that stem from the branching of a unique primordial dipole. Obviously, the assumption of statistical independence of the diffusion centers, which was needed for the factorization (2.10) to hold, is no longer justified.

So far, we have seen that nonlinear effects which go beyond the factorization formula (2.7) are necessary to preserve unitarity as soon as $n \sim 1/\alpha_s^2$. This came out of an analysis of Eq. (2.7) in the restframe of the target. The rapidity $y_{\rm BFKL}$ at which the system reaches this number of dipoles and hence at which the BFKL approach breaks down may be found from the form of the typical growth of n with y, namely $n(y) \sim e^{\bar{\alpha} y}$. Parametrically,

$$y_{\rm BFKL} \sim \frac{1}{\bar{\alpha}} \ln \frac{1}{\alpha_s^2}. \tag{2.16}$$

Now we may go to the center-of-mass frame, where Eq. (2.7) with $y' = y/2$ would describe the scattering amplitude in the absence of nonlinear effects. There, the typical number of dipoles in the projectile and in the target are well below $1/\alpha_s^2$: $n(y_{\rm BFKL}/2) \sim 1/\alpha_s$. We actually see that the evolution of the dipoles in each of theses systems remains linear until $y = 2y_{\rm BFKL}$. In that rapidity interval, nonlinear effects consist in the simultaneous scatterings of several dipoles from the target and the projectile but the evolution of n still obeys the BFKL equation. Now, performing a boost to the projectile restframe, the evolution goes into the target. Formula (2.3) should then apply for the amplitude A. But if the evolution of the target were kept linear, then the amplitude would break unitarity because the number of dipoles would be larger than $1/\alpha_s^2$. Hence, through some nonlinear mechanism, which was represented by multiple scatterings between linearly evolving objets in the center-of-mass frame, the dipole number density has to be kept effectively lower than $1/\alpha_s^2$ in order to preserve unitarity. This is called *parton saturation*. The precise saturation mechanism has not been formulated in QCD. It could be dipole recombinations due to gluon fusion, multiple scatterings inside the target which slow down the production of new dipoles [53], "dipole swing" as was proposed more recently [54, 55], or any other mechanism. Some of these mechanisms may be implemented in simplified toy models; see Chap. 3.

Hence, unitarity of the scattering amplitudes together with boost-invariance seem to require some sort of saturation of the density of partons. It is not clear whether such a mechanism is included in the B-JIMWLK formalism, since the latter is not obviously boost-invariant. What is clear is that some saturation mechanism lacks in the dipole model.

A pedagogical review of saturation and the discussion of the relationship between saturation and unitarity may be found in Ref. [56]. Original papers include Refs. [57, 58].

Visualizing saturation: Evolution in different models

We now wish to illustrate how the different schemes of unitarization (BK unitarization, multiple scatterings in the center-of-mass frame, explicit parton number saturation) affect the evolution of scattering amplitudes.

In Fig. 2.7, we plot the S-matrix element at different rapidity and as a function of the (logarithmic) dipole size resulting from the evolution of toy models with dynamics similar to QCD (The use of such models will be justified later, when we will establish the correspondence of high-energy QCD with more general processes). We see that S goes to zero in a region of sizes that extends with rapidity. This phenomenon is slower when there are saturation effects explicitly included in the evolution, as discussed above in this section.

2.1.6 The Pomeron language

So far, we have presented in detail a s-channel picture of hadronic interactions, and it is in this formalism that we will understand most easily the link with reaction-diffusion processes. In the s-channel formulation, all the QCD evolution happens in the form of quantum fluctuations of the interacting hadrons. However, a picture maybe more familiar to the reader belonging to the "traditional" QCD community is a t-channel picture, where the rapidity evolution is put in the t-channel, while the projectile and target stay in their bare states. This picture directly stems

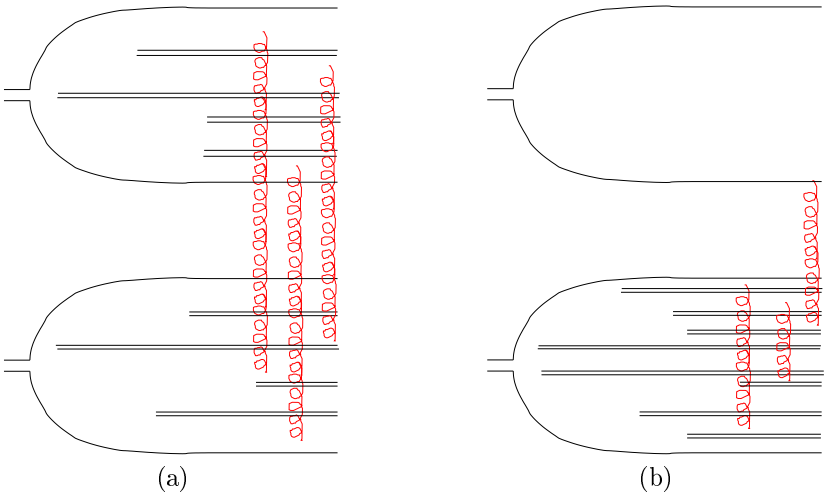

Figure 2.6: (a) Scattering in the dipole model in the center-of-mass frame. The evolution is shared between the target and the probe. The amplitude is unitarized through the multiple scatterings occurring between the two evolved wave-functions. (b) Boost of the previous graph to the restframe of the projectile. There is now twice as much evolution in the target and the nonlinear effects should occur inside its wave-function, in the course of the evolution. They may take the form of "internal" rescatterings (as depicted), or dipole merging...

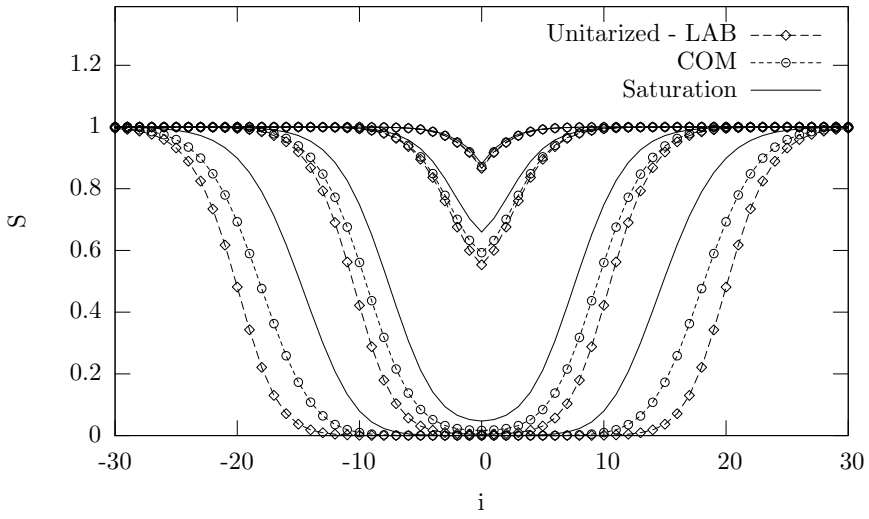

Figure 2.7: [From Ref. [59]] S-matrix element as a function of the logarithm of the dipole size for $y = 5, 10, 20, 30$ (from the center of the figure towards the outskirts). $1/\alpha^2 = 20$. For low rapidities ($y = 5$ and $y = 10$), the evolution is linear (of BFKL type). At $y = 20$, the unitarity limit has been reached in all calculations (S becomes zero in some region of sizes). Later ($y = 30$), the region in which $S = 0$ propagates outwards. Different unitarization mechanisms are tested: simple BK unitarization ("Unitarized-LAB"), center-of-mass unitarization ("COM") and intrinsic saturation.

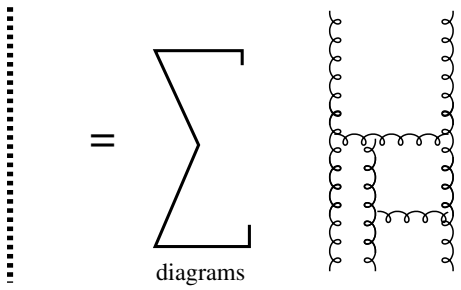

Figure 2.8: The BFKL Pomeron is a sum of t-channel gluon Feynman diagrams.

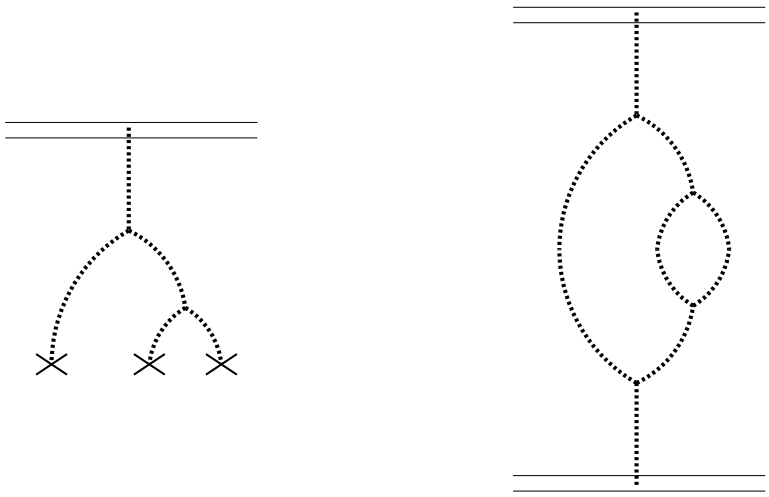

Figure 2.9: (a) Example of a diagram contributing to the BK equation in the t-channel representation (see Fig. 2.4). The dashed lines represent Pomerons. The rapidity is proportional to the length of the Pomeron lines in the t-channel. (b) Pomeron representation of a class of diagrams to which Fig. 2.6a belongs.

from the usual Lorentz-invariant formulation of quantum field theory, while the dipole picture (or the parton model) is derived in the framework of time-ordered perturbation theory.

Both pictures have their respective advantages and drawbacks. The covariant formulation seems to be more suited for higher-order systematic calculations, since for a given observable the number of diagrams is smaller than in the time-ordered (s-channel) formalism. The time-ordered formalism seems unpractical beyond the tree-level approximation. On the other hand, the latter gives maybe a more intuitive picture of scattering processes and seems to be particularly useful to study the approach to unitarity.

In the t-channel picture, classes of Feynam diagrams can be grouped into "Pomerons" (or Reggeized gluons, see Fig. 2.8), in terms of which scattering processes may be analyzed. (A pedagogical review on how to derive the BFKL equation in such a formalism is available from Ref. [60]). An effective action containing Pomeron fields and Pomeron vertices may be constructed. In these terms, the s-channel diagrams of Fig. 2.4 and 2.6a may be translated in terms of the diagrams of Fig. 2.9. The effective action formalism was initially developped in Refs. [61–63]. More recently, there has been some progress in the definition of the effective action [64], some of it with the help of the correspondence with statistical physics processes [65,66].

We will not expand on this formulation in the present review, because it is difficult to see the analogy with statistical physics in this framework. A s-channel picture is much more natural. However, a full solution of high-energy QCD may require to go back to that kind of calculation and compute accurately the $1 \to n$ Pomeron vertices. This program was formulated some time ago [67, 68], and there is continuing progress in this direction (see e.g. [69, 70]).

2.2 Analogy with reaction-diffusion processes

We are now in position to draw the relationship between high-energy QCD and reaction-diffusion processes. In the first section below, we will show that the BK equation is, in some limit, an equation that also appears in the context of statistical physics. Second, we will exhibit a simple reaction-diffusion model, and show in the final section how this model is related to scattering in QCD, even beyond the approximations implied in the BK equation.

2.2.1 The BK equation and the FKPP equation

Let us first show at the technical level that under some well-controlled approximations, the BK equation (2.11) may be mapped exactly to a parabolic nonlinear partial differential equation. This observation was first made in Ref. [39].

To simplify, we will look for impact-parameter independent solutions: $A(y,(x_0,x_1))$ is assumed to depend on y and x_{01} only, not on $\frac{x_0+x_1}{2}$. We switch to momentum space through the Fourier transformation

$$A(y,k) = \int \frac{d^2x_{01}}{2\pi x_{01}^2} e^{i\vec{k}\vec{x}_{01}} A(y,x_{01}). \tag{2.17}$$

This transformation greatly simplifies the BK equation [25, 26]. It now reads

$$\partial_{\bar{\alpha}y} A(y,k) = \chi(-\partial_{\ln k^2}) A(y,k) - A^2(y,k). \tag{2.18}$$

The first term on the right-hand side, which is a linear term, is actually an integral transform whose kernel, obtained by Fourier transformation of the BFKL kernel (first three terms on the right-hand side of Eq. (2.11)). It is most easily expressed in Mellin space since the powers $k^{-2\gamma}$ are its eigenfunctions, with the corresponding eigenvalues

$$\chi(\gamma) = 2\psi(1) - \psi(\gamma) - \psi(1-\gamma). \tag{2.19}$$

This kernel may be expanded around some real $\gamma = \gamma_0$, fixed between 0 and 1. Keeping the terms up to $\mathcal{O}((\gamma-\gamma_0)^2)$ is the well-known diffusive approximation, which is a good approximation at large rapidities. Introducing the notations $\chi_0 \equiv \chi(\gamma_0)$, $\chi_0' \equiv \chi'(\gamma_0)$ and $\chi_0'' \equiv \chi''(\gamma_0)$, the BK equation reads

$$\partial_{\bar{\alpha}y} A = \tfrac{\chi_0''}{2} \partial^2_{\ln k^2} A + (\gamma_0\chi_0'' - \chi_0') \partial_{\ln k^2} A + (\chi_0 - \gamma_0\chi_0' + \tfrac{\gamma_0^2\chi_0''}{2}) A - A^2. \tag{2.20}$$

Through the linear change of variable $(\bar{\alpha}y, \ln k^2) \to (t,x)$,

$$\begin{aligned} \bar{\alpha}y &= \frac{t}{\chi_0 - \gamma_0\chi_0' + \frac{\gamma_0^2\chi_0''}{2}} \\ \ln k^2 &= \sqrt{\frac{\chi_0''}{2(\chi_0 - \gamma_0\chi_0') + \gamma_0^2\chi_0''}}\, x - \frac{\gamma_0\chi_0'' - \chi_0'}{\chi_0 - \gamma_0\chi_0' + \frac{\gamma_0^2\chi_0''}{2}} t, \end{aligned} \tag{2.21}$$

one may get rid of the first-order partial derivative in the right handside. We then find that the rescaled function

$$u(t,x) = \frac{A(y(t), \ln k^2(t,x))}{\chi_0 - \gamma_0\chi_0' + \frac{\gamma_0^2\chi_0''}{2}} \tag{2.22}$$

obeys the equation

$$\frac{\partial u(t,x)}{\partial t} = \frac{\partial^2 u(t,x)}{\partial x^2} + u(t,x) - u^2(t,x), \tag{2.23}$$

which is the Fisher [37] and Kolmogorov-Petrovsky-Piscounov [38] (FKPP) equation. This equation was first written down as a model for gene propagation in a population in the limit of large number of individuals. But it turns out to apply directly or indirectly to many different physical situations, such as reaction-diffusion processes, but also directed percolation, and even mean-field spin glasses [71]. A recent comprehensive review on the known mathematics and the phenomenological implications of the FKPP equation can be found in Ref. [72].

As a side remark, we note that if γ_0 is chosen such that the equation $\chi(\gamma_0) = \gamma_0 \chi'(\gamma_0)$ is verified, then the mapping drastically simplifies. Actually, this choice has a physical meaning, as we will discover in Chap. 4 when we try and solve the BK equation.

Beyond the exact mapping (2.23) between an approximate form of the BK equation and the FKPP equation, the full BK equation is said to be in the *universality class* of the FKPP equation. All equations in this universality class share some common properties, as will be understood below. The exact form of the equation is unessential. As a matter of fact, recently, it has been checked explicitly that the BFKL equation with next-to-leading order contributions to the linear evolution kernel (but keeping the QCD coupling fixed) is also in the same universality class. A mapping to a partial differential equation (which involves higher-order derivatives in the rapidity variable) was exhibited [73]. What defines physically the universality class of the FKPP equation is a branching diffusion process with some saturation mechanism. The details seem unimportant.

We must however keep in mind that there is for the time being no theorem that would clearly state the necessary and sufficient conditions for a model to belong (or not) to the universality class of the FKPP equation: Our statements are nothing but conjectures, supported by arguments and checked against numerical simulations.

In the next section, we shall give a concrete example of a reaction-diffusion process: We will see how the FKPP equation appears as a fluctuationless (or "mean-field") limit of some stochastic reaction-diffusion process. In Ref. [39], it had not been realized that the analogy of QCD with such processes is in fact much deeper than the formal mapping between the BK equation and the FKPP equation that we have just outlined. But this is actually the case, as we shall shortly argue.

2.2.2 Reaction-diffusion processes: an example

We consider the reaction-diffusion model which was introduced in Ref. [74]. It consists in a set of particles which are evolving in discrete time on a one-dimensional lattice. The following rules define the dynamics of the system: At each timestep, a particle may jump to the nearest position on the left or on the right with respective probabilities p_l and p_r, and may split into two particles with probability λ. We also allow each of the $n(t,x)$ particles on site x at time t to die with probability $\lambda n(t,x)/N$.

We can guess what a realization of this evolution may look like at large times. The particles branch and diffuse (they undergo an evolution which can be represented by a linear finite difference equation) until their number n becomes of the order of N, at which point the probability that they "die" starts to be sizable, in such a way that their number never exceeds N by a large amount, on any site. If the initial condition is spread on a finite number of lattice sites, the linear branching-diffusion process may always proceed towards larger values of $|x|$, where there were no particles in the beginning of the evolution. Hence after some lapse of time (typically larger than $\ln N$) a realization will look like a double front connecting an ensemble of lattice sites where a quasi-stationary state in which the number of particles is N (up to fluctuations) has been reached, to an ensemble of empty sites. One front will move towards $x \to +\infty$, the other one towards $x \to -\infty$ as the branching diffusion process proceeds. Let us focus on the front traveling to the right. The position of the front $X(t)$ may be defined in different ways, leading asymptotically to equivalent determinations, up to a constant. For example, one may define $X(t)$ as the rightmost bin in which there are more than $N/2$ particles, or, alternatively, as the total number of particles

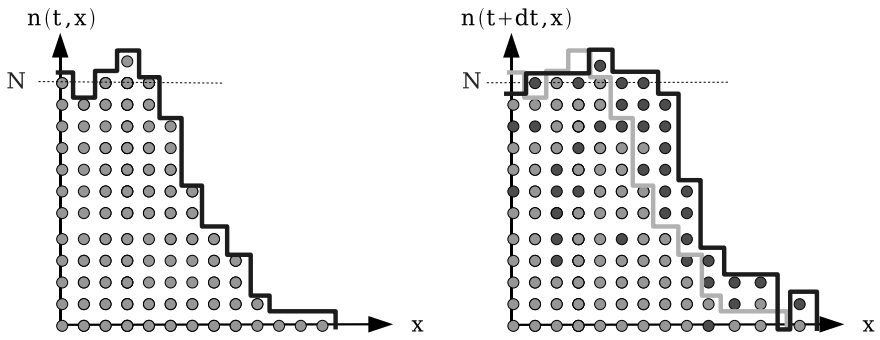

Figure 2.10: Picture of a realization of the system of particles at two successive times. In the bins in which the number of particles is of order N, some particles disappear, others are created by splittings, but overall the number of particles is conserved up to fluctuations of order $\sqrt{N}$. In the bins in which n is small compared to N, the dynamics is driven by branching diffusion. As a result, $n(t,x)$ looks like a noisy wave front moving to the right.

in the realization whose positions are greater than 0, scaled by $1/N$. A realization and its time evolution is sketched in Fig. 2.10.

Between times t and $t+\Delta t$, $n_l(t,x)$ particles out of $n(t,x)$ move to the left and $n_r(t,x)$ of them move to the right. Furthermore, $n_+(t,x)$ particles are replaced by their two offspring at x, and $n_-(t,x)$ particles disappear. Hence the total variation in the number of particles on site x reads

$$n(t+\Delta t,x)-n(t,x) = -n_l(t,x)-n_r(t,x)-n_-(t,x) + n_+(t,x)+n_l(t,x+\Delta x)+n_r(t,x-\Delta x). \quad (2.24a)$$

The numbers describing a timestep at position x have a multinomial distribution:

$$P(\{n_l,n_r,n_+,n_-\}) = \frac{n!}{n_l!n_r!n_+!n_-!\Delta n!} p_l^{n_l} p_r^{n_r} \lambda^{n_+} (\lambda n/N)^{n_-} (1-p_l-p_r-\lambda-\lambda n/N)^{\Delta n}, \quad (2.24b)$$

where $\Delta n = n-n_l-n_r-n_+-n_-$, and all quantities in the previous equation are understood at site x and time t. The evolution of $u \equiv n/N$ is obviously stochastic. One could write the following equation:

$$u(t+\Delta t,x) = \langle u(t+\Delta t,x)\rangle + \sqrt{\langle u^2(t+\Delta t,x)\rangle - \langle u(t+\Delta t,x)\rangle^2}\,\nu(t+\Delta t,x) \quad (2.25)$$

where the averages are performed over the time step that takes the system from t to $t+\Delta t$. They are conditioned to the value of u at time t. ν is a noise, i.e. a random function. The equation was written in such a way that it has zero mean and unit variance. Note that the noise is updated at time $t+\Delta t$ in this equation.

One can compute the mean evolution of $u \equiv n/N$ in one step of time which appears in the right-hand side of Eq. (2.25) from Eq. (2.24). It reads

$$\langle u(t+\Delta t,x)|\{u(t,x)\}\rangle = u(t,x)+p_l[u(t,x+\Delta x)-u(t,x)] + p_r[u(t,x-\Delta x)-u(t,x)]+\lambda u(t,x)[1-u(t,x)]. \quad (2.26)$$

The mean evolution of the variance of u that appears in Eq. (2.25) may also be computed. The precise form of the result is more complicated, but roughly speaking, the variance of u after evolution over a unit of time is of the order of u/N for small $u \sim 1/N$. This is related to the fact

that the noise has a statistical origin: Having n particles on the average in a system means that each realization typically consists in $n \pm \sqrt{n}$ particles.

When N is infinitely large, one can replace the u's in Eq. (2.26) by their averages: This would be a mean-field approximation. Obviously, the noise term drops out, and the equation becomes deterministic. Note that if we appropriately take the limits $\Delta x \to 0$ and $\Delta t \to 0$, setting

$$\lambda = \Delta t, \quad p_R = p_L = \frac{\Delta t}{(\Delta x)^2}, \tag{2.27}$$

the obtained mean-field equation is nothing but the FKPP equation (2.23). For the numerical simulations of this model that we will perform in Sec. 4, we will keep Δt and Δx fixed, which is more convenient for computer implementation.

Thus we have seen that the evolution of reaction-diffusion systems is governed by a stochastic equation (2.25) whose continuous limit ($\Delta t \to 0$, $\Delta x \to 0$) and mean-field limit ($N \gg 1$) is a partial differential equation of the form of (exactly actually, in our simple case study) the FKPP equation. We shall now argue that partons in high-energy QCD form a similar system.

2.2.3 Universality class of high-energy QCD

Let us come back to the QCD dipole model discussed in Sec. 2.1. We have seen that evolution proceeds through a branching diffusion process of dipoles. Let us denote by $T(y, r)$ the scattering amplitude of the probe dipole off one particular realization of the target at rapidity y and at a given fixed impact parameter. This means that we imagine for a while that we may freeze the target in one particular realization after the rapidity evolution y, and probe the latter with projectiles of all possible sizes. Of course, this is not doable in an actual experiment, not even in principle. But it is very important for the statistical picture to decompose the physical observables with the help of such a "gedanken observable". The amplitude A, which is related to the measurable total cross-section, is nothing but the average of T over all possible realizations of the fluctuations of the target, namely

$$A(y, r) = \langle T(y, r) \rangle. \tag{2.28}$$

The branching diffusion of the dipoles essentially occurs in the $\ln(1/r^2)$ variable. The scattering amplitude is roughly equal to the number of dipoles in a given bin of (logarithmic) dipole size, multiplied by α_s^2. From unitarity arguments and consistency with boost-invariance, we have seen that the branching diffusion process should (at least) slow down in a given bin as soon as the number of objects in that very bin is of the order of $N = 1/\alpha_s^2$, in such a way that effectively, the number of dipoles in each bin is limited to N. A typical realization of T is sketched in Fig. 2.11. As in the case of the reaction-diffusion process, from similar arguments, it necessarily looks like a front. The position of the front, defined to be the value r_s of r for which T is equal to some fixed number, say $\frac{1}{2}$, is related to the saturation scale defined in the Introduction: $r_s = 1/Q_s(y)$.

We now see that there is a very close analogy between what we are describing for QCD here and the model that we were introducing in the previous section. So in particular, one might be able to formulate interaction processes in QCD with the help of a stochastic nonlinear evolution equation for the "gedanken" amplitude T. We already know the equation that one should get in the mean-field limit in which N is very large: It is the BK equation, as was rigorously proven above. Thus we know the equivalent of the term $\langle u(t + \Delta t, x) \rangle$ in Eq. (2.25). The noise term is not known, but since it is of statistical origin, it must be of the order of the square root of the number of dipoles normalized to N, that is to say, of order $\sqrt{T/N}$. We may write an equation of the form

$$\partial_{\bar{\alpha} y} T(y, k) = \chi(-\partial_{\ln k^2}) T(y, k) - T^2(y, k) + \alpha_s \sqrt{2T(y, k)}\, \nu(y, k), \tag{2.29}$$

where ν is a noise, uncorrelated in rapidity and transverse momentum, with zero mean and unit variance. This equation is to be compared to the following one:

$$\partial_t u(t, x) = \partial_x^2 u(t, x) + u(t, x) - u^2(t, x) + \sqrt{\frac{2u(t, x)}{N}}\, \nu(t, x), \tag{2.30}$$

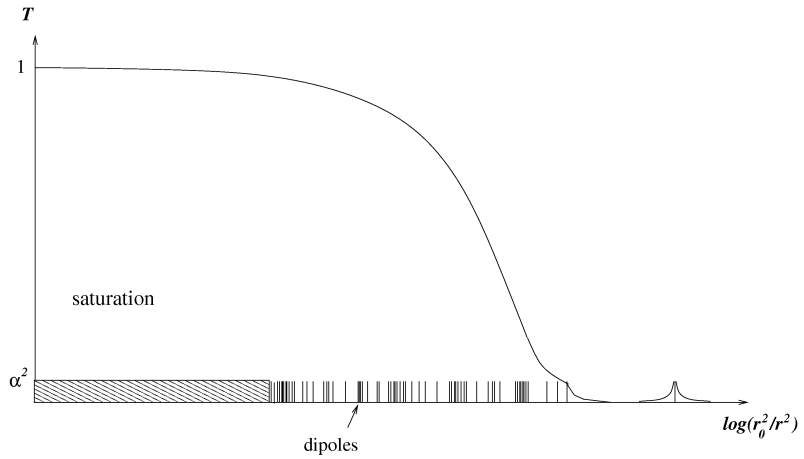

Figure 2.11: Sketch of the scattering amplitude T of a dipole of size r off a frozen partonic configuration. The small lines on the axis denote the dipoles ordered by their logarithmic sizes. Up to fluctuations, T looks like a wave front.

which is the so-called "Reggeon field theory" equation when the noise ν is exactly a normal Gaussian white noise, that is to say, whose non-vanishing cumulants read

$$\begin{aligned} \langle \nu(t,x) \rangle &= 0 \\ \langle \nu(t,x)\nu(t',x') \rangle &= \delta(t-t')\delta(x-x'). \end{aligned} \tag{2.31}$$

It is a stochastic extension of Eq. (2.23). If the noise term were of the form

$$\sqrt{\frac{2u(t,x)(1-u(t,x))}{N}}\,\nu(t,x) \tag{2.32}$$

instead, then this equation would be what is usually referred to as the *stochastic Fisher-Kolmogorov-Petrovsky-Piscounov equation*. The sFKPP equation and the physics that it represents is reviewed in Ref. [75].

Taking averages over events converts this equation into a hierarchy of coupled equations, which has a lot in common in its structure with the (modified) Balitsky hierarchy (2.9,2.12). A detailed study may be found in Ref. [76]. We will perform explicit calculations in this spirit within simpler models in Chap. 3 below.

Based on these considerations, we may establish a dictionary between QCD and reaction-diffusion processes. The correspondence is summarized in Tab. 2.1.

The mechanism for saturation of the parton densities (i.e. of the dipole number) is not known for sure in QCD. There is even some evidence that dipole degrees of freedom are no longer sufficient to describe scattering beyond some rapidity, as is understood from the appearance of sextupoles in the second equation of the full Balitsky hierarchy. There are also important differences between the reaction-diffusion model introduced above and QCD that lie in the "counting rule" of the particles (provided by the form of $T^{\rm el}$ in the QCD case). But from the general analysis of processes described by equations in the universality class of the stochastic FKPP equation and the underlying evolution mechanisms presented in Chap. 4, we will understand that most of the observables have universal properties in appropriate limits, which do not depend on the details of the mechanism at work. We draw the reader's attention to Refs. [77, 78], where a precise stochastic equation was searched for in QCD. Some of the problems one may face with the use and the very interpretation of such equations were studied in Ref. [79].

The way in which we view high energy QCD in this review is actually not particularly original: It is nothing but the QCD dipole model, which was implemented numerically in the form of a Monte

Reaction-diffusion	QCD
Occupation fraction $u(t,x)$	Scattering amplitude for the probe off a frozen realization of the target $T(y,k)$
Average occupation fraction $\langle u(t,x)\rangle$	Physical scattering amplitude $A = \langle T\rangle$
Space variable x	$\ln(k^2/\Lambda^2)$ or $\ln(1/x^2\Lambda^2)$
Time variable t	$\bar{\alpha}y$
Average maximum density of particles N	$1/\alpha_s^2$
Position of the front $X(t)$	Saturation scale $\ln(Q_s^2(y)/\Lambda^2)$
Branching-diffusion kernel $\omega(-\partial_x)$ ($\omega(-\partial_x) = \partial_x^2 + 1$ in the FKPP case)	BFKL kernel $\chi(-\partial_{\ln k^2})$ or its equivalent in coordinate space

Table 2.1: Dictionary between QCD and the reaction-diffusion model for the main physical quantities. Λ is a typical hadronic scale.

Carlo event generator by Salam [80–82] (see also [54] for another more recent implementation). He also devised and implemented a ad hoc saturation mechanism [53] that went beyond the original dipole model pictured in Fig. 2.6a, but which is necessary, as we argued before.

Before discussing more deeply the physical content of equations of the form of Eq. (2.29), we shall first study a model in which spatial dimensions are left out, that we will be able to formulate in different ways.

Chapter 3

The simplest saturation model

In the previous chapter, we have understood that scattering at high energy in QCD may be viewed as a branching-diffusion process supplemented by a saturation mechanism. We have exhibited a simple toy model with these characteristics, whose dynamics is represented by an equation of the type (2.30).

Unfortunately, even that toy model is too difficult to solve analytically. We shall study a still simplified model, where there is no diffusion mechanism: Realizations are completely specified by the number of particles that the system contains at a given time. Of course, in this case, a saturation scale cannot be defined, which limits the relevance of this model for QCD. However, we will be able to formulate this model in many different ways, and to draw parallels with QCD.

We start by defining precisely the model. Then, two approaches to the computation of the moments of the number of particles are presented. The first set of methods relies on field theory (Sec. 3.2). The second method relies on a statistical approach (Sec. 3.3) and will be extended in a phenomenological way to models with a spatial dimension in Chap. 4. We shall then draw the relation to a scattering-like formulation (Sec. 3.4). Finally (Sec. 3.5), some variants of the basic model are reviewed.

Contents

3.1 Definition

Let us consider a simple model in which at a given time t, the system is fully characterized by the number n_t of particles. The evolution rules are the following. Between times t and $t + dt$, each particle has a probability dt to split in two particles. For each pair of particles, there is a probability dt/N that they merge into one. We may summarize these rules by the following set of

equations:

$$n_{t+dt} = \begin{cases} n_t{+}1 \text{ proba } n_t dt \\ n_t{-}1 \text{ proba } \dfrac{n_t(n_t{-}1)dt}{N} \\ n_t \text{ proba } 1{-}n_t dt - \dfrac{n_t(n_t{-}1)dt}{N}. \end{cases} \tag{3.1}$$

From this, one can easily derive an equation for the time evolution of the probability $P(n,t)$ of observing n particles in the system at time t:

$$\frac{\partial P}{\partial t}(n,t) = (n-1)P(n-1,t) + \frac{n(n+1)}{N}P(n+1,t) - \left(n + \frac{n(n-1)}{N}\right)P(n,t). \tag{3.2}$$

This is the *master equation* for the Markovian process under consideration. The two first terms with a positive sign represent the process of going from one state containing n particles to an adjacent one containing $n+1$ or $n-1$ particles respectively, while the last term simply corrects the probability to keep it unitary.

By multiplying both sides of this equation by n and summing over n, we get an evolution equation for the average number of particles $\langle n_t \rangle$:

$$\frac{d\langle n_t \rangle}{dt} = \langle n_t \rangle - \frac{1}{N}\langle n_t(n_t-1) \rangle. \tag{3.3}$$

Obviously, this equation is not closed, and one would have to establish an equation for $\langle n_t(n_t{-}1)\rangle$, which would involve 3-point correlators of n_t, and so on, ending up with an infinite hierarchy of equations, exactly like in Chap. 2 for QCD (see Eqs. (2.9) and (2.12)).

This illustrates the difficulties one has to face before one can get an analytical expression for $\langle n_t \rangle$, even in such a simple model.

3.2 "Field theory" approach

In the next subsections, we will follow different routes to get analytical results on the moments of the number of particles in the system at a given time t. The first one will be similar to the s-channel picture of QCD (see Sec. 2), since it will consist in computing the time (equivalent to the rapidity in QCD) evolution of realizations of the system. The second one will be closer to the t-channel picture of QCD. We will see how "Pomerons" may appear in these simple systems. We will then examine a formulation in terms of a stochastic nonlinear partial differential equation, which is nothing but the sFKPP equation in which the space variable (x) has been discarded.

3.2.1 Particle Fock states and their weights

Statistical problems were first formulated as field theories by Doi [83] and Peliti [84]. Different authors have used these methods (see Ref. [85] for a review). We shall start by following the presentation given in Ref. [86].

We would like to interpret the master equation (3.2) as a quasi-Hamiltonian evolution equation of the type of the ones that appear in quantum mechanics. To this aim, we need to introduce the basis of states $|n\rangle$ of fixed number n of particles. We define the ladder operators a and $a^\dagger$ by their action on these states:

$$a|n\rangle = n|n-1\rangle, \; a^\dagger|n\rangle = |n+1\rangle \tag{3.4}$$

and which obey the commutation relation

$$[a, a^\dagger] = 1. \tag{3.5}$$

The n-particle state may be constructed from the vacuum (zero-particle) state by repeated application of the ladder operator:

$$|n\rangle = \left(a^\dagger\right)^n |0\rangle. \tag{3.6}$$

The normalization is not standard with respect to what is usually taken in quantum mechanics. In particular, the orthogonal basis $|n\rangle$ is defined in such a way that $\langle m|n\rangle = n!\delta_{m,n}$. This implies that the completeness relation reads

$$\sum_n \frac{1}{n!}|n\rangle\langle n| = 1. \tag{3.7}$$

We also introduce the state vector of the system at a time t as a sum over all possible Fock states weighted by their probabilities:

$$|\phi(t)\rangle = \sum_n P(n,t)|n\rangle. \tag{3.8}$$

It is straightforward to see that the master equation (3.2) is then mapped to the Schrödinger-type equation

$$\frac{\partial}{\partial t}|\phi(t)\rangle = -\mathcal{H}|\phi(t)\rangle, \tag{3.9}$$

where $\mathcal{H}$ is the "Hamiltonian" operator

$$\mathcal{H} = (1-a^\dagger)a^\dagger a - \frac{1}{N}(1-a^\dagger)a^\dagger a^2. \tag{3.10}$$

The first term represents the splitting of particles, while the second one, proportional to $1/N$, represents the recombination. We may rewrite $\mathcal{H}$ as

$$\mathcal{H} = \mathcal{H}_0 + \mathcal{H}_1, \tag{3.11}$$

where

$$\mathcal{H}_0 = a^\dagger a \tag{3.12}$$

is the "free" Hamiltonian whose eigenstates are the Fock states. We now go to the interaction picture by introducing the time-dependent Hamiltonian

$$\mathcal{H}_I(t) = e^{\mathcal{H}_0 t}\mathcal{H}_1 e^{-\mathcal{H}_0 t} \tag{3.13}$$

and the states $|\phi\rangle_I = e^{\mathcal{H}_0 t}|\phi\rangle$. The solution of the evolution reads

$$\begin{aligned} |\phi\rangle_I &= T\exp\left(-\int_0^t dt'\mathcal{H}_I(t')\right)|\phi_0\rangle_I \\ &= |\phi_0\rangle_I - \int_0^t dt'\mathcal{H}_I(t')|\phi_0\rangle_I + \int_0^t dt'\int_0^{t'} dt''\mathcal{H}_I(t')\mathcal{H}_I(t'')|\phi_0\rangle_I + \cdots \end{aligned} \tag{3.14}$$

We may then compute the weights of the successive Fock states by applying this formula. Let us show how it works in detail by computing the state of a single particle evolved from time 0 to time t, in the limit $N = \infty$ in which there are no recombinations. We follow the usual method to deal with such problems in field theory. We repeatedly insert complete bases of eigenstates of $\mathcal{H}_0$ into Eq. (3.14), namely

$$|\phi\rangle_I = |1\rangle - \int_0^t dt'\sum_{n_1}\frac{1}{n_1!}|n_1\rangle\langle n_1|\mathcal{H}_I(t')|1\rangle + \cdots \tag{3.15}$$

(We have kept the first two terms in Eq. (3.14) explicitely). Using the expression for $\mathcal{H}_I(t)$ as a function of $\mathcal{H}_0$ and $\mathcal{H}_1$, together with the knowledge that the Fock states are eigenstates of $\mathcal{H}_0$, we get

$$|\phi\rangle = e^{-t}|1\rangle - \sum_{n_1} e^{-n_1 t}\int_0^t dt' e^{n_1 t'-t'}\frac{1}{n_1!}|n_1\rangle\langle n_1|\mathcal{H}_1|1\rangle + \cdots \tag{3.16}$$

Inserting the expression for $\mathcal{H}_1$, one sees that in the infinite-N limit, there is only one possible elementary transition, namely the splitting. Performing the integration over t' and computing in the same manner the higher orders, one finally gets the expansion

$$|\phi\rangle = e^{-t}|1\rangle + e^{-t}(1-e^{-t})|2\rangle + \cdots + e^{-t}(1-e^{-t})^{n-1}|n\rangle + \cdots \tag{3.17}$$

from which one can read the probabilities of the successive Fock states. This expansion is similar to the expansion in dipole Fock states introduced in Sec. 2: The n-particle states correspond to n-dipole states in QCD, and their weights are computed by applying successive splittings to the system, whose rates are given by Eq. (2.1). (They are just unity in the case of the zero-dimensional model.)

We see that this method is well-suited to compute the probabilities of the lowest-lying Fock-states, and their successive corrections at finite N. But in general we are rather interested in averages such as $\langle n^k \rangle$, for which the weights of all Fock states are needed. We will develop a slightly different (but equivalent) formalism below, that will enable us to get these averages in a much more straightforward way.

3.2.2 "Pomeron" field theory

Let us introduce the generating function of the factorial moments of the distribution of the number of particles

$$Z(z,t) = \sum_n (1+z)^n P(n,t). \tag{3.18}$$

The evolution equation obeyed by Z can easily be derived from the master equation (3.2):

$$\frac{\partial Z}{\partial t} = z(1+z)\left(\frac{\partial Z}{\partial z} - \frac{1}{N}\frac{\partial^2 Z}{\partial z^2}\right). \tag{3.19}$$

We may represent this equation in a second-quantized formalism by introducing the operators

$$b^\dagger = z,\ b = \frac{\partial}{\partial z} = \bar{z} \tag{3.20}$$

acting on the set of states $|Z\rangle$ consisting in the analytic functions of z. Then we may write

$$\frac{\partial Z}{\partial t} = -\mathcal{H}^{\mathbb{P}} Z, \tag{3.21}$$

where

$$\mathcal{H}^{\mathbb{P}} = \mathcal{H}_0^{\mathbb{P}} + \mathcal{H}_1^{\mathbb{P}},\ \text{with}\ \mathcal{H}_0^{\mathbb{P}} = -b^\dagger b,\ \mathcal{H}_1^{\mathbb{P}} = -b^\dagger b^\dagger b + \frac{1}{N} b^\dagger (1+b^\dagger) b^2. \tag{3.22}$$

A basis for the states is

$$|k\rangle = z^k,\ \langle k| = \bar{z}^k \tag{3.23}$$

which is orthogonal with respect to the scalar product

$$\langle Z_1 | Z_2 \rangle = \int \frac{dz d\bar{z}}{2i\pi} e^{-|z|^2} \bar{Z}_1(z,\bar{z}) Z_2(z,\bar{z}), \tag{3.24}$$

and obeys the normalization condition $\langle k|l\rangle = k!\delta_{k,l}$. We shall call these states "k-Pomeron" states, by analogy with high-energy QCD. We may apply exactly the same formalism as before, since the operators b, $b^\dagger$ have the same properties as the a, $a^\dagger$.

From the definition of the scalar product, it is not difficult to see that the k-th factorial moment of n may be obtained by a mere contraction of the state vector $|Z\rangle$, computed by solving the Hamiltonian evolution, with a k-Pomeron state. The following identity holds:

$$\langle k|Z\rangle = \left\langle \frac{n!}{(n-k)!} \right\rangle, \tag{3.25}$$

where the average in the right-hand side goes over the realizations of the system. As for the initial condition, starting the evolution with one particle means taking as an initial condition the superposition $|0\rangle + |1\rangle$ of zero- and one-Pomeron states respectively. The zero-Pomeron state does not contribute to the evolution, hence effectively a one-Pomeron state is like a one-particle state.

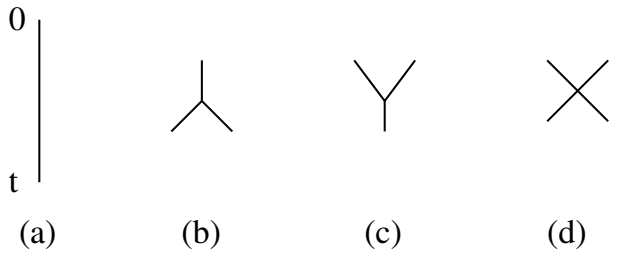

Figure 3.1: Propagator and vertices for the Pomeron field theory. Time flows from the top to the bottom.

In order to simplify the systematic computation of these moments, we may use a diagrammatic method and establish Feynman rules. To this aim, we write the contribution of the graphs with l-vertices (corresponding to the term of order l in the expansion of Eq. (3.14)), starting with a one-Pomeron state:

$$\langle k|Z\rangle \supset (-1)^l \int_0^t dt_1 \int_0^{t_1} dt_2 \cdots \int_0^{t_{l-1}} dt_l \sum_{n_1,\cdots,n_l} \langle k|n_l\rangle \frac{1}{n_l!}\langle n_l|\mathcal{H}_I^{\mathbb{P}}|n_{l-1}\rangle \cdots \frac{1}{n_1!}\langle n_1|\mathcal{H}_I^{\mathbb{P}}|1\rangle. \quad (3.26)$$

Each matrix element that appears in this equation is associated to a vertex, and propagators connect these vertices. We read on the expression for the Hamiltonian (3.22) that there is one propagator and three vertices in the theory: one splitting vertex ($1 \to 2$), one recombination ($2 \to 1$) and a $2 \to 2$ elastic diffusion vertex.

The method to compute the 1 to k Pomeron transition amplitude is standard. First, one draws all possible diagrams for this transition that contain l vertices, including all possible permutations. (Note that a splitting may occur in k different ways, if k is the number of Pomerons before the splitting; A recombination instead may occur in $k(k-1)/2$ ways). Then, the propagators (Fig. 3.1a) are replaced by

$$\langle 1|e^{-t\mathcal{H}_0^{\mathbb{P}}}|1\rangle = e^t, \quad (3.27)$$

(where t is the time interval they span). The n-Pomeron state propagates as $\langle n|e^{-t\mathcal{H}_0^{\mathbb{P}}}|n\rangle = e^{nt}$. Intermediate times are eventually integrated over. As for the vertices (Figs. 3.1b-d), the following factors have to be applied:

$$(1 \to 2): \ -1; \quad (2 \to 1): \ \frac{2}{N}; \quad (2 \to 2): \ \frac{2}{N}. \quad (3.28)$$

In addition, there is a $(-1)^{\#\text{vertices}}$ factor. Finally, an overall $k!$ factor leads to the expression for the factorial moment $\langle n(n-1)\cdots(n-k+1)\rangle$.

The lowest-order diagram for the average particle number, consisting in a simple propagator, reads $\langle n\rangle = e^t$. We now understand that this method leads to a more straightfoward computation of the moments of the number of particles than the one based on the computation of the probabilities of successive Fock states, for a single Pomeron already resums an infinity of particle Fock states. The Pomeron in this case is exactly like the BFKL Pomeron introduced in Sec. 2, which leads to an exponential increase of the scattering amplitudes with the rapidity (Eq. (3.27)).

We now move on to the computation of higher-order diagrams in which recombinations are absent. First, let us recover simple results by taking the infinite-N limit. We consider the diagrams in Fig. 3.2, which are the only ones that survive at infinite N in the evaluation of the moment $\langle n(n-1)\cdots(n-k+1)\rangle$. Using the Feynman rules, we get for each individual diagram

$$(-1)^k \times (-1)^k \times e^{kt} \int_0^t dt_1 e^{-t_1} \int_{t_1}^t dt_2 e^{-t_2} \cdots \int_{t_{k-1}}^t dt_k e^{-t_k} = \frac{1}{k!} e^{kt} \left(1 - e^{-t}\right)^{k-1}. \quad (3.29)$$

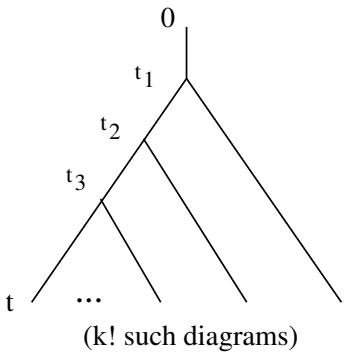

Figure 3.2: Diagrams contributing to the one Pomeron $\to k$-Pomeron transition, which gives the moments $\langle n(n-1)\cdots(n-k+1)\rangle$ at leading order in a $1/N$ expansion.

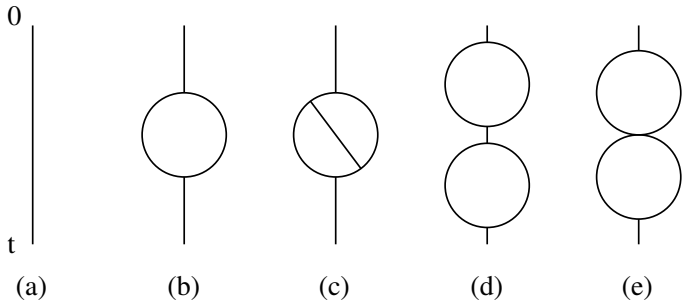

Figure 3.3: Diagrams up to order $1/N^2$ contributing to the average of the number of particles in the system after an evolution over the time interval t.

There are $k!$ such diagrams (corresponding to all possible permutations of the Pomerons), and there is an extra overall $k!$ factor to be added in order to get the relevant factorial moment:

$$\langle n(n-1)\cdots(n-k+1)\rangle = k! e^{kt}\left(1-e^{-t}\right)^{k-1}. \tag{3.30}$$

Next, we would like to perform the computation of the one-Pomeron $\to$ one-Pomeron transition (which provides the value of $\langle n\rangle$) within the full theory, including the recombinations. Some of the lowest-order diagrams are shown in Fig. 3.3. A straightforward application of the Feynman rules edicted above leads to the following results for the graphs that are depicted in Fig. 3.3:

$$\begin{aligned}
\langle n\rangle|_{\text{tree, Fig. 3.3a}} &= e^t \\
\langle n\rangle|_{\text{1 loop, Fig. 3.3b}} &= -2!\frac{e^{2t}}{N}\left(1-e^{-t}(1+t)\right) \\
\langle n\rangle|_{\text{2 loops, Fig. 3.3c}} &= 3!\frac{e^{3t}}{N^2}\left(1+4e^{-t}(1-t)-e^{-2t}(2t+5)\right) \\
\langle n\rangle|_{\text{2 loops, Fig. 3.3d}} &= 4\frac{e^{2t}}{N^2}\left(t-3+e^{-t}\left(\tfrac{t^2}{2}+2t+3\right)\right) \\
\langle n\rangle|_{\text{2 loops, Fig. 3.3e}} &= 4\frac{e^{2t}}{N^2}\left(t-2+e^{-t}\left(t+2\right)\right)
\end{aligned} \tag{3.31}$$

We may classify these different contributions according to their order in e^t/N: We see on the explicit expressions that the leading terms for large t and $e^t/N \sim 1$ are always of the form $N(e^t/N)^{1+\#\text{loops}}$. It turns out that we may compute easily these dominant terms at any number

of loops. They stem from the graphs in which all splittings occur before all recombinations (such as 3.3b and 3.3c). These terms build up a series that reads

$$\langle n \rangle = \sum_{k=1}^{\infty} (-1)^{k-1} k! \frac{e^{kt}}{N^{k-1}}. \tag{3.32}$$

This series is factorially divergent, but is easy to resum with the help of the Borel transformation. Indeed, using the identity

$$k! = \int_0^{+\infty} db\, b^k e^{-b}, \tag{3.33}$$

replacing it in Eq. (3.32), then exchanging the integration over b and the sum over the number of Pomerons k, one gets

$$\langle n \rangle = N^2 e^{-t} \int_0^{+\infty} db \frac{1}{1+\frac{1}{b}} e^{-Ne^{-t}b} = N\left(1 - Ne^{Ne^{-t}}\Gamma(0, Ne^{-t})\right), \tag{3.34}$$

where Γ is the incomplete Gamma function.

This result was obtained for the first time using a diagrammatic method in Ref. [87]. The authors of the latter paper also computed the next-to-leading order, that is to say, the terms of relative order $1/N$ after the resummation has been performed. The equivalent of the diffractive processes known in QCD were also investigated by these very authors in Ref. [88]. More results were obtained on that kind of models by another group in Ref. [89,90], using different techniques, which go beyond the perturbative approach. Remarkably, the latter calculations can be applied to some extent to QCD [91,92].

3.2.3 Stochastic evolution equations

The model may also be formulated in the form of a stochastic evolution equation for the number of particles n_t it contains at each time t. The most straightforward way of doing this would be to first compute the mean and variance of n_{t+dt} given n_t, with the help of the master equation (3.2). This would enable one to write the time evolution of n_t in terms of a drift and of a noise of zero mean and normalized variance, namely:

$$\frac{dn_t}{dt} = n_t - \frac{n_t(n_t-1)}{N} + \sqrt{n_t + \frac{n_t(n_t-1)}{N}}\nu_{t+dt}, \tag{3.35}$$

where ν is such that $\langle \nu_t \rangle = 0$ and $\langle \nu_t \nu_{t'} \rangle = \delta(t-t')$. This equation is similar to Eqs. (2.29) and (2.30), except for it does not have a spatial dimension where some diffusion could take place. The noise term is of order $\sqrt{n}$, as it should according to the argumentation of Chap. 2. Note that the distribution of ν depends on n_t and is not a Gaussian. This last point is easy to understand: The evolution of ν_t is intrinsically discontinuous, since it stems from a rescaling of n_t, which is an integer at all times. A Brownian evolution (i.e. with a Gaussian noise) would necessarily be continuous. For completeness, we write the statistics of ν_{t+dt}, which is deduced from the evolution of n:

$$\nu_{t+dt} = \begin{cases} \frac{1}{\sigma\, dt} - \frac{\Delta}{\sigma} & \text{proba } n_t\, dt \\ -\frac{\Delta}{\sigma} & \text{proba } 1 - n_t\, dt - \frac{n_t(n_t-1)}{N} dt \\ -\frac{1}{\sigma\, dt} - \frac{\Delta}{\sigma} & \text{proba } \frac{n_t(n_t-1)}{N} dt, \end{cases} \tag{3.36}$$

where $\Delta = n_t - \frac{n_t(n_t-1)}{N}$ and $\sigma = \sqrt{n_t + \frac{n_t(n_t-1)}{N}}$. There are jumps, represented by the large terms proportional to $1/dt$.

This formulation is not of great interest, neither for analytical calculations nor for numerical simulations, since it is much easier to just implement the rules that define the model in the first place (Eq. (3.1)) in the form of a Monte Carlo event generator.

There is a better way to arrive at a stochastic evolution equation for this model, although it is a bit more abstract. (It is actually equivalent to the Pomeron field theory formulated before.) Instead of following states with a definite number of particles like above, we may introduce coherent states

$$|z\rangle = e^{-z+za^\dagger}|0\rangle, \tag{3.37}$$

where z is a complex number. For real positive values of z, the state $|z\rangle$ is nothing but a Poissonian state, which is a superposition of $|k\rangle$-particle states, where the weight of each term follows the Poisson law of parameter z. For the simplicity of the argument, let us restrict ourselves to Poissonian states. By applying the Hamiltonian $\mathcal{H}$ (defined in Eq. (3.10)) to a Poissonian state $|z_t\rangle$, one gets a new state $|\phi_{t+dt}\rangle$:

$$|\phi_{t+dt}\rangle = |z_t\rangle - dt\,\mathcal{H}|z_t\rangle. \tag{3.38}$$

Of course, that new state is not itself a Poissonian state in general, but may be written as a superposition of such states. One writes

$$|\phi_{t+dt}\rangle = \int dz\, f(z)|z\rangle = \int dz\, f(z) \sum_n e^{-z}\frac{z^n}{n!}|n\rangle. \tag{3.39}$$

The idea is to interpret the weight function $f(z)$ as the probability to observe a given Poissonian state $|z\rangle$. Hence the evolution is viewed as a stochastic path

$$\cdots \to z_{t-dt} \to z_t \to z_{t+dt} \to z_{t+2dt} \to \cdots \tag{3.40}$$

with well-defined transition rates from one Poissonian state to the next one. Inserting the explicit expression for the Hamiltonian (3.10) and the decomposition (3.39) in Eq. (3.38), one gets for each Fock state $|n\rangle$

$$\int dz\, e^{-z} f(z)\frac{z^n}{n!} = e^{-z_t}\frac{z_t^n}{n!} - dt\, e^{-z_t}\left[\frac{z_t^n}{(n-1)!} - \frac{z_t^{n-1}}{(n-2)!} - \frac{1}{N}\left(\frac{z_t^{n+1}}{(n-1)!} - \frac{z_t^n}{(n-2)!}\right)\right]. \tag{3.41}$$

Finally, this equation can be inverted for $f(z)$ by a weighted integration over n, $\int \frac{dn}{2i\pi} z_{t+dt}^{-n-1}$, along an appropriate contour in the complex plane. After some straightforward algebra, we get

$$f(z_{t+dt}) = \delta(z_{t+dt} - z_t) + dt\left(z_t - \frac{z_t^2}{N}\right)\delta'(z_{t+dt} - z_t) + \frac{1}{2}\left[2dt\left(z_t - \frac{z_t^2}{N}\right)\delta''(z_{t+dt} - z_t)\right]. \tag{3.42}$$

This is a representation for the Gaussian law centered at $z_t + dt(z_t - \frac{z_t^2}{N})$ of variance $2dt(z_t - \frac{z_t^2}{N})$. Introducing a normal Gaussian noise ν_t which satisfies

$$\langle \nu_t \rangle = 0 \quad \text{and} \quad \langle \nu_t \nu_{t'} \rangle = \delta(t - t'), \tag{3.43}$$

we may write

$$\frac{dz_t}{dt} = z_t - \frac{z_t^2}{N} + \sqrt{2\left(z_t - \frac{z_t^2}{N}\right)}\nu_{t+dt} \tag{3.44}$$

where one must be careful to take the noise at time $t + dt$, and hence, this equation is to be interpreted in the Ito sense. If $z_{t=0}$ is a real number between 0 and N, then the equation keeps it in this range. But of course the equation is valid for more general coherent states, with complex z_t.

This equation is suitable for numerical simulations: One may discretize the time in small steps $\Delta t \ll 1$ in which case ν_t is distributed as

$$p(\nu_t) = \frac{1}{\sqrt{2\pi\Delta t}} \exp\left(-\frac{\nu_t^2}{2\Delta t}\right). \tag{3.45}$$

(In many cases, one has to use more sophisticated methods, see e.g. Ref. [93]; A more rigorous and general derivation of this stochastic formulation may be obtained from a path integral formalism starting from the Hamiltonian (3.10), see Ref. [85]). Analytical manipulations of this equation using Ito's calculus are also quite easy. We are going to give an example of such a calculation below, avoiding unnecessary formalism. (We refer again the reader to [93] for a textbook on a more mathematical handling of stochastic equations).

We may transform the stochastic equation (3.44) to a hierarchy of equations for the factorial moments of the number of particles, using the relation

$$\langle z_t^k \rangle = \langle n(n-1)\cdots(n-k+1)\rangle \equiv n^{(k)}. \tag{3.46}$$

First, let us write Eq. (3.44) in a discretized form:

$$z_{t+dt} = z_t + dt\left(z_t - \frac{z_t^2}{N}\right) + dt\sqrt{2\left(z_t - \frac{z_t^2}{N}\right)}\nu_{t+dt}. \tag{3.47}$$

We then take the k-th power of the left and the right-hand side, and we average the result over realizations. Expanding in powers of dt for small dt, we get

$$\begin{aligned}\left\langle z_{t+dt}^k \right\rangle = \langle z_t^k\rangle + dt\, k\left\langle z_t^k - \frac{z_t^{k+1}}{N}\right\rangle + dt\, k\left\langle z_t^{k-1}\sqrt{2\left(z_t - \frac{z_t^2}{N}\right)}\right\rangle \langle \nu_{t+dt}\rangle \\ + dt^2\,\frac{k(k-1)}{2}\left\langle 2\left(z_t^{k-1} - \frac{z_t^k}{N}\right)\right\rangle \langle \nu_{t+dt}^2\rangle + \cdots\end{aligned} \tag{3.48}$$

We have factorized the averages over the time intervals $[t, t+dt]$ and $[0,t]$, since the noise ν is uncorrelated in time. The term proportional to dt vanishes thanks to the fact that ν_{t+dt} averages to zero. One may think that the next term could be neglected for it is apparently proportional to dt^2. Actually, it gives a contribution of order dt, because for discretized t, $\langle \nu_{t+dt}^2\rangle = 1/dt$. The dots stand for terms of order dt^2 at least. Using Eq. (3.46) to identify the factorial moments of n, we eventually get

$$\frac{dn^{(k)}}{dt} = k\left(n^{(k)} - \frac{n^{(k+1)}}{N}\right) + k(k-1)\left(n^{(k-1)} - \frac{n^{(k)}}{N}\right) \tag{3.49}$$

This equation is similar to the (modified) Balitsky hierarchy in high-energy QCD. Indeed, let us write explicitly the equations for the first two moments:

$$\begin{aligned}\frac{d\langle n\rangle}{dt} &= \langle n\rangle - \frac{1}{N}\langle n(n-1)\rangle, \\ \frac{d\langle n(n-1)\rangle}{dt} &= 2\left(1-\frac{1}{N}\right)\langle n(n-1)\rangle - \frac{2}{N}\langle n(n-1)(n-2)\rangle + 2\langle n\rangle.\end{aligned} \tag{3.50}$$

We note the similarity in structure with Eqs. (2.9), (2.12), except for the term $2\langle n\rangle$ in the right-hand side of the second equation. This term stems precisely from the particle recombinations, and was absent in the B-JIMWLK/BK formalism.

3.3 Statistical methods

The field theory methods presented above provide a systematics to solve the evolution of the system to arbitrary orders in $1/N$, at least theoretically. (In practice, identifying and resumming the relevant diagrams becomes increasingly difficult). However, it would look quite unreasonable to get into such an involved formalism if one were only interested in computing the lowest order in a large-N expansion. Indeed, as we shall demonstrate it below, in the case of this simple model, an intuitive and economical calculation leads to the right answer [94]. We work it out here because

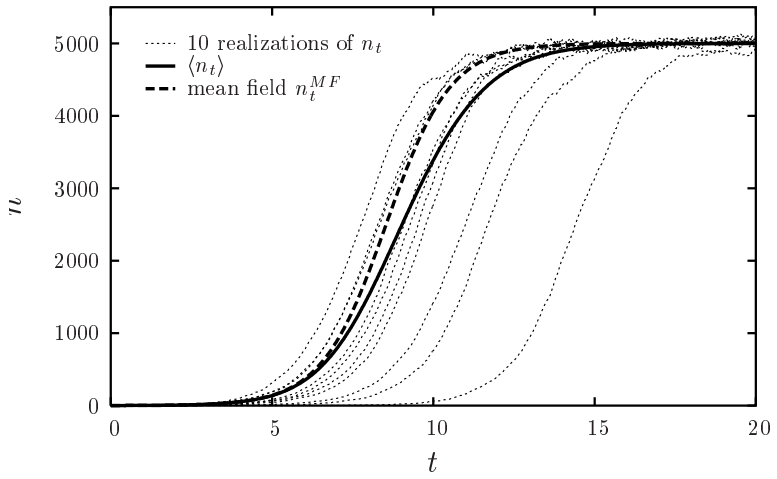

Figure 3.4: [From Ref. [94]] Ten different realizations of the stochastic evolution of the zero-dimensional model (dotted lines; $N = 5 \times 10^3$). All realizations look the same, up to a shift in time. They are all parallel to the solution to the mean-field equation (3.52) (dashed line). Note the significant difference between the latter and the average of the particle number over the realizations (full line).

this line of reasoning is at the basis of the solution of more complicated models, closer to QCD, that we shall address in the next chapter (Chap. 4).

As before, we denote by n_t the value of the number of particles in a given realization of the system. We further introduce $p_{\bar{n}}(\bar{t})$ the distribution of the times at which the number of particles in the system reaches some given value $\bar{n}$ for the first time, and $\langle n_t | n_{\bar{t}} \rangle$ the conditional average number of particles at time t given that there were $n_{\bar{t}}$ particles in the system at time $\bar{t}$. One may write the following factorization formula:

$$\langle n_t \rangle = \int_0^\infty d\bar{t} p_{\bar{n}}(\bar{t}) \langle n_t | n_{\bar{t}} \rangle. \tag{3.51}$$

This formula holds exactly for any value of $\bar{n}$. In particular, if N is large enough, one may choose $\bar{n}$ such that $1 \ll \bar{n} \ll N$.

Observing at a few realizations generated numerically (Fig. 3.4), one sees that the curves that represent n_t look like the solution to the mean-field equation obtained by neglecting the noise term in Eq. (3.35), up to a translation of the origin of times by some random t_0. (The curves look also slightly noisy around the average trend, but the noise would still be much weaker for larger values of N.) This suggests that once there are enough particles in the system (for $n_t > \bar{n} \gg 1$), the evolution becomes essentially deterministic and in that stage of the evolution, the noise can safely be discarded. Thus stochasticity only manifests itself in the initial stages of the evolution, but in a crucial way. Indeed, as one can see in Fig. 3.4, after averaging, $\langle n_t \rangle$ differs significantly from the mean-field result, and this difference stems from rare realizations in which the particle number stays low for a long time. Therefore, in individual realizations, stochasticity should be accurately taken into account as long as $n_t < \bar{n}$. Fortunately, when the number of particles in the system is small compared to the parameter N that fixes the typical maximum number of particles in a realization, the stochastic evolution is essentially governed by a linear equation.

Thanks to this discussion, we may assume that the evolution is linear as long as there are less than $\bar{n}$ particles in the system and deterministic when $n_t > \bar{n}$. It is then enough to compute $p_{\bar{n}}(\bar{t})$ for an evolution without recombinations, and $\langle n_t | n_{\bar{t}} \rangle$ for an evolution without noise. The second quantity is most easily computed by replacing the averages of powers of n_t in Eq. (3.3) by n_t^{MF}

and discarding the term of order $1/N$. One gets a closed equation for n_t^{MF} in the form

$$\frac{dn_t^{\mathrm{MF}}}{dt} = n_t^{\mathrm{MF}} - \frac{(n_t^{\mathrm{MF}})^2}{N} \tag{3.52}$$

which is solved by

$$n_{t-\bar{t}|\bar{n}}^{\mathrm{MF}} = \frac{N}{1+\frac{N}{\bar{n}}e^{-(t-\bar{t})}} \tag{3.53}$$

where the initial condition has been chosen in such a way that $n_0 = \bar{n}$.

As for the distribution $p_{\bar{n}}(\bar{t})$ for the waiting times $\bar{t}$ to observe $\bar{n}$ particles in the system, its derivation is a bit more subtle.

Let us introduce $R(n,t)$ the probability distribution of the first passage time at the given population size $\bar{n}$, starting with n individuals at time 0. The probability $p_{\bar{n}}(\bar{t})$ we are looking for is nothing but $R(1,\bar{t})$.

We now establish an evolution equation for R. Recall that the evolution equation for P was obtained by considering the variation in the number of particles in the system between times t and $t+dt$. Here we consider the beginning of the time evolution, between times 0 and dt. The probability that the system has $\bar{n}$ particles for the first time at $t+dt$ starting with n particles at time 0, $R(n,t+dt)$, is the probability ndt that the system gains a particle between times 0 and dt multiplied by $R(n+1,t)$, minus a unitarity-preserving term. In this way, after having taken the limit $dt \to 0$, we get

$$\frac{\partial R(n,t)}{\partial t} = n\left(R(n+1,t) - R(n,t)\right), \text{ with the condition } R(\bar{n},t) = \delta(t). \tag{3.54}$$

This equation is valid when we neglect recombination processes, which is the relevant approximation here since we stick to the dilute regime. In order to find a solution, we introduce the generating function for the moments of n:

$$G(u,t) = \sum_{n=0}^{\infty} u^n R(n,t) \tag{3.55}$$

and the Laplace transform

$$\tilde{G}(u,s) = \int_0^{+\infty} dt\, e^{-st} G(u,t). \tag{3.56}$$

The evolution of R implies the following equation for $\tilde{G}$:

$$(1-u)\frac{d\tilde{G}}{du} = \left(s + \frac{1}{u}\right)\tilde{G}. \tag{3.57}$$

This equation is straightforward to integrate. Its solution reads

$$\tilde{G}(u,s) = Cu(1-u)^{-1-s}. \tag{3.58}$$

The constant C must be determined from the initial condition, namely from the equation $R(\bar{n},t) = \delta(t)$, which after Laplace transform reads $\tilde{R}(\bar{n},s) = 1$. The latter means that the $\bar{n}$-th order in the expansion of $\tilde{G}$ in powers of u should be set to one, which writes

$$C\frac{\Gamma(s+\bar{n})}{\Gamma(s+1)\Gamma(\bar{n})} = 1. \tag{3.59}$$

For large $\bar{n}$, the Stirling formula enables one to cast the equation in the simplified form $C = \Gamma(s+1)\bar{n}^{-s}$. We then see that $\tilde{R}(1,s) = \Gamma(1+s)\bar{n}^{-s}$. The inverse Laplace transform of this function is just the Gumbel distribution:

$$R(1,\bar{t}) = p_{\bar{n}}(\bar{t}) = \bar{n}e^{-\bar{t}-\bar{n}e^{-\bar{t}}}. \tag{3.60}$$

Plugging Eqs. (3.60) and (3.53) into Eq. (3.51), we get for the average number of particles after t time units of evolution:

$$\langle n_t \rangle = N \int_0^\infty d\bar{t} \frac{\bar{n} e^{-\bar{t}-\bar{n}e^{-\bar{t}}}}{1+\frac{N}{\bar{n}}e^{-(t-\bar{t})}}. \tag{3.61}$$

Because the Gumbel distribution is strongly damped for $\bar{t} < 0$, the lower integration boundary may safely be extended to $-\infty$. Indeed, it is easy to see that a conservative upper bound for the contribution of the domain $]-\infty, 0]$ to the integral is $e^{-\bar{n}}$, which is very small in the limit $\bar{n} \gg 1$. Finally, we perform the change of variable $b = \bar{n}e^{t-\bar{t}}/N$ to arrive at the form

$$\langle n_t \rangle = N^2 e^{-t} \int_0^\infty db \frac{1}{1+\frac{1}{b}} e^{-Ne^{-t}b}. \tag{3.62}$$

It can be checked that it is exactly the form found through the diagrammatic approach to Pomeron field theory (compare Eq. (3.62) to Eq. (3.34)).

The factorization in Eq. (3.51) and the convenient approximations that it subsequently allows are actually very important. Indeed, we realized that we may write the average number of particles at time t, whose expression would *a priori* be given by the solution of a *nonlinear stochastic differential equation*, by solving two much simpler problems. The key observation was the following. When the number of particles in the system is low compared to the maximum average number of particles N allowed by the reaction process, then the nonlinearity is not important, but the noise term is instead crucial. On the other hand, when the number of particles is large compared to 1, then the noise may be discarded, but the nonlinearity of the evolution equation, which corresponds to recombinations of particles, must be treated accurately. From this method, one gets an expression for $\langle n_t \rangle$ for any time up to relative corrections of order $1/N$.

When we address the problem of reaction-diffusion with one spatial dimension, we will rely on the very same observation. It is essentially the latter which will enable us to find analytical results also in that case.

3.4 Relation to high energy scattering and the parton model approach

So far, we have focussed on the factorial moments of the number n of particles in the system. We have seen how they may be computed from "Pomeron" diagrams, which are quite similar to the diagrams that appear in effective formulations of high-energy QCD. However, the relation to scattering amplitudes, which are the observables in QCD, may not be clear to the reader at this stage. In particular, we do not understand yet what would correspond to boost invariance of the QCD amplitudes. The aim of this section is to try and clarify these points.

Let us consider a realization of the system of particles, evolved up to time t, that we may call the projectile. A convenient formalism to compute the weights of Fock states was presented in Sec. 3.2.1. At time t, the system of particles scatters off a target consisting of a single particle, and can have at most one exchange with the target, which "costs" a factor $1/N$. All the particles in the system have an equal probability to scatter. Hence the probability that the system scatters reads $T = n_t/N$.

This way of viewing the evolution of the system makes it obviously very similar to the QCD dipole model introduced in Chap. 2, provided one identifies the number of particles to the number of dipoles and the time to the rapidity variable. The average of T over realizations is the elastic scattering amplitude.

From this analogy, there is a property similar to boost invariance that should hold. Instead of putting all the evolution in the projectile, we may share it between the projectile and the target. Let us call $n_{t'}$ the number of particles in the projectile at the time of the interaction, and $m_{t-t'}$ the number of particles in the target. The total evolution time is the same as before. To establish the expression for T in this frame, it is easier to work with the probability $S = 1 - T$ that there

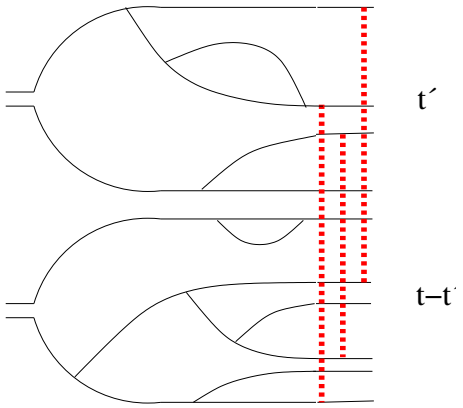

Figure 3.5: Representation of the scattering of two systems of particles. The systems evolve in time from the left to the right. The horizontal lines represent the particles, and the vertical dashed lines the interactions between the systems. Each of the elementary scatterings comes with a power of $1/N$. Note the strong similarity with the QCD diagram in Fig. 2.6a, except that in the present case, recombinations are included in the evolution of each of the systems.

is no interaction. If any number of interactions were allowed between each pair of particles from the projectile and the target, then one would simply write $S = \exp(-n_{t'} m_{t-t'}/N)$. But since the number of scatterings should be limited to one per particle, one has to decrease n and m for each new power of $1/N$, i.e. for each additional rescattering:

$$S = 1 - \frac{1}{N} nm + \frac{1}{2!}\frac{1}{N^2}[n(n-1)][m(m-1)] - \frac{1}{3!}\frac{1}{N^3}[n(n-1)(n-2)][m(m-1)(m-2)]\cdots \tag{3.63}$$

where the time dependences are understood, in order to help the reading. This is like a "normal ordering" of the expression to which we would arrive by assuming any number of exchanges. Note that S is not necessarily positive in a given event, and hence looses its probabilistic interpretation once one has performed the normal ordering.

Taking the average over realizations, one gets

$$\langle S \rangle = \sum_{k=0}^{\infty} \left\langle \frac{n!}{(n-k)!} \right\rangle_{t'} \left\langle \frac{m!}{(m-k)!} \right\rangle_{t-t'} \frac{(-1)^k}{k! N^k}. \tag{3.64}$$

Let us analyze this expression.

First, if $t' = t - t'$ ("center-of-mass frame"), the first two factors in each term of the series are of course identical after averaging. The sum runs over the number of actual exchanges between the probe and the target. A realization of the evolution, which would correspond to an event in QCD, is represented in Fig. 3.5. Note that the figure is very similar to Fig. 2.6a, except that particle mergings are allowed, while they have not been properly formulated in QCD yet.

Second, this expression should be independent of t'. It is not difficult to check that this is indeed true by taking the derivative of $\langle S \rangle$ with respect to t'. Expressing the averages of the factorial moments of the number of particles with the help of the probability distributions $P(n, t')$ and $P(m, t - t')$ respectively, each term of the sum over k and m, n reads

$$\left.\frac{d\langle S \rangle}{dt'}\right|_{n,m,k \text{ fixed}} = (\dot{P}_n P_m - P_n \dot{P}_m) \frac{n!}{(n-k)!} \frac{m!}{(m-k)!} \frac{(-1)^k}{k! N^k}. \tag{3.65}$$

The time dependence is again implicit, and we introduced the notation $P_n = P(n, \cdot)$ and $\dot{P}_n = \partial_t P(n, \cdot)$ to get a more compact expression. The time variabe that should be used for each factor

is unambiguous since it is in one-to-one correspondence with the particle number index. We may use the master equation (3.2) to express the time derivatives:

$$\dot{P}_n P_m - P_n \dot{P}_m = \left[(n-1)P_{n-1} + \frac{n(n+1)}{N} P_{n+1} - \left(n + \frac{n(n-1)}{N} \right) P_n \right] P_m - [n \leftrightarrow m]. \quad (3.66)$$

Recalling that there are sums over m, n and k which go from 0 to ∞, one may shift first the indices m and n in order to factorize $P_n P_m$ in each term. The factors $1/N$ may then be absorbed by shifting k for the relevant terms. Then cancellations occur between the terms of both squared brackets in such a way that once the summations over n, m and k have been performed, the global result is 0. This proves the independence of $\langle S \rangle$ upon t', that is, "boost invariance" in a quantum field theory language.

We have seen that we may formulate scattering amplitudes in the zero-dimensional toy model, exactly in the same way as in QCD. We have seen in particular how crucial it is to include particle mergings consistently with the form of the interaction between the states of the projectile and of the target at the time of the interaction, in order to get a boost-invariant amplitude.

3.5 Alternative models in zero dimension

For the sake of completeness, we shall now construct some variants of the zero-dimensional model introduced above, since the latter were also discussed in the literature. We review two of the most popular models.

3.5.1 Allowing for multiple scatterings between pairs of particles

Instead of assuming that there is at most one single exchange between each pairs of partons, one may allow for any number of exchanges. Then the definition of S is modified as follows:

$$\langle S \rangle = \left\langle e^{-\frac{nm}{N}} \right\rangle = \sum_{n,m \geq 1} P(n,t') P(m, t-t') e^{-\frac{mn}{N}}. \quad (3.67)$$

One sees immediately that if the probabilities P satisfy the master equation (3.2), then this expression cannot be boost-invariant (i.e. independent of t'). Indeed, if Eq. (3.2) holds, then

$$P(n, t \to \infty) = \delta_{n,N} \text{ and } P(n, t=0) = \delta_{n,1}. \quad (3.68)$$

It follows that in the frame in which the projectile is at rest,

$$\langle S \rangle_{t'=0, t \to \infty} = e^{-1} \quad (3.69)$$

while in the center-of-mass frame (if the projectile and the target share an equal fraction of the evolution),

$$\langle S \rangle_{t'=\frac{t}{2}, t \to \infty} = e^{-N} \quad (3.70)$$

which is very different. Actually, in this model, the average number of particles cannot saturate at a fixed value N. It would not be compatible with boost invariance.

In order to preserve boost-invariance, one has to modify the master equation. We may write the following general equation for the evolution of the probability:

$$\dot{P}_n = \sum_{k \neq 0} (\alpha_{n-k}^k P_{n-k} - \alpha_n^k P_n). \quad (3.71)$$

The coefficients α_n^k are the transition rates from a $(n-k)$-particle state to a n-particle state. We determine the α_n^k from the boost-invariance requirement. Actually, only the coefficient $\alpha_n^{k=1}$ is needed in the case of this model.

Using the same method as the one employed for checking the boost invariance in the previous model, we write

$$\frac{d\langle S\rangle}{dt'} = \sum_{n,m} (\dot{P}_n P_m - P_n \dot{P}_m) \left\langle e^{-\frac{mn}{N}} \right\rangle , \tag{3.72}$$

and express $\dot{P}_n, \dot{P}_m$ with the help of the master equation. Requiring that the sum over n and m in the right-hand side cancels leads to the rates

$$\alpha_n^1 = N \left(1 - e^{-n/N}\right), \tag{3.73}$$

where the overall constant is determined from the rate in the unsaturated version of the model, which should hold for small values of $n \ll N$. This model was first proposed by Mueller and Salam [53].

We see that the saturation mechanism is quite different than in the previous model. Indeed, the average number of particles in the system keeps growing, but at a rate that slows down and depends on the number of particles in the system itself. Unitarity of the scattering probability T is ensured first by multiple scatterings rather than by the saturation of the number of particles to a constant number N (up to fluctuations).

This model was studied in detail in Ref. [95]. The conclusions drawn in there is that the saturation mechanism implied by the above model is likely to be quite close to the one at work in QCD. We could get analytical results for this model using one of the methods presented above. In particular, the statistical method outlined in Sec. 3.3 would apply and lead in a straightforward way to the expression for $\langle n\rangle$, up to corrections of relative order $1/N$.

3.5.2 Reggeon field theory

Starting from the field theory formulation in Sec. 3.2.2, we may discard the 4-Pomeron vertex (term $(b^\dagger)^2 b^2/N$ in Eq. (3.22)). The new Hamiltonian then reads

$$\mathcal{H}^{RFT} = -b^\dagger b - (b^\dagger)^2 b + \frac{1}{N} b^\dagger b^2. \tag{3.74}$$

The stochastic formulation reads

$$\frac{dz}{dt} = z - \frac{z^2}{N} + \sqrt{2z}\,\nu_{t+dt} \tag{3.75}$$

(Compare to Eq. (3.44)). This is the zero-dimensional version of the stochastic equation defining the so-called Reggeon field theory, which was intensely studied in the 70's as a pre-QCD model for hadronic interactions.

This model has peculiar properties if one insists on interpreting it as a particle model. Indeed, the Hamiltonian (3.74) corresponds to a generating function for the factorial moments of the number n of particles in the system at a given time t that satisfies

$$\frac{\partial Z(z,t)}{\partial t} = z(1+z)\frac{\partial Z(z,t)}{\partial z} - \frac{z}{N}\frac{\partial^2 Z(z,t)}{\partial z^2} \tag{3.76}$$

and the corresponding master equation, obeyed by the probability $P(n,t)$ to find n particles in the system at time t, writes

$$\begin{aligned}\frac{\partial P(n,t)}{\partial t} = &-nP(n,t) + (n-1)P(n-1,t) \\ &+ \frac{1}{N}(n+1)(n+2)P(n+2,t) - \frac{1}{N}n(n+1)P(n+1,t).\end{aligned} \tag{3.77}$$

One can read off this equation the rates for particle creation/disappearance. One has a $1 \to 2$ splitting, with rate dt; a $2 \to 0$ annihilation with rate dt/N; and a $2 \to 1$ recombination with rate

$-dt/N$. This is a negative number, and of course, it is unacceptable for a physical probability not to take its values between 0 and 1. But we should not reject *a priori* negative probabilities as a formal calculation tool [96], as long as the physical probabilities are well-defined. However, a Monte-Carlo code based on these negative rates turns out to be extremely unstable, and thus of no practical use.[1]

Note that the statistical approach teaches us that in the large $N \gg 1$ limit, the moments of the number of particles in the system should not be very different than for the model with 3 and 4-Pomeron vertices, since it is essentially the form of the fluctuations in the dilute regime which determines the moments at all times.

A detailed study of the special properties of this model as well as a comparison with reaction-diffusion-like models may be found in Ref. [97].

[1] We thank Al Mueller and Bo-Wen Xiao for interesting discussions on this topic, and Krzysztof Golec-Biernat for having brought Ref. [96] to our attention.

Chapter 4

General results on stochastic traveling-wave equations

In chapter 2, we have shown the relevance of the stochastic FKPP equation for high-energy QCD. The latter represents (classical) particle models that undergo a branching-diffusion process in one dimension, supplemented by a saturation mechanism. Chapter 3 was dedicated to a detailed study, from different points of view, of simplified models obtained from the former ones by switching off diffusion. We now go back to the study of one-dimensional models. We proceed by steps: First, we shall address the deterministic FKPP equation (which is equivalent to the BK equation in QCD) (Sec. 4.1). Second, we shall introduce fluctuations to get solutions for equations in the universality class of the sFKPP equation (Sec. 4.2 and 4.3).

Contents

4.1 Deterministic case: the FKPP equation

We address the simplest reaction-diffusion equation, namely the FKPP equation

$$\partial_t u = \partial_x^2 u + u - u^2. \tag{4.1}$$

This equation was found to describe scattering in QCD under some assumptions, see Chap. 2.

It is a mathematical theorem [98] that this equation admits *traveling waves* as solutions, that is to say, solitonic-like solutions such that

$$u(t,x) = u(x - vt) \tag{4.2}$$

where v is the velocity of the wave. u is a front that smoothly connects 1 (for $x \to -\infty$) to 0 (for $x \to +\infty$). The velocities of the traveling waves and their shapes for large x are also known mathematically. Starting with some given initial condition which itself is not necessarily a traveling

wave such as Eq. (4.2) (but which satisfies some conditions, see below), the FKPP equation turns it into a stationary wave front at large times, namely a function which may be written in the form (4.2). The front velocity during this phase may also be predicted asymptotically. We informally review these results in this section.

4.1.1 General analysis and wave velocity

The FKPP equation (4.1) encodes a diffusion in space (through the term $\partial_x^2 u$ in the right-hand side), a growth (term u), and a saturation of this growth (term $-u^2$). It admits two fixed-points: the constant functions $u(t,x) = 0$ and $u(t,x) = 1$. A linear stability analysis shows that 0 is unstable, while 1 is stable. Indeed, thanks to the growth term u in the right-hand side, a small perturbation $u(t,x) = \varepsilon \ll 1$ grows exponentially with time. On the other hand, a perturbation near 1 of the form $u(t,x) = 1 - \varepsilon$ goes back to the fixed point 1 through evolution. Hence the FKPP equation describes the transition from an unstable to a stable state. Therefore, we expect that the linear part of the equation drives the motion of the traveling wave, since the role of the nonlinear term is just to stabilize the fixed point $u = 1$.

We shall cast the linear part of the equation into a more general form:

$$\partial_t u(t,x) = \omega(-\partial_x) u(t,x), \tag{4.3}$$

where $\omega(-\partial_x)$ is a branching diffusion kernel. It may be an integral or differential operator. An appropriate kernel is, in practice, an operator such that the "phase velocity" $v_\phi(\gamma) = \omega(\gamma)/\gamma$ (see below) has a minimum in its domain of analyticity. The FKPP equation is obtained from the choice $\omega(-\partial_x) = \partial_x^2 + 1$.

Let us follow the wave front in the vicinity of a specific value of u. To this aim, we define a new coordinate x_{WF} such that

$$x = x_{\mathrm{WF}} + vt. \tag{4.4}$$

The solution of the linearized equation (4.3) writes most generally

$$u(t,x) = \int_{\mathcal{C}} \frac{d\gamma}{2i\pi} u_0(\gamma) \exp\left[-\gamma(x_{\mathrm{WF}} + vt) + \omega(\gamma)t\right], \tag{4.5}$$

where $\omega(\gamma)$ is the Mellin transform of the linear kernel $\omega(-\partial_x)$ (and thus γ corresponds to $-\partial_x$), and defines the dispersion relation of the linearized equation. $u_0(\gamma)$ is the Mellin transform of the initial condition $u(t = 0, x)$. Let us assume for definiteness that the initial condition is a function smoothly connecting 1 at $x = -\infty$ to 0 at $x = +\infty$, with asymptotic decay of the form $u(t = 0, x) \sim e^{-\gamma_0 x}$. Then $u_0(\gamma)$ has singularities on the real negative axis, and on the positive axis starting from $\gamma = \gamma_0$ and extending towards $+\infty$. Let us take a concrete example: If $u(0, x \leq 0) = 1$ and $u(0, x > 0) = e^{-\gamma_0 x}$, then $u_0(\gamma) = 1/\gamma + 1/(\gamma_0 - \gamma)$. The integration contour $\mathcal{C}$ should go parallel to the imaginary axis in the complex γ-plane and cross the interval $[0, \gamma_0]$.

Each partial wave of wave number γ has a phase velocity

$$v_\phi(\gamma) = \frac{\omega(\gamma)}{\gamma}, \tag{4.6}$$

whose expression is found by imposing that the exponential factor in the integrand of Eq. (4.5) be time-independent when the velocity v of the frame is set to $v = v_\phi(\gamma)$.

We are interested in the large-time behavior of $u(t,x)$. The integrand in Eq. (4.5) admits a saddle point at a value γ_c of the integration variable such that

$$\omega'(\gamma_c) = v, \tag{4.7}$$

that is to say, when v coincides with the group velocity of the wave packet. But the large-time solution is not necessarily given by the saddle point: This depends on the initial condition $u_0(\gamma)$.

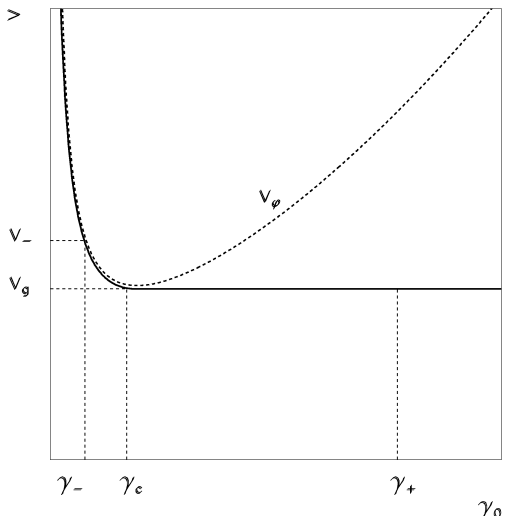

Figure 4.1: Front velocity as a function of its asymptotic decay rate γ_0 (dashed curve). It has a minimum at $\gamma = \gamma_c$. The full line represents the actual velocity that would be selected starting with an initial condition decaying as $e^{-\gamma_0 x}$ for large x. If $\gamma_0 = \gamma_- < \gamma_c$ (initial condition less steep than γ_c), then the asymptotic velocity is the phase velocity of a front which has the same asymptotics as the initial condition. For any $\gamma_0 = \gamma_+ > \gamma_c$, the velocity of the front is the minimum of the phase velocity $v_\phi(\gamma)$.

In order to understand this point, let us work out in detail the simple example of initial condition quoted above. The integral has two contributions for large t:

$$u(t,x) = e^{-\gamma_0(x_{\rm WF}+vt)+\omega(\gamma_0)t} + \kappa e^{-\gamma_c(x_{\rm WF}+vt)+\omega(\gamma_c)t}, \tag{4.8}$$

up to a relative $\mathcal{O}(1)$ factor κ. The time invariance of $u(t,x)$ in the frame of the wave may only be achieved by tuning v to one of the following two values:

$$(i)\ \ v_0 = \frac{\omega(\gamma_0)}{\gamma_0}, \quad (ii)\ \ v_c = \frac{\omega(\gamma_c)}{\gamma_c} = \omega'(\gamma_c). \tag{4.9}$$

In the second case, v coincides with the minimum of the phase velocity $\omega(\gamma)/\gamma$ and in particular, $v_c \leq v_0$. The relevant value of v depends on the shape of the initial condition:

- If $\gamma_0 < \gamma_c$, i.e. the decay of the initial condition is less steep than the decay of the wave from the saddle-point, then one has to pick the first choice *(i)* for the velocity. Indeed, this is the only one for which the first term in Eq. (4.8) is time-independent, and the second term vanishes at large time. Due to the fact that $v_c < v_0$, choice *(ii)* would make the first term in Eq. (4.8) blow up exponentially, $u \sim e^{\gamma_0(v_0-v_c)t}$.

- If instead $\gamma_0 > \gamma_c$, then it is the second choice *(ii)* that has to be made. The saddle point dominates, and the wave velocity at large time is independent of the initial condition.

Figure 4.1 summarizes these two cases.

The limiting case $\gamma_0 = \gamma_c$ requires a special treatment. Since it is not relevant for the physics of QCD traveling waves, we refer the interested reader to the review paper of Ref. [72] for a complete treatment also of that case.

There exists a rigorous mathematical proof of these solutions in the case of the straight FKPP equation [98]. These results are largely confirmed in numerical simulations for various other

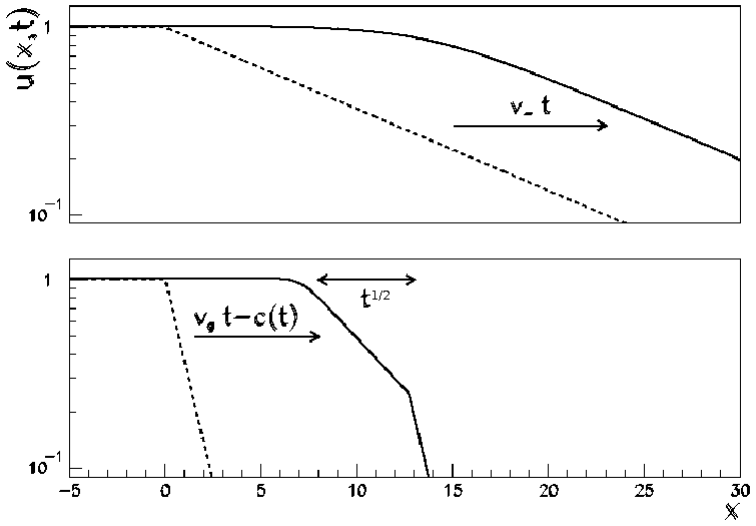

Figure 4.2: Sketch of the shape of the front according to the large-x behavior of the initial condition $u(t=0,x) \sim e^{-\gamma_0 x}$. *Top:* $\gamma_0 < \gamma_c$. The asymptotic shape of the initial condition is conserved. The relaxation of the front is fast. *Bottom:* $\gamma_0 > \gamma_c$. The asymptotic shape of the front is $e^{-\gamma_c x}$, and the velocity for $t = \infty$ is $v_c = \omega(\gamma_c)/\gamma_c$. The asymptotic shape is reached over a distance $\sqrt{t}$ ahead of the front, and the velocity at finite time is less than the asymptotic velocity by $\frac{3}{2\gamma_c t}$.

branching diffusion kernels, including the ones of interest for QCD (see e.g. [74, 99], and Ref. [34, 100, 101] for earlier simulations of the BK equation).

Actually, in QCD as well as in many problems in statistical physics, the initial condition is localized or has a finite support, and hence, its large-x decay is always very steep. Thus for the physical processes of interest in this review, the asymptotic front velocity, that we shall denote by V_∞ for reasons that will become clear later, reads

$$V_\infty = v_c = \frac{\omega(\gamma_c)}{\gamma_c} = \omega'(\gamma_c), \tag{4.10}$$

where the last equality defines γ_c as the value of γ for which $v_\phi(\gamma) = \omega(\gamma)/\gamma$ is minimum. Note that in the context of particle physics, this result was already known from the work of Gribov, Levin, Ryskin [14], and was rederived later in the framework of the BK equation [35, 36, 102].

So far, we have discussed the asymptotic velocity of the solutions to the FKPP equation as a function of the initial condition. When the initial condition is steep enough, then the asymptotic front velocity takes a fixed value which is the minimum of $\omega(\gamma)/\gamma$. In the opposite case, the shape of the initial condition is retained (see Fig. 4.2). We wish to know more detailed properties of the wave front, such as its shape and the way its velocity approaches the asymptotic velocity. There are several methods to arrive at this result (which is known from rigorous mathematics, see [98]). At the level of principle, they all rely on a matching between a solution near the fixed point $u = 1$, and a solution of the linearized equation which holds in the tail $u \ll 1$.

4.1.2 Diffusion equation with a boundary and the approach to the asymptotic traveling wave

We now come back to the original FKPP equation (4.1). We have seen that the nonlinearity $-u^2$ has the effect of taming the growth induced by the linear term u, when u gets close to 1. But

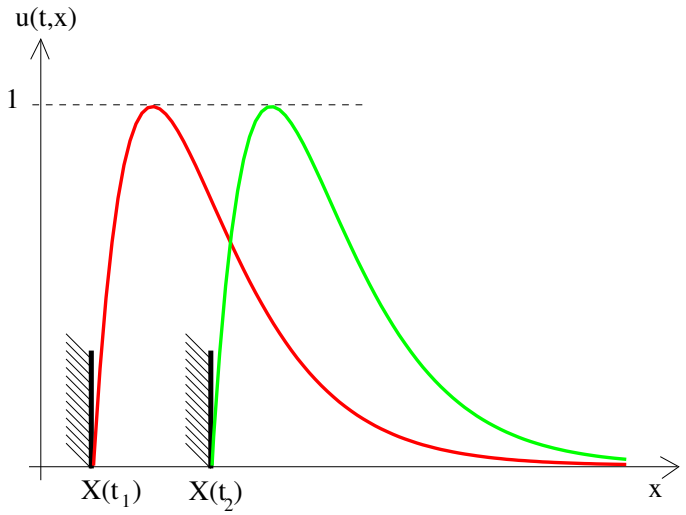

Figure 4.3: Shape of the solution of the branching diffusion equation (4.11) with a moving cutoff, whose position is adjusted in such a way that the maximum of $u(t,x)$ be 1 at all times. The solution is represented at two different times t_1 and t_2, showing the soliton-like behavior of the solution.

nonlinear partial differential equations are very difficult to address mathematically. It may be much simpler to address the linear equation

$$\partial_t u = \partial_x^2 u + u \tag{4.11}$$

supplemented with an absorptive (moving with time) boundary condition that ensures that $u(t,x)$ has a maximum value of 1 at any time. We need to work out the solution of Eq. (4.11) with this kind of boundary condition. Here, we reformulate the approach proposed in the QCD context by Mueller and Triantafyllopoulos [36] (see also Ref. [103] for an account of the next-to-leading order BFKL kernel).

A solution to Eq. (4.11) with the initial condition $u(t=0,x) = \delta(x - x_0)$ is given, for positive times, by

$$u(t,x) = \frac{1}{\sqrt{4\pi t}} \exp\left(t - \frac{(x-x_0)^2}{4t}\right). \tag{4.12}$$

This solution holds if the boundary condition is at spatial infinity.

We note that the lines x of constant $u(t,x) = C$ are given by

$$x = x_0 + 2t - \frac{1}{2}\ln t - \ln(C\sqrt{4\pi}) + \text{terms vanishing for } t \to \infty. \tag{4.13}$$

(We have selected the rightmost front $x > x_0$). This would be the correct expression of the position of the front if it were enough to solve the linearized FKPP equation, to stay around some line of constant amplitude closing an eye on the exponential growth behind the latter line (which would be tamed by the nonlinearity). The asymptotic velocity is 2, which coincides with the critical velocity v_c of the FKPP equation discussed above. It is corrected by a logarithmic term. We will see that the actual solution has the same logarithm except for the coefficient. We will be able to get the solution by setting an appropriate absorptive boundary which will be time dependent. We will proceed by steps, implementing first some fixed boundary condition in order to gain intuition on the form of the solution.

So if instead of the boundary condition at infinity there is an absorptive barrier at say $x = X$, i.e. if $u(t, x = X) = 0$ for any t, then a solution may be found through a linear combination of

the latter solution with different initial conditions, in such a way as the sum vanishes at $x = X$. This is known as the method of images. It is based on the elementary observation that any linear combination of Eq. (4.12) also solves Eq. (4.11). From the solution with initial condition $\delta(x-x_0)$, we subtract the solution of the same equation but with initial condition $\delta(x-(2X-x_0))$, in such a way that this linear combination vanishes for $x = X$, at any time. We get

$$u_X(t,x) = \frac{e^t}{\sqrt{4\pi t}}\left(e^{-\frac{(x-x_0)^2}{4t}} - e^{-\frac{(x-2X+x_0)^2}{4t}}\right). \tag{4.14}$$

At this point, let us already comment that we do not expect the solution to this problem to represent accurately the solution to the full FKPP equation near the boundary $x \sim X$ since in that region, the details of the nonlinearity must matter. So the region of interest will be significantly ahead of the boundary, while the starting point x_0 of the evolution is at some finite distance of the boundary:

$$x - X \gg 1 \quad \text{and} \quad x_0 - X \sim 1. \tag{4.15}$$

One may then expand the two Gaussian terms:

$$u_X(t,x) = \frac{x_0 - X}{\sqrt{4\pi}}\frac{x-X}{t^{3/2}}\exp\left(t - \frac{(x-X)^2}{4t}\right). \tag{4.16}$$

But in this equation, X does not yet depend on time. We cannot implement in a straightforward way a time-dependent absorptive boundary. We may get to such a solution by successive iterations: The main trick is to go to a frame in which the solution of the branching diffusion with a boundary is stationary for large times. We went through the steps of this procedure in Ref. [1]. Here we wish to simply argue the form of the solution from the elements we have learned so far.

As we see in Eq. (4.16), the presence of the boundary at X requires u to vanish linearly at $x \sim X$. We expect this property to be preserved when we promote X to a function of time. Moreover, we know from our earlier investigations that the large-x asymptotic shape is $e^{-(x-X(t))}$. From Eq. (4.16), we see that this shape is reached diffusively; Hence there must be a factor of the form $e^{-(x-X(t))^2/(4t)}$.

Putting everything together, we are lead to the ansatz

$$u(t,x) = Ce^{-X}(x-X(t))e^{-(x-X(t))}\exp\left(-\frac{(x-X(t))^2}{4t}\right), \tag{4.17}$$

where C and X are constants.

We know that the front velocity at large time is $X'(t) \sim v_c = 2$ and we expect a logarithmic correction $c(t) \sim \ln t$, so we write

$$X(t) = 2t - c(t). \tag{4.18}$$

Inserting Eq. (4.17) and (4.18) into Eq. (4.11) and setting $x = X(t) + a$ (a is a constant), we arrive at the equation

$$c'(t)\left[2t(a-1) + a^2\right] = 3a \tag{4.19}$$

which means that for large a and t, $c(t) \sim \frac{3}{2}\ln t$. Hence

$$X(t) \equiv x - x_2 + X = 2t - \frac{3}{2}\ln t + \mathcal{O}(1). \tag{4.20}$$

The latter quantity is the position of the absorptive boundary for large times, and thus also the position of the front. The constant X is the position of the front in the moving frame (while $X(t)$ is its position in the initial reference frame). Setting $X = -1$ and $C = 1$, the maximum of u is reached at $x = X(t) + 1$, and is indeed equal to 1.

For large t or in the region $x - X(t) \leq \sqrt{t}$ which expands with time, the Gaussian factor goes to 1, and we see that $u(t,x)$ only depends on one single variable $x - X(t)$. This was expected: It is precisely the defining property of traveling waves. But in addition to these asymptotic solutions, we get from this calculation the first finite-t correction to the front shape and front velocity.

Actually, the speed of the front is intimately related to its shape. At time t, the front has reached its asymptotic shape over the distance $\sqrt{t}$ from the saturation point. This remark will be important in the following.

We have derived the solution of a problem that was not exactly the initial one, however, we believe that the shape of the front in its forward part ($u \ll 1$, namely for $x - X(t) \gg 1$) as well as its velocity are quite universal. Heuristically, these properties are completely derived from the linear part of the equation. For this reason, the front is said to be "pulled" by its tail. The nonlinearity only tames the growth of u near $u \sim 1$, and so its precise form should not influence the front position itself, at least at large enough times. Thus we expect these solutions to have a broad validity, only depending on the diffusion kernel, and so, may be obtainable from our calculation up to the replacement of the relevant parameters.

For the more general branching diffusion kernel in Eq. (4.3), the velocity of the front would read

$$\frac{dX(t)}{dt} = \frac{\omega(\gamma_c)}{\gamma_c} - \frac{3}{2\gamma_c t} + \cdots \tag{4.21}$$

where γ_c solves $\omega(\gamma_c) = \gamma_c \omega'(\gamma_c)$, as was explained in Sec. 4.1.1. The front shape in its forward part $x - X(t) \gg 1$ is represented by the equation

$$u(t,x) \propto (x - X(t)) e^{-\gamma_c (x - X(t))} \exp\left(-\frac{(x - X(t))^2}{2\omega''(\gamma_c) t} \right), \tag{4.22}$$

up to an overall constant. Fig. 4.3 represents a sketch of the solution at two different times. The large-time shape is an exponential decay,

$$u(t,x) \sim e^{-\gamma_c (x - X(t))} \tag{4.23}$$

up to a linear growth, and from Eq. (4.22), this shape extends over a range

$$L = x - X(t) \sim \sqrt{2\omega''(\gamma_c) t}. \tag{4.24}$$

In other words, the time needed for the front to reach its asymptotic shape over a range L reads

$$t \sim \frac{L^2}{2\omega''(\gamma_c)}. \tag{4.25}$$

Through our simple arguments and calculation, we got the lowest order in an expansion of the front shape and position at large times. The next corrections to $X(t)$ would be of order 1 (this constant depends on the way we define the position of the front), followed by an algebraic series in t whose terms all vanish at large t. The first next-to-leading term in the series has been computed (see Ref. [104]): It turns out to be of order $1/\sqrt{t}$. We will not reproduce the calculations that lead to it because they are rather technical and there is already a comprehensive review paper available on the topic [72]. But let us write the result for the position and the shape of the front at that level of accuracy, for the more general branching diffusion kernel given by Eq. (4.3). To that accuracy, the front position reads [104, 105]

$$X(t) = \frac{\omega(\gamma_c)}{\gamma_c} t - \frac{3}{2\gamma_c} \ln t - \frac{3}{\gamma_c^2} \sqrt{\frac{2\pi}{\omega''(\gamma_c)}} \frac{1}{\sqrt{t}} + \mathcal{O}(1/t). \tag{4.26}$$

For the simple FKPP case, we recall that $\omega(-\partial_x) = \partial_x^2 + 1$, then $\gamma_c = 1$ and $\omega(\gamma_c) = 2$. The first two terms in the last equations match the ones found in Eq. (4.21). The shape of the front in its

forward part has the following form [104, 105]:

$$u(t,x) = C_1 e^{-\gamma_c(x-X(t))} \exp\left(-z^2\right) \times \left\{ \gamma_c(x-X(t))] + C_2 + \left(3 - 2C_2 + \frac{\gamma_c \omega^{(3)}(\gamma_c)}{\omega''(\gamma_c)}\right) z^2 - \left(\frac{2}{3}\frac{\gamma_c\omega^{(3)}(\gamma_c)}{\omega''(\gamma_c)} + \frac{1}{3}{}_2F_2\left[1,1;\tfrac{5}{2},3;z^2\right]\right) z^4 + 6\sqrt{\pi}\left(1 - {}_1F_1\left[-\tfrac{1}{2},\tfrac{3}{2};z^2\right]\right) z + \mathcal{O}(1/\sqrt{t}) \right\}, \quad (4.27)$$

where

$$z = \frac{x - X(t)}{\sqrt{2\omega''(\gamma_c)t}}. \quad (4.28)$$

C_1 and C_2 are constants, and ${}_2F_2$, ${}_1F_1$ are generalized hypergeometric functions. The terms in the first and second lines match with the result of our calculation (Eq. (4.22)). These expressions should apply also to QCD, up to the relevant replacements given in Tab. 2.1.

So far, we have considered equations of the type of Eq. (4.1) as saturation equations, in the sense that they describe the diffusive growth of a continuous function u until it is tamed for $u \sim 1$. We will see below that these equations may actually be given a different physical interpretation.

Relevance of this formalism to the BK equation

In order to check that the formalism used to arrive at a solution to FKPP-like equation applies to the BK equation in QCD, we performed in Ref. [74] a numerical simulation of the BK equation. We compared the velocity of the obtained traveling wave with Eq. (4.26), using either the full expression with three terms or a truncation of it keeping only the two dominant terms. We defined the saturation scale by the equation $A(y, Q_s(y)) = \kappa$, and we chose different values of κ. We see in the plot of Fig. 4.4 that the numerical result is consistent with the analytical expectations (using the dictionary in Tab. 2.1), although the complete discussion is quite subtle. All details of the numerics and the discussion of the results were published in Ref. [74].

4.1.3 Discrete branching diffusion

We have investigated the solutions of the FKPP equation in a mathematical way, without discussing the physics that may lead to such an equation. The absorptive boundary that we have put replaces the nonlinear term in the FKPP equation, whose role is to make sure that u never exceeds the limit $u = 1$. Hence we have thought of this boundary as a way to enforce the *saturation* of some density of particles. Actually, the FKPP equation (4.1) may stem from a branching diffusion process in which the number of particles is unlimited, and thus, for which there is no saturation at all. As a matter of fact, this is what the BK equation describes in QCD: An exponentially growing number of dipoles, stemming from the rapidity evolution of a hadronic probe, scatters off some target. The overall interaction probability is unitary because multiple scatterings are allowed (the interaction probability of n dipoles is actually of the form $1 - e^{-\alpha_s^2 n}$), but not because there is a saturation of the number of dipoles in the wavefunction of the probe. We refer the reader back to Fig. 2.4 for a picture of the process.

To illustrate how the FKPP equation arises in such a simple model of branching diffusion, let us consider a set of particles on a line, each of them being indexed by a continuous variable x. (Such a model was considered for instance in Ref. [71]). We let the system evolve according to the following rules. During the time interval dt, each particle has a probability dt to split in 2 particles. Unless it splits, it moves of the small random amount δx, which is a Gaussian variable distributed like

$$p(\delta x) = \frac{1}{\sqrt{4\pi dt}} \exp\left(-\frac{(\delta x)^2}{4dt}\right). \quad (4.29)$$

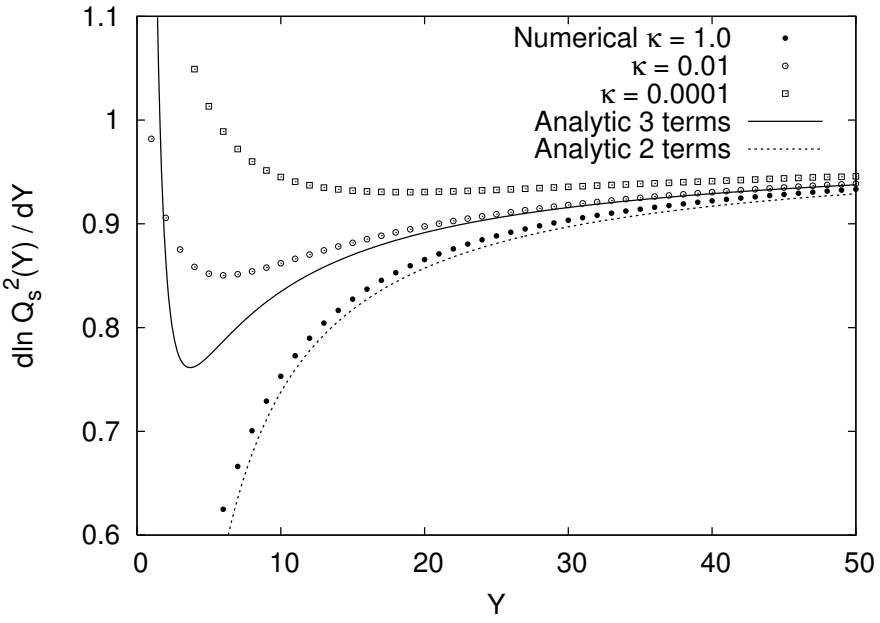

Figure 4.4: Velocity of the QCD traveling wave as a function of the rapidity. The different curves correspond to the numerical simulation, the saturation scale being defined in various ways with the help of the parameter κ (see the text for the definition of the latter), and to the analytical formula of Eq. (4.26), either truncated after the second term ("Analytic 2 terms"), or complete ("Analytic 3 terms") (see the dictonary in Tab. 2.1 for the notations).

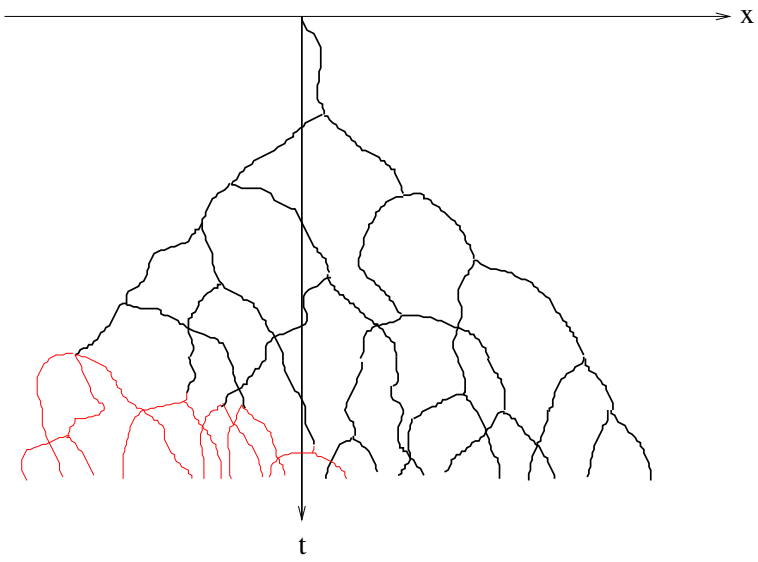

Figure 4.5: Example of branching diffusion process on a line (see the text for a mathematical description of the evolution rules). If the number of individuals is limited by a selection process which, at each new branching, eliminates the individual sitting at the smallest x as soon as the total number of individuals reaches say N ($N = 10$ in this figure), then only the branches drawn in thick line survive.

Let us consider the number of particles $n(t,x)$ contained in an interval of given size Δx centered around the coordinate x. At time $t=0$, the system is supposed to consist in a single particle sitting at the origin $x=0$. A sketch of a realization of this model is shown in Fig. 4.5. From the evolution rules, we easily get an equation for the average number of particles $\langle n\rangle$:

$$\langle n(t+dt,x)\rangle = dt\, 2\langle n\rangle + (1-dt)\int d(\delta x)p(\delta x)\langle n(t,x-\delta x)\rangle \tag{4.30}$$

which reads, after replacing p by Eq. (4.29) and after the limit $dt\to 0$ has been taken,

$$\frac{\partial\langle n\rangle}{\partial t} = \langle n\rangle + \frac{\partial^2\langle n\rangle}{\partial x^2}. \tag{4.31}$$

All the dependence on the size Δx of the "bin" is contained in the initial condition. It is clear that for large enough times, the solution to this equation is given by Eq. (4.12).

Let us now define

$$S(t,x) = e^{-n(t,x)/N} \tag{4.32}$$

where N is some (large) constant. This definition is reminiscent of the S-function, related to the scattering amplitude, introduced in the discussion of the BK equation in Chap. 2. At a fixed time and for large enough x, $n(t,x)\ll N$ and thus $1-S(t,x)\simeq n(t,x)/N\to 0$. For any x, the exponential makes sure that S ranges between 0 and 1. Thus S (or $1-S$) has the shape of a traveling wave. Its position $X(t)$ is the value of x for which $n(t,x)$ is some given constant say of the order of N. In the mean-field limit in which n is replaced by its average $\langle n\rangle$, it is very easy to compute $X(t)$ from the form of the solution (4.12). We get (see Eq. (4.13))

$$X(t) = 2t - \frac{1}{2}\ln t \tag{4.33}$$

up to a constant.

On the other hand however, the average of S over events, namely $A=1-\langle S\rangle$ obeys the FKPP equation. Indeed

$$\langle S(t+dt,x)\rangle = dt\langle S(t,x)\rangle^2 + (1-dt)\int d(\delta x)p(\delta x)\langle S(t,x-\delta x)\rangle. \tag{4.34}$$

In the limit $dt\to 0$ and rewriting the equation with the help of A, we get

$$\frac{\partial A}{\partial t} = \frac{\partial^2 A}{\partial x^2} + A - A^2. \tag{4.35}$$

Hence A is a traveling wave at large times, and its position $X(t)$ is given by Eq. (4.20). It is obviously behind by a term $\ln t$ with respect to the value of x for which the average number of particles has a given constant value (compare Eq. (4.20) and Eq. (4.13)). Furthermore, the probability distribution of the position of the rightmost particle (or of the k-th rightmost particle for any given k) may also be derived from the FKPP equation. (Brunet and Derrida have recently given an advanced discussion of the statistics of the position of these particles, see Ref. [106,107]). It turns out that in any event, the average x for which $n(t,x)$ has a given value, say n_0, moves with the FKPP velocity which can be read off from Eq. (4.20). This is much slower than the rate of change of $X(t)$ when the latter is defined as the implicit solution of the equation $\langle n(t,X(t))\rangle = n_0$.

All this may seem a bit paradoxical. But actually, it is just related to the fact that $\langle e^{-n/N}\rangle$ cannot be approximated by $e^{-\langle n\rangle/N}$. We may understand it in the following way. By taking the average of n, we have somewhat forgotten a fundamental property of n: its *discreteness*. Indeed, it only takes integer values, and in particular, the distribution of n in a realization has a finite support: At any time, there is a value of x to the right of which there are no particles at all. n obeys a stochastic equation. This is not the case for $\langle n\rangle$, which just obeys an ordinary branching diffusion equation.

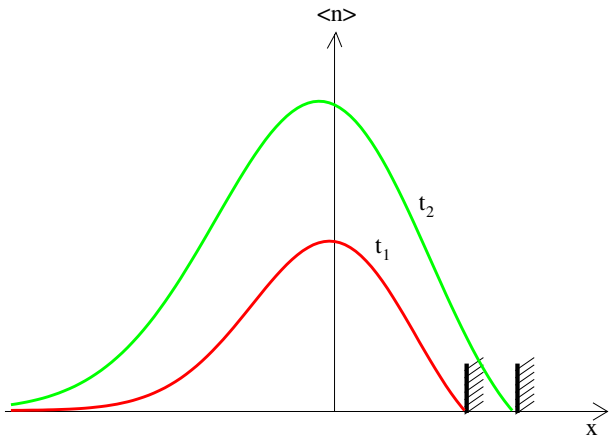

Figure 4.6: Solution of the branching diffusion equation (4.36) with a moving absorptive boundary that forces $\langle n \rangle$ to vanish at the point $X(t)$ such that $\langle n(t, X(t) - 1) \rangle = 1$. Two different times are represented.

In order to recover the effect of the discreteness of n and compute the velocity, we may again use the absorptive boundary trick. Let us solve the linear equation

$$\partial_t \langle n \rangle = \partial_x^2 \langle n \rangle + \langle n \rangle \tag{4.36}$$

with an absorptive boundary. The latter will be placed in such a way that at a distance of order one to its left (we will focus on the right-moving wave), $\langle n \rangle = 1$ (see Fig. 4.6). There is no difference in principle with the boundary calculation that we have performed before, except that the absorptive boundary is now placed to the right of the front (i.e. $x_0 < X$ in the notations used above). Thus we find without any further calculation that the realizations of n move, on the average, with the FKPP velocity (4.21).

4.2 Combining saturation and discreteness

We have seen that physically, the FKPP equation (or the BK equation in QCD) may be interpreted either as an equation for the growth, diffusion and saturation of a continuous function, or as the evolution equation for the average of a bounded function of a discrete (thus stochastic) branching diffusion process. For each of these interpretations, we may find the main features of the solutions by imposing one absorptive boundary on the linear partial differential equation encoding branching diffusion. In one case, the boundary is a cutoff that prevents u to be larger than 1: It represents saturation, i.e. the explicit nonlinearity present in the FKPP equation. In the other case, the boundary forces the function n that represents the number of particles to vanish quickly when n becomes less than 1. Formally, it actually models the stochasticity due to the intrinsic discreteness of the number n of particles, and avoids to address a stochastic equation directly.

In physical cases such as reaction-diffusion processes for finite N, we define $u(t, x)$ as the number of particles per site (or per bin) in x normalized to N. Hence it takes discrete values: $1/N$, $2/N$ etc... While for large N discreteness is unlikely to play a role in the region $u \sim 1$, it is expected to be crucial when $u \sim 1/N$. It is thus natural to impose the two boundaries: one representing saturation of the particle number, the other one taking care of the discreteness of the same quantity. A model that these two cutoffs may represent is for example, the branching diffusion model in Sec. 4.1.3, but in which the total number of particles is limited to N by keeping only the N rightmost ones at each new branching. It is clear that the function $\mathcal{U}(t, x)$ defined to be the number of particles to the right of some position x normalized to the maximum number N is, for large enough times, a front connecting 1 (for $x \to -\infty$) to 0 (for $x \to +\infty$) (see Fig. 4.7).

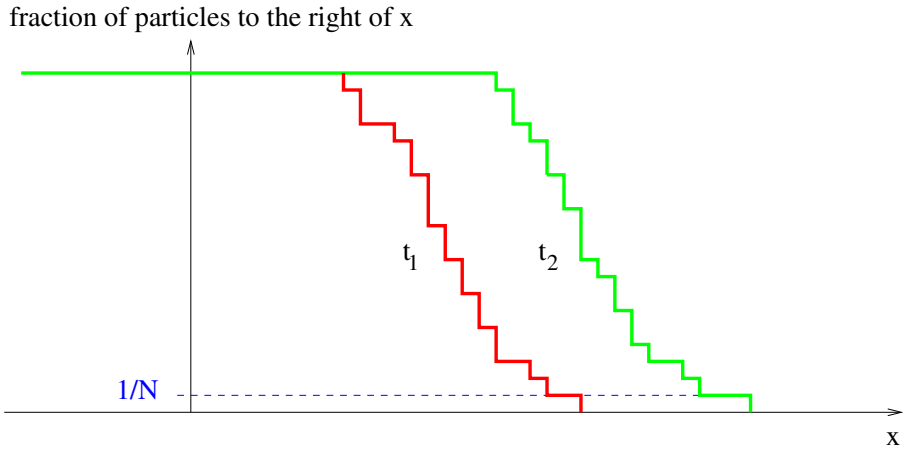

Figure 4.7: Branching diffusion model of Sec. 4.1.3 with selection that limits the total number of particles to N. The function $\mathcal{U}(t,x)$, which is the number of particles to the right of x normalized to the maximum number of particles N, is represented. One sees that the fraction of particles to the right of x looks like a traveling wave front.

Reaction-diffusion problems (described by nonlinear stochastic partial differential equations) were interpreted as branching diffusion problems taking place between two absorptive boundaries for the first time by Brunet and Derrida in Ref. [108] and later, independently, by Mueller and Shoshi in the case of QCD in Ref. [40]. Note however that in the context of the QCD parton model, the present interpretation of the cutoffs was only found in Ref. [41]. Mueller and Shoshi introduced the both cutoffs for reasons related to the boost-invariance of the QCD amplitude. (The discreteness cutoff was thought as the symmetric of the saturation cutoff under some boost). The duality of the two boundaries, that is to say of the dense and dilute regimes of the traveling wave, was studied more deeply in Refs. [109–113].

Before moving on to the technical derivation of the shape and position of the front in this case, let us figure out what we expect to find.

Starting from the initial condition which we assume to be one or a few particles, the front builds up and its velocity increases with t (see Eq. (4.21)) until it reaches its asymptotic shape, which is a decreasing exponential $e^{-\gamma_c(x-X(t))}$ that holds for all $x - X(t) \gg 1$. ($X(t)$ is here the position of the bulk of the front, say for example of the leftmost surviving particle). But if the front is made of discrete particles, then it has a finite support, and the exponential shape may not extend to infinity to the right, since $u(t,x)$ has to be either larger than $1/N$, or zero. It cannot take values that would be a fraction of $1/N$ in realizations, and thus, we cannot accommodate the shape $e^{-\gamma_c(x-X(t))}$ for arbitrarily large values of x, since it would mean authorizing arbitrarily small positive values of $u(t,x)$. From Eq. (4.25) and from the shape of the asymptotic front (4.23), the exponential shape sets down to $u = 1/N$ at time

$$t_{\rm relax} = \frac{c}{2\omega''(\gamma_c)} \left(\frac{\ln N}{\gamma_c} \right)^2 . \tag{4.37}$$

Beyond, the front cannot develop any longer, and thus, its shape and velocity remain fixed. $t_{\rm relax}$ is the time that is needed for the front to relax from any perturbation, which is why we have put the subscript "relax".

From Eq. (4.21) evaluated at $t = t_{\rm relax}$, we get the new asymptotic velocity, which takes into account the effects of discreteness, in the form

$$\frac{dX(t)}{dt} = \frac{\omega(\gamma_c)}{\gamma_c} - \frac{3}{c} \frac{\gamma_c \omega''(\gamma_c)}{\ln^2 N}. \tag{4.38}$$

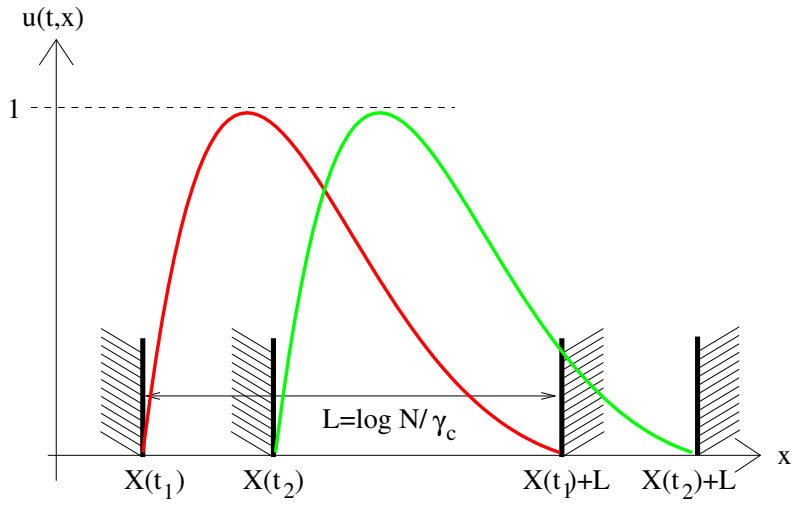

Figure 4.8: Sketch of the solution to the branching diffusion equation with two boundaries.

The calculation of the constant c requires a proper account of the exact shape of the front. We shall turn to this calculation now.

As announced, we are now going to solve the linear branching diffusion equation with two absorptive boundaries: one representing saturation, the other one discreteness. Using the intuition gained from the study of the deterministic FKPP equation, we write the ansatz

$$u(t,x) = e^{-\gamma_c(x-X(t))} L\psi\left(\frac{2\omega''(\gamma_c)t}{L^2}, \frac{x-X(t)}{L}\right). \tag{4.39}$$

L is a constant which will represent the size of the front, which is essentially equal to $L_0 = \ln N/\gamma_c$ for large N. When ω is expanded to second order around the eigenvalue γ_c, then ψ obeys the partial differential equation

$$\partial_y \psi = \frac{1}{4}\partial_\rho^2 \psi + \frac{\gamma_c L^2}{2\omega''(\gamma_c)}(\omega'(\gamma_c) - X'(t))\psi, \tag{4.40}$$

where we have defined

$$y = \frac{2\omega''(\gamma_c)t}{L^2} \quad \text{and} \quad \rho = \frac{x-X(t)}{L}. \tag{4.41}$$

We have only kept the dominant terms for large L. We see that $\omega'(\gamma_c) - X'(t)$ has to scale like $1/L^2$ for all terms of this equation to be relevant, as was already guessed heuristically. The coefficient of $1/L^2$ must be chosen in such a way that in the large-y limit, there is a nontrivial stationary solution. We will check that the correct ansatz is

$$X'(t) = \omega'(\gamma_c) - \frac{\pi^2 \omega''(\gamma_c)}{2\gamma_c L^2} + o(1/L^2) \tag{4.42}$$

Equation (4.40) then becomes

$$\partial_y \psi = \frac{1}{4}\partial_\rho^2 \psi + \frac{\pi^2}{4}\psi, \tag{4.43}$$

up to higher-order terms when L is large.

We now implement the absorptive boundaries at $\rho = 0$ and another one at $\rho = 1$ (which corresponds to a distance L between the boundaries in x-coordinates, i.e. to the natural size of the stationary front). The boundary conditions formally read

$$\psi(y, \rho = 0) = 0 \quad \text{and} \quad \psi(y, \rho = 1) = 0. \tag{4.44}$$

As for the initial condition, for reasons that will become clear later, put a localized mass close to the rightmost boundary, namely we write

$$\psi(y=0,\rho) = \delta(\rho - 1 + \bar{a})\frac{e^{\gamma_c \delta}}{L^2}, \tag{4.45}$$

where $\bar{a}$ is a constant of order $1/L$, and therefore $\bar{a} \ll 1$. The value of the weight $e^{\gamma_c \delta}$ actually corresponds to putting one single particle at a distance δ to the *right* of the rightmost boundary. As we will see, such a weight corresponds to a fluctuation added to a stationary solution. But in this section, we shall only focus on the large-time behavior: The initial condition will be forgotten through the time evolution.

The solution of Eq. (4.43) with the conditions (4.44) and (4.45) reads

$$\psi_\delta(y,\rho) = \frac{2e^{\gamma_c \delta}}{L^2}\sum_{n=1}^{\infty}(-1)^{n+1}\sin \pi n\bar{a}\,\sin \pi n\rho\, e^{-\frac{\pi^2(n^2-1)y}{4}}. \tag{4.46}$$

While the full solution with all harmonics will be of interest later, we shall discuss here only the stationary solution. We see that for large y, the higher harmonics are suppressed exponentially with respect to the fundamental mode $n = 1$, which gives the following contribution:

$$\psi_{\delta_0}(y,\rho) = \frac{2e^{\gamma_c \delta_0}}{L^2}\sin \pi\bar{a}\sin \pi\rho \underset{\bar{a}\ll 1}{\simeq} \frac{2\pi\bar{a}e^{\gamma_c \delta_0}}{L^2}\sin \pi\rho. \tag{4.47}$$

Thanks to the choice (4.42) for $X'(t)$, this solution has no y dependence, and leads to a stationary u in the frame of the front. The expression (4.47) is independent of the initial condition except for the overall normalization. The value of δ_0, which characterizes the initial condition, will be adjusted later. Undoing the changes of variables which trade u for ψ, x for ρ and t for y (Eq. (4.39)), the stationary solution u_{δ_0} reads

$$u_{\delta_0}(t,x) = e^{-\gamma_c(x-X(t))}\frac{2\pi\bar{a}e^{\gamma_c \delta_0}}{L^2}\left[L\sin\frac{\pi(x-X(t))}{L}\right]. \tag{4.48}$$

We further require that $u_0(t,x) \sim 1$ for $x = X(t) + aL$, where aL is a constant of order 1. This condition is satisfied if we set $\delta_0 \sim 3\ln L/\gamma_c$. Indeed, with this choice,

$$u_{\delta_0}(t, X(t)+aL) \simeq 2\pi^2\bar{a}aL^2 e^{-\gamma_c aL}. \tag{4.49}$$

Since $\bar{a}L$ and aL are constants, the right-hand side is just a number of order 1.

All in all, the final solution reads

$$u(t,x) \propto \kappa\, e^{-\gamma_c(x-X(t))}L\sin\frac{\pi(x-X(t))}{L} \tag{4.50}$$

(see Fig. 4.8) where the size of the front is

$$L = \frac{\ln N}{\gamma_c} \tag{4.51}$$

and its velocity reads, from Eq. (4.42),

$$v_{\mathrm{BD}} \equiv \frac{dX(t)}{dt} = V_\infty - \frac{\pi^2\omega''(\gamma_c)}{2\gamma_c L^2} = \frac{\omega(\gamma_c)}{\gamma_c} - \frac{\pi^2\gamma_c\omega''(\gamma_c)}{2\ln^2 N}. \tag{4.52}$$

The subscript BD stands for "Brunet-Derrida" after the first authors who wrote down such an expression. In the FKPP case, namely for $\omega(\gamma) = \gamma^2 + 1$, $\gamma_c = 1$ and $\omega(\gamma_c) = \omega''(\gamma_c) = 2$.

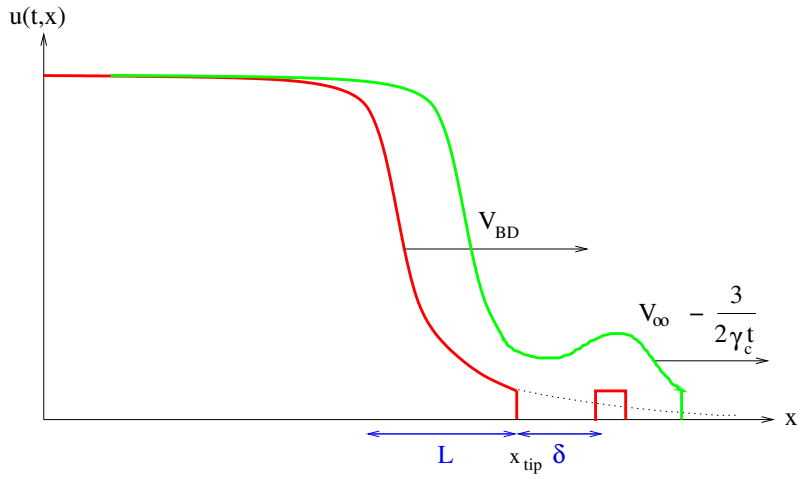

Figure 4.9: Evolution of the front with a forward fluctuation. At time t_0, the primary front extends over a size L and is a solution of the branching diffusion equation with two appropriate boundaries. An extra particle is stochastically generated at a distance δ with respect to the tip of the primary front. At a later time, the latter grows deterministically into a secondary front that is a bit slower, and that will add up to the primary one. The overall effect, after relaxation, is a shift to the right of the distance $R(\delta)$ with respect to the position of the front if a fluctuation had not occured.

4.3 Beyond the deterministic equations: Effect of the fluctuations

So far, we have actually solved deterministic equations although we were addressing a model with a discrete number of particles, that therefore had necessarily fluctuations. Our procedure gave the leading effects. We shall now incorporate more fluctuation effects, in a phenomenological way. (We shall essentially review Ref. [114]).

4.3.1 Phenomenological model and analytical results

The two-boundary procedure has led to the following result: The front propagates at a velocity $v_{\rm BD}$ in Eq. (4.52) lower than the velocity predicted by the mean-field equation (4.21), and its shape is the decreasing exponential $e^{-\gamma_c(x-X(t))}$ down to the position

$$x_{\rm tip}(t) = v_{\rm BD}t + \frac{\ln N}{\gamma_c}, \tag{4.53}$$

at which it is sharply cut off by an absorptive boundary. This boundary was meant to make the front vanish typically over one unit in x, hence to implement discreteness on a deterministic equation.

But since the evolution is not deterministic, it may happen that a few extra particles are sent stochastically ahead of the tip of the front (See Fig. 4.9). Their evolution would pull the front forward. To model this effect, we assume that the probability per unit time that there be a particle sent at a distance δ ahead of the tip simply continues the asymptotic shape of the front, that is to say, the distribution of δ is

$$p(\delta) = C_1 e^{-\gamma_c \delta}, \tag{4.54}$$

where C_1 is a constant. Heuristic arguments to support this assumption were presented in Ref. [114]. Note that while the exponential shape is quite natural since it is the continuation

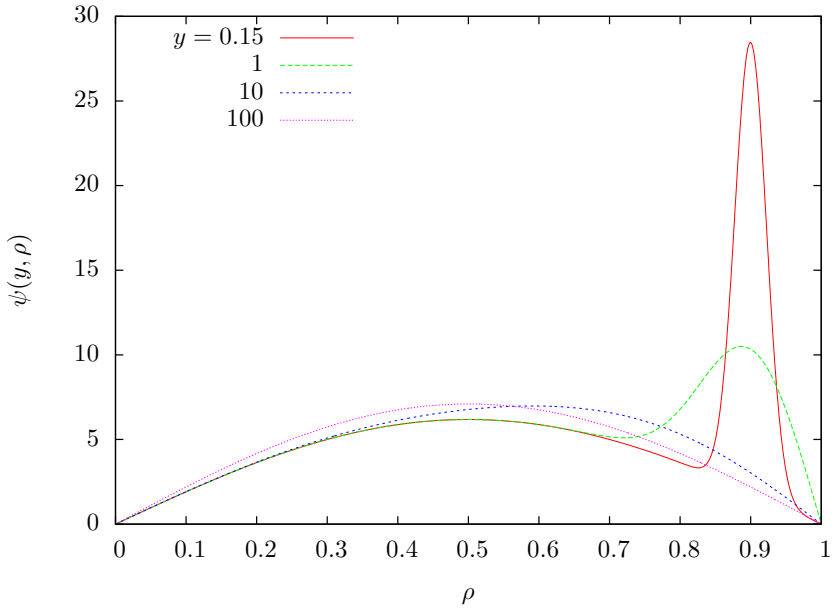

Figure 4.10: $\psi_{\delta_0}(y,\rho) + \psi_\delta(y,\rho)$ [see Eqs. (4.47), (4.46)] for different values of the reduced time variable y after a fluctuation of size $\delta = 5$ has occurred at $y = 0$. In this plot, the size of the front is $L = 10$, and $\bar{a} = 0.1$. We see how the fluctuation, initially localized at the tip of the front, gets smeared uniformly over the width of the front as y gets large. Eventually, a small forward shift $X \to X + R$ would be needed in order to absorb it and recover the stationary front.

of the deterministic solution (4.22) in the linear regime, the fact that C_1 need to be strictly constant (and cannot be a slowly varying function of δ) is a priori more difficult to argue.

Once a particle has been produced at position $x_{\rm tip} + \delta$, say at time t_0, it starts to multiply (see Fig. 4.9) and it eventually develops its own front (after a time $t_{\rm relax}$ of the order of L^2), that will add up to the deterministic primary front made of the evolution of the bulk of the particles.

Note that the philosophy of our phenomenological approach to the treatment of the fluctuations is identical to the spirit of the statistical approach in Sec. 3.3 developped for the zero-dimensional model. Whenever the number of particles is larger than $\bar{n}$ ($\bar{n} = 1$ here), we apply a deterministic nonlinear evolution. Fluctuations instead are produced with a probability which stems from a linear equation. The difficulty here is that we are unable to solve either of these equations for arbitrary initial conditions and thus we have to make conjectures on the form of their solutions.

Let us estimate the shift in the position of the front induced by these extra forward particles. The solution of the diffusion equation is the superposition of the large-time stationary solution u_{δ_0} given by Eq. (4.48) with $\delta_0 = 3 \ln L/\gamma_c$, and of the solution u_δ of the diffusion equation with the generic initial condition characterized by δ (see Eq. (4.46)), up to a multiplicative constant C_2 of order 1 that we do not control in this calculation, since it certainly depends on the detailed shape of the fluctuations. We write

$$u(t,x) = u_{\delta_0}(t,x) + C_2 u_\delta(t,x) = e^{-\gamma_c(x - X(t))} L\left[\psi_{\delta_0}(y,\rho) + C_2 \psi_\delta(y,\rho)\right] \tag{4.55}$$

up to the replacement of the variables by their expressions (4.41). The presence of the second term alters the shape of the front (the front eventually relaxes back to the sine shape in Eq. (4.48)), see Fig. 4.10. But of course, we want to keep the normalization condition for u, namely for some appropriate value of x, u is required to equate Eq. (4.49) at all t. This is possible by shifting the value of x at which we enforce the normalization condition from $x = X(t) + aL$ to say $x = X(t) + aL + R(t,\delta)$. This is equivalent to shifting the position of the front $X(t) \to X(t) + R(t,\delta)$.

Equation (4.55) then leads to

$$u(t, X(t) + aL + R(t,\delta)) = 2\pi^2 \bar{a} a L^2 e^{-\gamma_c a L - \gamma_c R(t,\delta)} \left[1 + C_2 \frac{\psi_\delta(y,a)}{2\pi^2 \bar{a} a\, L}\right]. \tag{4.56}$$

Equating the right-hand sides of Eq. (4.56) and Eq. (4.49), we get

$$R(t,\delta) = \frac{1}{\gamma_c} \ln \left[1 + C_2 \frac{\psi_\delta\left(\frac{2\omega''(\gamma_c)t}{L^2}, a\right)}{2\pi^2 \bar{a} a\, L}\right], \tag{4.57}$$

where only the lowest orders in $\bar{a}$, a in the expansion of ψ_δ must be kept. With the help of Eq. (4.46), it is then straightforward to arrive at an explicit expression of R.

In the large time limit in which only the fundamental mode survives in the expression of ψ, we get the shift

$$R(\delta) = \frac{1}{\gamma_c} \ln \left(1 + C_2 \frac{e^{\gamma_c \delta}}{L^3}\right). \tag{4.58}$$

The probability distribution (4.54) and the front shift (4.58) due to a forward fluctuation define an effective theory for the evolution of the position of the front $X(t)$:

$$X(t+dt) = \begin{cases} X(t) + v_{\rm BD}\, dt & \text{proba. } 1 - dt \int_0^\infty d\delta p(\delta) \\ X(t) + v_{\rm BD}\, dt + R(\delta) & \text{proba. } p(\delta) d\delta dt. \end{cases} \tag{4.59}$$

From these rules, we may compute all cumulants of $X(t)$, by writing the evolution of their generating function, deduced from the effective theory (4.59):

$$\frac{\partial}{\partial t} \ln \left\langle e^{\lambda X(t)} \right\rangle = \lambda v_{\rm BD} + \int d\delta\, p(\delta) \left(e^{\lambda R(\delta)} - 1\right). \tag{4.60}$$

The left hand-side is a power series in λ whose coefficients are the time derivatives of the cumulants of $X(t)$. Identifying the powers of λ in the left and right-hand sides, we get

$$\begin{aligned} V - v_{\rm BD} &= \int d\delta p(\delta) R(\delta) = \frac{C_1 C_2}{\gamma_c} \frac{3 \ln L}{\gamma_c L^3} \\ \frac{[n\text{-th cumulant}]}{t} &= \int d\delta p(\delta) [R(\delta)]^n = \frac{C_1 C_2}{\gamma_c} \frac{n! \zeta(n)}{\gamma_c^n L^3}. \end{aligned} \tag{4.61}$$

We see that the statistics of the position of the front still depend on the product $C_1 C_2$ of the undetermined constants C_1 and C_2. We need a further assumption to fix its value.

We go back to the expression for the correction to the mean-field front velocity, given in Eq. (4.52). From the expressions of $R(\delta)$ (Eq. (4.58)) and of $p(\delta)$ (Eq. (4.54)), we see that the integrand defining $V - v_{\rm BD}$ in Eq. (4.61) is almost a constant function of δ for $\delta < \delta_0 = 3 \ln L/\gamma_c$, and is decaying exponentially for $\delta > \delta_0$. Furthermore, $R(\delta_0)$ is of order 1, which means that when a fluctuation is sent out at a distance $\delta \sim \delta_0$ ahead of the tip of the front, it evolves into a front that matches in position the deterministic primary front. We also notice that when a fluctuation has $\delta < \delta_0$, its evolution is completely linear until it is incorporated to the primary front, whereas fluctuations with $\delta > \delta_0$ evolve nonlinearly but at the same time have a very suppressed probability. We are thus led to the natural conjecture that the average front velocity is given by $v_{\rm BD}$ in Eq. (4.52), with the replacement

$$L \to L_{\rm eff} = \frac{\ln N}{\gamma_c} + \delta_0 = \frac{\ln N}{\gamma_c} + 3 \frac{\ln \ln N}{\gamma_c}, \tag{4.62}$$

namely

$$V = \frac{\omega(\gamma_c)}{\gamma_c} - \frac{\pi^2 \omega''(\gamma_c)}{2\gamma_c \left(\frac{\ln N}{\gamma_c} + \frac{3 \ln \ln N}{\gamma_c}\right)^2}. \tag{4.63}$$

The large-N expansion of the new expression of the velocity yields a correction of the order of $\ln\ln N/\ln^3 N$ to the Brunet-Derrida result, more precisely

$$V = \frac{\omega(\gamma_c)}{\gamma_c} - \frac{\pi^2\gamma_c\omega''(\gamma_c)}{2\ln^2 N} + \pi^2\gamma_c\omega''(\gamma_c)\frac{3\ln\ln N}{\ln^3 N}. \tag{4.64}$$

Eqs. (4.61) and (4.64) match for the choice

$$C_1C_2 = \pi^2\omega''(\gamma_c). \tag{4.65}$$

From this determination of C_1C_2, we also get the full expression of the cumulants of the position of the front:

$$\frac{[n\text{-th cumulant}]}{t} = \pi^2\gamma_c^2\omega''(\gamma_c)\frac{n!\zeta(n)}{\gamma_c^n\ln^3 N}. \tag{4.66}$$

We note that all cumulants are of order unity for $t \sim \ln^3 N$, which is the sign that the distribution of the front position is far from being a trivial Gaussian. This makes it particularly interesting. On the other hand, the cumulants are proportional to $\kappa = t/\ln^3 N$, which is the sign that the position of the front is the result of the sum of κ independent random variables, and as such, becomes Gaussian when κ is very large. The properties of the statistics of the front position were investigated in some more details in Ref. [115].

Thanks to our discussion in Chap. 2, we see that these results should apply to QCD with the relevant substitution of the kernel ω and of the parameter N according to Tab. 2.1.

4.3.2 Numerical simulations

The results obtained so far rely on a number of conjectures that no-one has been able to prove so far. In order to check our results, let us consider again the model introduced in Sec. 2.2.2. The first step to take before being able to apply our results to this particular model is to extract from the linear part of Eq. (2.26) the corresponding function $\omega(\gamma)$, and then to compute γ_c. Setting $\Delta x = \Delta t = 1$, we get

$$\omega(\gamma) = \ln\left[1 + \lambda + p_l(e^{-\gamma} - 1) + p_r(e^{\gamma} - 1)\right], \tag{4.67}$$

and γ_c is defined by $\omega(\gamma_c) = \gamma_c\omega'(\gamma_c)$.

For the purpose of our numerical study, we set

$$p_l = p_r = 0.1 \quad \text{and} \quad \lambda = 0.2\,. \tag{4.68}$$

Simulated realizations for this set of parameters are shown in Fig. 4.11.

From (4.67), this choice leads to

$$\begin{aligned} &\gamma_c = 1.352\cdots\ , \quad \omega'(\gamma_c) = 0.2553\cdots\ , \\ &\omega''(\gamma_c) = 0.2267\cdots\ . \end{aligned} \tag{4.69}$$

Predictions for all cumulants of the position of the front are obtained by replacing the values of these parameters in Eqs. (4.64),(4.66).

Technically, in order to be able to go to very large values of N, we replace the full stochastic model by its deterministic mean field approximation $u \to \langle u\rangle$, where the evolution of $\langle u\rangle$ is given by Eq. (2.26), in all bins in which the number of particles is larger than 10^3 (that is, in the bulk of the front). Whenever the number of particles is smaller, we use the full stochastic evolution (2.24). We add an appropriate boundary condition on the interface between the bins described by the deterministic equation and the bins described by the stochastic equation so that the flux of particles is conserved [116]. This version of the model will be called "model I". Eventually, we shall use the mean field approximation everywhere except in the rightmost bin (model II): at each time step, a new bin is filled immediately on the right of the rightmost nonempty site with a number of particles given by a Poisson law of average $\theta = N\langle u(x,t+1)|\{u(x,t)\}\rangle$. We checked numerically

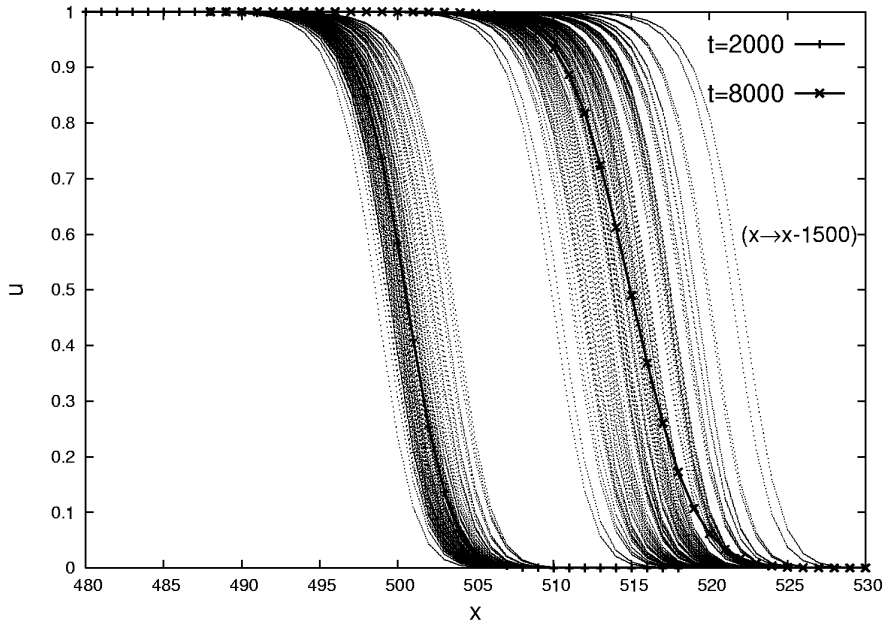

Figure 4.11: 1000 realizations of the model introduced in Sec. 2.2.2 at two different times (dotted lines), and the average of u over the realizations (full line). One clearly sees that $\langle u \rangle$ does not keep its shape upon time evolution, which shows that the traveling wave property of the FKPP equation is lost due to the stochasticity. This point is addressed in some detail in Chap. 6.

that this last approximation gives indistinguishable results from those obtained within model I as far as the statistics of the position of the front is concerned.

We define the position of the front at time t by

$$X_t = \sum_{x=0}^{\infty} u(x,t). \tag{4.70}$$

We start at time $t = 0$ from the initial condition $u(x,0) = 1$ for $x \leq 0$ and $u(x,0) = 0$ for $x > 0$. We evolve it up to time $t = \ln^2 N$ to get rid of subasymptotic effects related to the building of the asymptotic shape of the front, and we measure the mean velocity between times $\ln^2 N$ and $16 \times \ln^2 N$. For model I (many stochastic bins), we average the results over 10^4 such realizations. For model II (only one stochastic bin), we generate 10^5 such realizations for $N \leq 10^{50}$ and 10^4 realizations for $N > 10^{50}$. In all our simulations, models I and II give numerically indistinguishable results for the values of N where both models were simulated, as can be seen on the figures (results for model I are represented by a circle and for model II by a cross).

Our numerical data for the cumulants is shown in Fig. 4.12 together with the analytical predictions obtained from (4.64),(4.66) (dotted lines in the figure). We see that the numerical simulations get very close to the analytical predictions at large N. However, higher-order corrections are presumably still important for the lowest values of N displayed in the figure.

We try to account for these corrections by replacing the factor $(\ln N)/\gamma_c = L_0$ in the denominator of the expression for the cumulants in Eqs. (4.64),(4.66) by the ansatz

$$L_{\text{eff}} = L_0 + \frac{3\ln(\ln N)}{\gamma_c} + c + d\frac{\ln(\ln N)}{\ln N} \ . \tag{4.71}$$

The two first terms in the r.h.s. are suggested by our model. We have added two subleading terms which go beyond our theory: a constant term, and a term that vanishes at large N. The latter

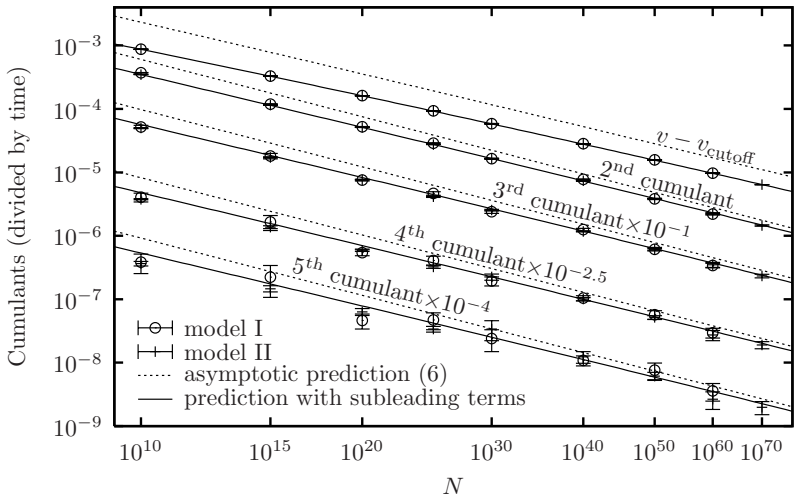

Figure 4.12: [From Ref. [114]] From top to bottom, the correction to the velocity given by the cutoff theory and the cumulants of orders 2 to 5 of the position of the front in the stochastic model. The numerical data are compared to our parameter-free analytical predictions (4.64),(4.66), represented by the dashed line.

are naturally expected to be among the next terms in the asymptotic expansion for large N. We include them in this numerical analysis because in the range of N in which we are able to perform our numerical simulations, they may still bring a significant contribution.

We fit (4.71) to the numerical data obtained in the framework of model II, restricting ourselves to values of N larger than 10^{30}. In the fit, each data point is weighted by the statistical dispersion of its value in our sample of data. We obtain a determination of the values of the free parameters $c = -4.26 \pm 0.01$ and $d = 5.12 \pm 0.27$, with a good quality of the fit ($\chi^2/d.o.f \sim 1.15$).

Now we see that with this modification of the expression of the size of the front, the results for the cumulants shown in figure 4.12 (full lines) are in excellent agreement with the numerical data over the whole range of N.

Chapter 5

Spatial correlations

So far, all models and calculations aimed at describing QCD scattering amplitudes assumed uniformity in impact-parameter space, or, decoupling of the evolution between different points in the transverse space. Indeed, we considered one-dimensional models while to fully describe the impact parameter, two dimensions are necessary. We shall address here the issue of the correlations of the QCD evolution between different impact parameters.

Contents

5.1 Relevance of one-dimensional models

So far, we have argued that high-energy scattering in QCD at fixed coupling and fixed impact parameter is in the universality class of the stochastic FKPP equation (Chap. 2), which is an equation with one evolution variable (time or rapidity in QCD), and one spatial dimension (x generically, or $\ln k^2 \sim \ln(1/r^2)$ in QCD). From the very beginning, we have simply discarded the impact parameter dependence. It is important to understand that the spatial variable and the impact parameter play different roles, and thus, the impact parameter may a priori not be accounted for by a two-dimensional extension of the FKPP equation.

There are general arguments to support the assumption that the QCD evolution is local enough for the different impact parameters to decouple through the rapidity evolution, which we are now going to present.

Let us start with a single dipole at rest, and bring it gradually to a higher rapidity. As was explained in Chap. 2, during this process, this dipole may be replaced by two new dipoles, which themselves may split, and so on, eventually producing a chain of dipoles. Figure 2.2 pictures one realization of such a chain.

According to the splitting rate given in Eq. (2.1), splittings to smaller-size dipoles are favored, and thus, one expects that the sizes of the dipoles get smaller on the average, and that in turn, the successive splittings become more local. The dipoles around region "1" and those around region "2" should have an independent evolution beyond the stage pictured in Fig. 2.2: Further splittings

will not mix in impact parameter space, and thus, the traveling waves around these regions should be uncorrelated. For a dipole in region 1 of size r to migrate to region 2, it should first split into a dipole whose size is of the order of the distance Δb between regions 1 and 2, up to some multiplicative factor of order 1. (We assume in this discussion that the dipoles in region 2 relevant to the propagation of the local traveling waves, that is, those which are in the bulk of the wave front, also have sizes of order r). Roughly speaking, the rate of such splittings may be estimated from the dipole splitting probability (2.1): it is of order $\bar{\alpha}(r^2/(\Delta b)^2)^2$, while the rate of splittings of the same dipole into a dipole of similar size in region 1 is of order $\bar{\alpha}$. Thus the first process is strongly suppressed as soon as regions 1 and 2 are more distant than a few units of r. Note that for $\Delta b \gtrsim 1/Q_s$, saturation may further reduce the emission of the first, large, dipole leading to an even stronger suppression of the estimated rate.

What could also happen is that some larger dipole has, by chance, one of its endpoints tuned to the vicinity of the coordinate one is looking at (at a distance which is at most $|\Delta r| \ll 1/Q_s(y)$), and easily produces a large number of dipoles there. In this case, the position of the traveling wave at that impact parameter would suddenly jump. If such events were frequent enough, then they would modify the average wave velocity and thus the one-dimensional sFKPP picture. We may give a rough estimate of the rate at which dipoles of size smaller than Δr are produced. Assuming local uniformity for the distribution n of the emitting dipoles, the rate (per unit of $\bar{\alpha}y$) of such events can be written

$$\int_{r_0>\Delta r} \frac{d^2 r_0}{r_0^2} \int_{\varepsilon<\Delta r} d^2\varepsilon \, n(r_0) \left(\frac{\varepsilon}{r_0}\right)^2 \frac{1}{2\pi} \frac{r_0^2}{\varepsilon^2 (r_0-\varepsilon)^2}, \tag{5.1}$$

where we integrate over large dipoles of size $r_0 > \Delta r$ emitting smaller dipoles (of size $\varepsilon < \Delta r$) with a probability $d^2\varepsilon \, r_0^2/(2\pi\varepsilon^2(r_0-\varepsilon)^2)$. The factor $(\varepsilon/r_0)^2$ accounts for the fact that one endpoint of the dipole of size r_0 has to be in a given region of size ε in order to emit the dipoles at the right impact parameter. To estimate this expression, we first use $n(r_0) = T(r_0)/\alpha_s^2$ and approximate T by

$$T(r_0) = \theta(r_0 - 1/Q_s) \, + \, (r_0^2 Q_s^2)^{\gamma_c} \, \theta(1/Q_s - r_0). \tag{5.2}$$

The front is replaced by 1 above the saturation scale (for $r_0 > 1/Q_s$) and by an exponentially decaying tail for $r_0 < 1/Q_s$. Using $r_0 - \varepsilon \approx r_0$ in the emission kernel, the integration is then easily performed and one finds a rate whose dominant term is

$$\frac{\pi}{2\alpha_s^2} \frac{((\Delta r)^2 Q_s^2)^{\gamma_c}}{1-\gamma_c}. \tag{5.3}$$

For $(\Delta r)^2 \ll (\alpha_s^2)^{1/\gamma_c}/Q_s^2$, i.e. ahead of the bulk of the front, this term is parametrically less than 1 and is in fact of the order of the probability to find an object in this region that contributes to the normal evolution of the front [114]. Hence there is no extra contribution due to the fact that there are many dipoles around at different impact parameters.

The arguments given here are based on estimates of average numbers of dipoles, on typical configurations, and we are not able to account analytically for the possible fluctuations. As we have seen through this review, the latter often play an important role. As a matter of fact, in the physics of disordered systems, rare events sometimes dominate. So before studying the phenomenological consequences of the statistical picture of high-energy QCD based on a one-dimensional equation, one should check more precisely the locality of the evolution in impact parameter.

A numerical check was achieved in the case of a toy model that has an impact-parameter dependence in Ref. [117]. Let us briefly describe the model, before presenting the main numerical results.

5.1.1 A model incorporating an impact-parameter dependence

In order to arrive at a model that is tractable numerically, we only keep one transverse dimension instead of two in 3+1-dimensional QCD. However, we cannot consider genuine 2+1-dimensional

QCD because we do not wish to give up the logarithmic collinear singularities at $x_2 = x_0$ and $x_2 = x_1$. Moreover, QCD with one dimension less has very different properties at high energies [118]. Starting from Eq. (2.1), a splitting rate which complies with our requirements is:

$$\frac{dP}{d(\bar{\alpha}y)} = \frac{1}{4}\frac{|x_{01}|}{|x_{02}||x_{12}|}dx_2. \tag{5.4}$$

We can further simplify this probability distribution by keeping only its collinear and infrared asymptotics (as in Ref. [119]). If $|x_{02}| \ll |x_{01}|$ (or the symmetrical case $|x_{12}| \ll |x_{01}|$), the probability reduces to $dx_2/|x_{02}|$ ($dx_2/|x_{12}|$ resp.). The result of the splitting is a small dipole (x_0, x_2) together with one close in size to the parent. So for simplicity we will just add the small dipole to the system and leave the parent unchanged. In the infrared region, a dipole of size $|x_{02}| \gg |x_{01}|$ is emitted with a rate given by the large-$|x_{02}|$ limit of the above probability. The probability laws (2.1),(5.4) imply that a second dipole of similar size should be produced while the parent dipole disappears. To retain a behavior as close as possible to that in the collinear limit, we will instead just generate a single large dipole and keep the parent. To do this consistently one must include a factor of two in the infrared splitting rate, so as not to modify the average rate of production of large dipoles.

Let us focus first on the distribution of the sizes of the participating dipoles. (The simplifying assumptions made above enable one to choose the sizes and the impact parameters of the dipoles successively). We call r the modulus of the emitted dipole, r_0 the modulus of its parent and we define $Y = \bar{\alpha}y$. The splitting rate (5.4) reads, in this simplified model

$$\frac{dP_{r_0\to r}}{dY} = \theta(r - r_0)\frac{r_0 dr}{r^2} + \theta(r_0 - r)\frac{dr}{r}, \tag{5.5}$$

and the original parent dipole is kept. Logarithmic variables are the relevant ones here, so we introduce

$$\rho = \log_2(1/r) \qquad \text{or} \qquad r = 2^{-\rho}. \tag{5.6}$$

We can thus rewrite the dipole creation rate as

$$\frac{dP_{\rho_0\to\rho}}{dY} = \theta(\rho_0 - \rho)\, 2^{\rho-\rho_0}\, \log 2\, d\rho + \theta(\rho - \rho_0)\, \log 2\, d\rho. \tag{5.7}$$

To further simplify the model, we discretise the dipole sizes in such a way that ρ is now an integer. This amounts to restricting the dipole sizes to negative integer powers of 2. The probability that a dipole at lattice site i (*i.e.* a dipole of size 2^{-i}) creates a new dipole at lattice site j is

$$\frac{dP_{i\to j}}{dY} = \int_{\rho_j}^{\rho_{j+1}} \frac{dP_{\rho_i\to\rho}}{dY} = \begin{cases} \log 2 & j \geq i \\ 2^{j-i} & j < i \end{cases}. \tag{5.8}$$

The rates $dP_{i\pm}/dY$ for a dipole at lattice site i to split to any lattice site $j \geq i$ or $j < i$ respectively are then given by

$$\frac{dP_{i+}}{dY} = \sum_{j=i}^{L-1} \frac{dP_{i\to j}}{dY} = \log 2(L - i), \quad \frac{dP_{i-}}{dY} = \sum_{j=0}^{i-1} \frac{dP_{i\to j}}{dY} = 1 - 2^{-i}, \tag{5.9}$$

where we have restricted the lattice to $0 \leq i < L$, for obvious reasons related to the numerical implementation.

Now we have to address the question of the impact parameter of the emitted dipole. In QCD, the collinear dipoles are produced near the endpoints of the parent dipoles. Let us take a parent of size r_0 at impact parameter b_0. We set the emitted dipole (size r) at the impact parameter b such that

$$b = b_0 \pm \frac{r_0 \pm r \times s}{2} \tag{5.10}$$

where s has uniform probability between 0 and 1. It is introduced to obtain a continuous distribution of the impact parameter unaffected by the discretisation of r. This prescription is quite arbitrary in its details, but the latter do not influence significantly the physical observables. Each of the two signs that appear in the above expression is chosen to be either $+$ or $-$ with equal weights. We apply the same prescription when the emitted dipole is larger than its parent.

Now that we have introduced a branching process similar to QCD dipole evolution, we must define the scattering amplitude. We have explained above (see Sec. 2.1) that in QCD, the scattering amplitude of an elementary probe dipole of size $r_i = 2^{-i}$ with a dipole in an evolved Fock state is proportional to the number of objects which have a size of the same order of magnitude and which sit in a region of size of order r_i around the impact point of the probe dipole. Since in our case, the sizes are discrete, the amplitude is just given, up to a factor, by the number of dipoles that are exactly in the same bin of size as the probe, namely

$$T(i, b_0) = \alpha_s^2 \times \#\{\text{dipoles of size } 2^{-i} \text{ at impact parameter } b \text{ satisfying } |b - b_0| < r_i/2\}. \quad (5.11)$$

Finally, we must enforce unitarity, that is, the condition

$$T(i, b) \leq 1 \quad (5.12)$$

for any i and b. This condition is expected to hold due to gluon saturation in QCD. However, saturation is not included in the original dipole model. The simplest choice is to veto splittings that would locally drive the amplitude to values larger than 1. In practice, for each splitting that gives birth to a new dipole of size i at impact parameter b, we compute $T(i, b)$ and $T(i, b \pm r_i/2)$, and throw away the produced dipole whenever one of these numbers gets larger than one.

Given the definition of the amplitude T, this saturation rule implies that there is a maximum number of objects in each bin of size and at each impact parameter, which is equal to $N_{\rm sat} = 1/\alpha_s^2$.

5.1.2 Numerical evaluation of the correlators

We have implemented this model numerically. Let us discuss how we operated this implementation and the results we obtained.

We take as an initial condition a number $N_{\rm sat}$ of dipoles of size 1 ($i = 0$), uniformly distributed in impact parameter between $-r_0/2$ and $r_0/2$. The impact parameters b_j that are considered are respectively 0, 10^{-6}, 10^{-4}, 10^{-2} and 10^{-1}. The number of events generated is typically 10^4,which allows one to measure the mean and variance of the position of the traveling waves to a sufficient accuracy.

We have checked that at each impact parameter, we get traveling waves whose positions grow linearly with rapidity at a velocity less than the expected mean-field velocity for this model. $N_{\rm sat}$ was varied from 10 to 200.

Figure 5.1 represents the correlations between the positions of the wave fronts at different impact parameters, defined as

$$\langle \rho_{\rm s}(Y, b_1)\rho_{\rm s}(Y, b_2)\rangle - \langle \rho_{\rm s}(Y, b_1)\rangle\langle \rho_{\rm s}(Y, b_2)\rangle. \quad (5.13)$$

We set $N_{\rm sat}$ to 25 in that figure, but we also repeated the analysis for different values of $N_{\rm sat}$ between 10 and 200.

We see very clearly the successive decouplings of the different impact parameters in Fig. 5.1, from the most distant to the closest one, as rapidity increases. Indeed, the correlation functions flatten after some given rapidity depending on the difference in the probed impact parameters, which means that the evolutions decouple. This decoupling is expected as soon as the traveling wave front reaches dipole sizes which are smaller than the distance between the probed impact parameters, *i.e.* at Y such that $|b_2 - b_1| \approx 1/Q_s(Y) = 2^{-\rho_{\rm s}(Y)}$. (We shall further comment on this decoupling in the next section). From the data for $\rho_{\rm s}(Y)$, we can estimate quantitatively the values of the rapidities at which the traveling waves decouple between the different impact

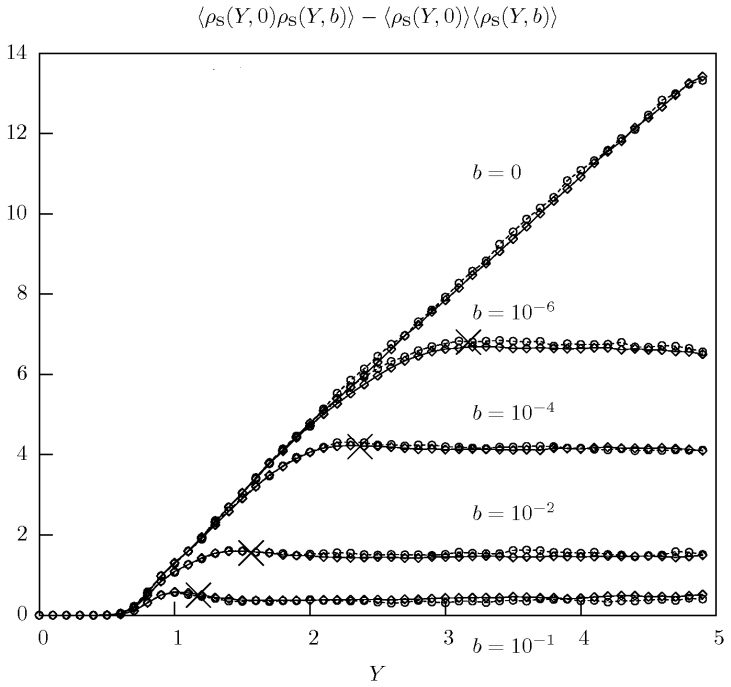

Figure 5.1: Correlations of the positions of the traveling wave fronts between different impact parameters in the toy model of Sec. 5.1. The points where the correlations flatten correspond to the decoupling of the waves in the corresponding regions of impact parameter.

parameters. (It is enough to invert the above formula for the relevant values of $b_2 - b_1$). These rapidities are denoted by a cross in Fig. 5.1 for the considered impact parameter differences. Our numerical results for the correlations are nicely consistent with this estimate, since the correlations start to saturate to a constant value precisely on the right of each such cross.

We conclude that the different impact parameters indeed decouple, as was expected from a naive analytical estimate. What is true for our toy model should go over to full QCD, since we have included the main features of QCD. When looking at the data more carefully however, it turns out that the model with impact parameter does not reduce exactly to a supposedly equivalent one-dimensional model of the sFKPP type. This is a point that would deserve more work. We refer the reader to Ref. [117] for all details of our numerical investigations.

However, even if one takes the statistical decoupling of impact parameters as soon as $\Delta b > 1/Q_s(Y)$ for granted, there may still be some effective correlations persisting at large rapidities since two points in impact-parameter space share some common history. Indeed, fluctuations need some rapidity to affect saturation scales, and history may be remembered way after the rapidity at which the decoupling happened. Such effects are negligible at small rapidities, as was just shown numerically, but may be crucial at large rapidities. We shall now investigate this point.

5.2 Computing the correlations

Our method will consist in proposing a simple toy model which contains the main physical features of QCD, which may be implemented as a Monte-Carlo event generator and for which analytical calculations will be possible. In these respects, our approach follows the one developed in the previous section, but while the latter work was purely numerical, our main results will consist in analytical expressions of the correlation of the saturation scale between two points in impact-

parameter space, as a function of the distance between the points and as a function of the rapidity. The content of this section was published in Ref. [120, 121].

The model that we will study will have the following characteristics. With respect to QCD, we assume the following simplifications: *(i)* Dipoles evolve by giving birth to one dipole of half size (the left or the right half of the parent dipole), or to one dipole of double size (in such a way that the parent be the left or right half of its offspring) at some fixed rates, *(ii)* dipoles do not disappear in the evolution, that is to say, the parent dipoles are not removed, *(iii)* the positions and dipole sizes are discrete, and *(iv)* the configuration space of the dipoles is a line instead of the full two-dimensional space. We thus give up two main properties of the QCD dipole model: The collinear singularities, which cause the dipole endpoints to emit an arbitrary number of dipoles of arbitrarily small sizes, and the continuous and two-dimensional nature of the dipole sizes and positions. The first simplification is the diffusion approximation, which has been studied in the context of BFKL physics (see e.g. Ref. [122]), but which was not assumed in the previous model. The second simplification was instead already assumed in there. These model simplifications may introduce some artefacts, but that we believe are under control, and many results which we will obtain within such simple models are likely to apply to QCD since they will not depend on the details.

Let us now specify completely the model. According to the evolution rules given above, starting from a dipole of size 1, the sizes of all dipoles present in the system after evolution are powers of 2. In practice, we shall only consider fractions of 1, i.e. the sizes may be written as 2^{1-k}, where $k \geq 1$. For each value of k, there are 2^{k-1} possible values of the position b of the center of the dipoles: $b = -\frac{1}{2} + 2^{-k}, -\frac{1}{2} + 3 \times 2^{-k}, \cdots, \frac{1}{2} - 3 \times 2^{-k}, \frac{1}{2} - 2^{-k}$. Let us number these bins by the index $0 \leq j \leq 2^{k-1} - 1$ running from the negative to the positive positions. The model may be represented as a hierarchy of bins that contain a discrete number of dipoles, see Fig. 5.2. Note that to any given impact parameter b between $-\frac{1}{2}$ and $\frac{1}{2}$ corresponds one unique bin at each level of size. For example, at position $b = -\frac{1}{2}$, one sees the bins $(k = 1, j = 0)$, $(k = 2, j = 0)$, $(k = 3, j = 0)$ etc... At position -0.2, one sees the bins $(k = 1, j = 0)$, $(k = 2, j = 0)$, $(k = 3, j = 1)$ etc... More generally, at position $-\frac{1}{2} + \Delta b$, one sees $(k, [\Delta b \times 2^{k-1}])$, where the square brackets represent the integer part.

During the rapidity (or time) interval dt, a dipole in the bin (k, j) has a probability αdt to give birth to a dipole in the bin $(k + 1, 2j)$, αdt to give a dipole in the bin $(k + 1, 2j + 1)$, and $\beta dt/2$ to give a dipole in the bin $(k - 1, j/2)$ if j is even and $(k - 1, (j - 1)/2)$ if j is odd. Note that dt may be infinitesimal (which is generally speaking convenient for analytical calculations), but also finite (which is convenient for numerical simulations).

As for the saturation mechanism, we assume the simplest one: We veto splittings to bins which already host the number N of dipoles.

We can consider that the number density of "gluons" of a given size seen at one impact parameter is proportional to the number of dipoles in the corresponding bin (k, j). As rapidity is increased, the occupation of the bins with low values of k gets higher until the number of objects they contain reaches N. The subsequent filling of the bins indexed by larger values of k (smaller dipole sizes) can be seen as the propagation of traveling wave fronts at each impact parameter, with possibly complicated relationships between them. The (logarithm of the) saturation scale $X(b, t)$ at impact parameter b is related to the position of the front seen there at time t. There are several equivalent ways to define the position of the front. It could be, for example, the largest value of k for which the number of objects becomes some given fraction of N. (Later, we will use a slightly different definition).

5.2.1 Basic features of the model

Let us denote by $n_{(k,j)}(t)$ the number of dipoles present in the bin (k, j) at time t. Then, according to the rules given above, we can write the following stochastic evolution equation:

$$n_{(k,j)}(t + dt) = \min \left[N, n_{(k,j)}(t) + \delta^{\alpha}_{(k-1,[j/2])}(t) + \delta^{\beta/2}_{(k+1,2j)}(t) + \delta^{\beta/2}_{(k+1,2j+1)}(t) \right], \tag{5.14}$$

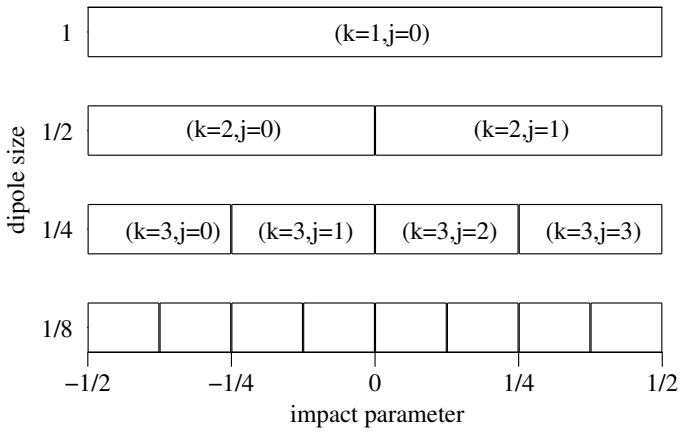

Figure 5.2: The hierarchical structure of the model. Each box represents a bin which may contain up to N dipoles of given sizes (vertical axis) and positions in impact-parameter space (horizontal axis). The conventional numbering of the bins that we have chosen is also shown for $k = 1, 2, 3$.

where the $\delta^x_{(k,j)}$ are drawn according to the binomial distribution

$$\text{Proba}\left[\delta^x_{(k,j)}(t) = l\right] = \binom{n_{(k,j)}(t)}{l} (xdt)^l (1 - xdt)^{n_{(k,j)}(t)-l}. \tag{5.15}$$

This is a rather complicated equation which we do not know how to solve except numerically.

This model does not a priori look like a stochastic FKPP model. We may assume uniformity in impact parameter: This would amount to imposing the same δ^α and $\delta^{\beta/2}$ respectively for all j at any given k. In this case, the model would be projected to the FKPP class, but by definition, this would wash out the fluctuations between the different impact parameters. This simplified model, that we call "FIP" (for "Fixed Impact Parameter", since effectively, the model is completely defined by a single impact parameter) is nevertheless useful since it provides a benchmark to evaluate how the fluctuations between different impact parameters may alter the FKPP picture. In this paper, we will rely on (and check again in the case of our model) the conclusion reached in Ref. [117] that thanks to saturation, locally at each impact parameter, the full model is still well-described by a one-dimensional FKPP equation, and the fluctuations between different positions in impact-parameter space do not qualitatively change the picture.

Let us first apply the treatment of FKPP equations exposed in Chap. 4 to the FIP case. We know that the large-rapidity realizations of the model are stochastic traveling waves, whose main features can be determined from a simple analysis of the linear part of the evolution equation. In this model, only the number of dipoles n_k in the bins say $(k, 0)$ (i.e. at impact parameter $-\frac{1}{2}$) is relevant. The evolution equation reads[1]

$$n_k(t + dt) = \min\left[N, n_k(t) + \delta^\alpha_{k-1}(t) + \delta^\beta_{k+1}(t)\right]. \tag{5.16}$$

The mean-field (or Balitsky-Kovchegov) approximation to the evolution leads to the equation

$$n_k(t + dt) = \min\left[N, n_k(t) + \alpha dt\, n_{k-1}(t) + \beta dt\, n_{k+1}(t)\right], \tag{5.17}$$

[1] We could also write $2\delta^{\beta/2}_{k+1}(t)$ instead of the last term in Eq. (5.16). (This may even be a more literal implementation of the FIP approximation). But this would not make a large difference, which anyway, we would be unable to capture analytically.

where the n_k are now real functions of k. The linearized equation (equivalent to the BFKL equation) is simply obtained by discarding the "min" in the previous equation:

$$n_k(t+dt) = n_k(t) + \alpha dt\, n_{k-1}(t) + \beta dt\, n_{k+1}(t). \tag{5.18}$$

From standard arguments, we know that for asymptotically large t and N, the velocity of the wave front, that is the time derivative of the position $X(t)$ of the front, is given by

$$v_0 = \frac{dX}{dt} = \omega'(\gamma_c), \tag{5.19}$$

where $\omega(\gamma)$ is the eigenvalue of the kernel of the linearized evolution equation (5.18) corresponding to the eigenfunction $e^{-\gamma k}$, namely

$$\omega(\gamma) = \frac{1}{dt} \ln\left(1 + \alpha dt\, e^{\gamma} + \beta dt\, e^{-\gamma}\right), \tag{5.20}$$

and γ_c minimizes $\omega(\gamma)/\gamma$. We recall that dt may be finite or infinitesimal, in which case Eq. (5.20) is to be understood as the derivative of $\ln(1+\cdot)$ at the origin.

Our aim is to study the correlations between the point at position $b = -\frac{1}{2}$ in transverse space (left edge of the system, see Fig. 5.2) and the one at position $b = -\frac{1}{2} + \Delta b$ with $0 \leq \Delta b < 1$. We calculate the average of the squared difference of the positions of the front between these points, which is formally related to the two-point correlation function of (the logarithm of) the saturation scales, and which we deem a good estimator of the spatial fluctuations of the saturation scale. In the hierarchical model, all bins with index k less than or equal to $k_{\Delta b} \equiv 1 + [-\log_2 \Delta b]$ (the notation "$[\cdots]$" stands for the integer part) and $j = 0$ overlap both impact parameters, and thus the dipoles of size larger than $2^{-k_{\Delta b}}$ seen at these points are exactly the same. For $k > k_{\Delta b}$ instead, the bins seen at the two points are distinct and nonoverlaping. So in particular, in our model with $\beta = 0$, as soon as the position of the front at one point or at the other is larger than $k_{\Delta b}$, that is to say, as soon as there are of the order of N dipoles in the bin $(k_{\Delta b}, j = 0)$, then the evolutions are completely uncorrelated at the two points in the corresponding bins. (We expect that for finite β of order 1, the discussion would not be qualitatively changed.) This matches to the picture that we may infer for the QCD dipole model: The dipoles at two positions in impact-parameter space separated by a distance larger than the typical saturation scales in that region evolve (almost) independently towards larger rapidities. Note that choosing pairs of points around impact parameter 0, one with positive impact parameter and another one with negative impact parameter, would not satisfy this property, due to the rigidity of the sizes and positions of the dipoles. Indeed, these two points would decorrelate very soon in the evolution since their common ancestors necessarily sit in the bin $(k = 1, j = 0)$, see Fig. 5.2.

As a consequence of these features of QCD reproduced in the toy model, studying two-point correlations between points in impact-parameter space as a function of their distance Δb and of the time (=rapidity) t is equivalent to studying the time dependence of the correlations of the saturation scales of two realizations of the model whose evolutions are identical until the tip of the front reaches $k_{\Delta b}$. On the average, it takes a time $t_{\Delta b} = (k_{\Delta b} - 1)/v$, v being the mean velocity of the individual fronts, for the front whose tip is at $k_{\Delta b} = 1$ at the beginning of the evolution to have its tip at $k_{\Delta b}$. Then the bins such that $k > k_{\Delta b}$ evolve independently between the two realizations over the remaining time interval

$$\Delta t = t - t_{\Delta b}, \quad \text{with} \quad t_{\Delta b} = \frac{[-\log_2 \Delta b]}{v}. \tag{5.21}$$

Note that this is very close to assuming that the realizations are identical for $t \leq t_{\Delta b}$ and completely uncorrelated for $t > t_{\Delta b}$.

From this discussion, we see that the basic input of our calculation will be the mechanism for the propagation of a FKPP front which was explained in Chap. 4. We will review it in the next subsection, then we will proceed to the formulation of the calculation of the correlations.

5.2.2 Formulation of the calculation of the correlations

In line with the above discussion, we wish to compute the correlations of the position of two fronts whose evolutions are identical for $t \leq t_{\Delta b}$ and uncorrelated for $t > t_{\Delta b}$. Note that strictly speaking, we would need to keep the content of all bins $k \leq k_{\Delta b}$ identical between the two realizations at all times, even after time $t_{\Delta b}$. But these two formulations give quantitatively similar results.

Let us introduce $X(t_0, t)$ the position of the front at time t in the frame in which $X(t_0, t_0) = 0$. We focus on what happens slightly before the initial time t_0. According to the mechanism of front propagation explained in Chap. 4, on one hand, $X(t_0 - dt_0, t) = X(t_0, t) + v_{\rm BD} dt_0$ if no fluctuation has occurred between times $t_0 - dt_0$ and t_0, on the other hand, $X(t_0 - dt_0, t) = X(t_0, t) + v_{\rm BD} dt_0 + R(t - t_0, \delta)$ if a fluctuation has occurred at a position δ ahead of the front (which happens with probability $p(\delta) d\delta \, dt_0$). $v_{\rm BD}$ was defined in Eq. (4.52), $R(t, \delta)$ in Eq. (4.57) and $p(\delta)$ in Eq. (4.54). It is straightforward to write an equation for the generating function of the cumulants of X:

$$-\frac{d}{dt_0} \ln \left\langle e^{\lambda X(t_0,t)} \right\rangle = \lambda v_{\rm BD} + \int d\delta \, p(\delta) \left(e^{\lambda R(t-t_0,\delta)} - 1 \right). \tag{5.22}$$

One now considers two such independent fronts and add up the generating functions. One gets

$$-\frac{d}{dt_0} \ln \left(\left\langle e^{\lambda X_1(t_0,t)} \right\rangle \left\langle e^{-\lambda X_2(t_0,t)} \right\rangle \right) = \int d\delta \, p(\delta) \left(e^{\lambda R(t-t_0,\delta)} + e^{-\lambda R(t-t_0,\delta)} - 2 \right). \tag{5.23}$$

Expanding for λ close to 0, the coefficients of the second power of λ obey the equation

$$\frac{d}{dt} \left\langle (X_1 - X_2)^2 \right\rangle = 2 \int d\delta \, p(\delta) R^2(t - t_0, \delta), \tag{5.24}$$

where we have used the fact that X_1 and X_2 are independent random variables for $t > t_0$, and we have traded t_0 for t in the derivative, taking advantage of the fact that both $X_1 - X_2$ and R only depend on $t - t_0$. In practice, t_0 will be equal to $t_{\Delta b}$, the time at which the tip of the single front reaches $k_{\Delta b}$. From Eq. (5.21), this time is $[-\log_2 \Delta b]/v$.

We see that the basic ingredient is the time evolution of the shift of the front due to a forward fluctuation. This shift was given in Eq. (4.57). It involved the expression for ψ_δ in Eq. (4.46). In order to write a compact expression for R, it is interesting to note that ψ_δ is related to some Jacobi ϑ function [123]. Since

$$\vartheta_4(z|q) = 1 + 2 \sum_{n=1}^{\infty} (-1)^n \cos(2nz) q^{n^2}, \tag{5.25}$$

we may rewrite Eq. (4.46) as

$$\psi_\delta(y, \rho) = \frac{e^{\gamma_c \delta}}{2L^2} \frac{1}{q} \left[\vartheta_4 \left(\frac{\pi(\bar{a} + \rho)}{2} \middle| q \right) - \vartheta_4 \left(\frac{\pi(\bar{a} - \rho)}{2} \middle| q \right) \right]. \tag{5.26}$$

The notation

$$q \equiv e^{-\frac{\pi^2 y}{4}} = e^{-\frac{\pi^2 \omega''(\gamma_c) t}{2L^2}} \tag{5.27}$$

has been introduced. Using Eq. (4.57) and performing the appropriate expansion for small $\bar{a}$ and a, we arrive at an expression for $R(t, \delta)$ in terms of the ϑ_4-function which is particularly compact:

$$R(t, \delta) = \frac{1}{\gamma_c} \ln \left[1 - C_2 \frac{e^{\gamma_c \delta}}{2L^3} \partial_q \vartheta_4(0|q) \right], \tag{5.28}$$

with

$$-\partial_q \vartheta_4(0|q) = 2 \sum_{n=1}^{+\infty} (-1)^{n+1} n^2 q^{n^2 - 1}. \tag{5.29}$$

It is actually quite natural that the Jacobi theta functions appear, since the latter are defined as solutions of the one-dimensional heat equation with periodic boundary conditions.

We turn to the analysis of the obtained result. First, for large y, only the fundamental mode contributes significantly to ψ_δ. Looking back at Eq. (4.46), we see that higher harmonics would give a series of exponentially decreasing corrections. But at a finite time, a large number of modes have to be taken into account, typically all modes such that $n \leq (L/\pi)\sqrt{2/\omega''(\gamma_c)t}$. A few low-lying modes are not enough to describe the small-time behavior. Instead, it is a saddle point (in an appropriate integral reformulation) that dominates the sum (4.46). In this regime, it would be useful to find a way to write the series of harmonics such that at asymptotically large y, only the first term contributes instead of the whole series. This is actually possible using the Poisson summation formula

$$\sum_{n=-\infty}^{+\infty} f(n) = \sum_{k=-\infty}^{+\infty} \int dx\, f(x) e^{-2i\pi kx}. \tag{5.30}$$

In order to get $R(t,\delta)$, we need the value of ψ_δ at $\rho = a$. Hence we choose

$$f(x) = -\frac{e^{\gamma_c \delta}}{L^2} \sin \pi x \bar{a} \sin \pi x a\, q^{x^2-1} e^{i\pi x}. \tag{5.31}$$

We then perform the integral over x in the r.h.s. of Eq. (5.30). Introducing $\gamma_+ = \bar{a} + a$ and $\gamma_- = \bar{a} - a$, we get the following expression for ψ_δ:

$$\psi_\delta(y,a) = \frac{e^{\gamma_c\delta}}{4L^2} \frac{1}{q} \sqrt{\frac{\pi}{-\ln q}} \sum_{k=-\infty}^{+\infty} \left(e^{\frac{(2k-1+\gamma_+)^2\pi^2}{4\ln q}} + e^{\frac{(2k-1-\gamma_+)^2\pi^2}{4\ln q}} - e^{\frac{(2k-1+\gamma_-)^2\pi^2}{4\ln q}} - e^{\frac{(2k-1-\gamma_-)^2\pi^2}{4\ln q}} \right). \tag{5.32}$$

Since we eventually want to apply Eq. (4.57) in order to get an expression of the shift of the front, we expand the latter formula for $\bar{a}, a \ll 1$. The leading order reads

$$\psi_\delta(y,a) = \frac{\sqrt{\pi}}{2} \frac{e^{\gamma_c\delta}}{q(-\ln q)^{5/2}} \frac{\pi^2 \bar{a} a}{L^2} \sum_{k=1}^{+\infty} \left[\pi^2(2k-1)^2 + 2\ln q\right] e^{\frac{(2k-1)^2\pi^2}{4\ln q}}. \tag{5.33}$$

The shift of the front due to a fluctuation is obtained from ψ_δ with the help of Eq. (4.57):

$$R(t,\delta) = \frac{1}{\gamma_c} \ln \left\{ 1 + C_2 \frac{\sqrt{2} L^2 e^{\gamma_c\delta}}{(\pi\omega''(\gamma_c)t)^{5/2}} e^{\frac{\pi^2\omega''(\gamma_c)t}{2L^2}} \sum_{k=1}^{+\infty} \left[(2k-1)^2 - \frac{\omega''(\gamma_c)t}{L^2} \right] e^{-\frac{(2k-1)^2 L^2}{2\omega''(\gamma_c)t}} \right\}. \tag{5.34}$$

q is the function of t given by Eq. (5.27). This formula is extremely useful, since the series indexed by k converges fast. Even for moderately large values of t, a few terms accurately describe the whole function. This is actually the best formula for numerical evaluations of R.

We shall now examine the limit of small t ($y \ll 1$). Then only the term $k = 1$ has to be kept. The expression for R boils down to

$$R(t,\delta) = \frac{1}{\gamma_c} \ln \left(1 + C_2 \frac{\sqrt{2} e^{\gamma_c\delta} L^2}{(\pi\omega''(\gamma_c))^{5/2}} \frac{e^{-\frac{L^2}{2\omega''(\gamma_c)t}}}{t^{5/2}} \right). \tag{5.35}$$

As a final remark, let us note that the Poisson summation (5.30) that we have used to rewrite the series of harmonics corresponds to a Jacobi identity for the ϑ functions [123]. Equation (5.34) results from Eq. (5.28) with the replacement

$$-\partial_q \vartheta_4(0|q) = \frac{\sqrt{\pi}}{2} \frac{1}{q(-\ln q)^{5/2}} \sum_{k=1}^{+\infty} \left(\pi^2(2k-1)^2 + 2\ln q\right) e^{\frac{(2k-1)^2\pi^2}{4\ln q}}. \tag{5.36}$$

5.2.3 Analytical expression for the correlations

With the elements presented in the previous sections, we can write the expression for $\sigma_{12}^2 \equiv \langle (X_1 - X_2)^2 \rangle$. It is enough to insert the expression for the probability of fluctuations (Eq. (4.54)) and for the time-dependent shift (Eq. (5.28)) into Eq. (5.24):

$$\frac{d\sigma_{12}^2}{dt} = \frac{2C_1}{\gamma_c^2} \int_0^{+\infty} d\delta \, e^{-\gamma_c \delta} \ln^2 \left[1 - C_2 \frac{e^{\gamma_c \delta}}{2L^3} \partial_q \vartheta_4(0|q) \right], \tag{5.37}$$

where for $\partial_q \vartheta_4(0|q)$ we use either one of the equivalent expressions (5.29), (5.36) according to the limit that we want to investigate. We now have to fix the value of L. In Ref. [114], L was taken to be a constant. (The phenomenological model predicted $L = L_0 \equiv \ln N/\gamma_c$, but empirically, we saw that it was better to add a subdominant correction, namely $L = L_0 + \frac{3}{\gamma_c} \ln L_0 + \text{const.}$) In this case, a change of variable can be made in the integrand. All the parameters may be factored out, leaving us with a simple numerical integral to perform:

$$\int_0^{+\infty} \frac{dx}{x^2} \ln^2(1+x) = 2\zeta(2) = \frac{\pi^2}{3}. \tag{5.38}$$

Thus

$$\frac{d\sigma_{12}^2}{dt} = \frac{\pi^2 C_1 C_2}{3\gamma_c^3 L^3} \left[-\partial_q \vartheta_4(0|q) \right]. \tag{5.39}$$

Replacing the product of the unknown constants by Eq. (4.65) and q by Eq. (5.27) and integrating over the time variable between 0 and $\Delta t = t - t_{\Delta b}$, we arrive at a parameter-free expression for σ_{12}^2 as a function of Δt, namely

$$\sigma_{12}^2 = \frac{2\pi^2}{3\gamma_c^3 L} \int_{e^{-\frac{\pi^2 \omega''(\gamma_c)\Delta t}{2L^2}}}^1 \frac{dq}{q} \left[-\partial_q \vartheta_4(0|q) \right]. \tag{5.40}$$

We now investigate the two interesting limits, i.e. $\Delta t \gg L^2$ and $\Delta t \ll L^2$. For large Δt, the integral is dominated by the region $q \to 0$, thus $-\partial_q \vartheta_4(0|q)$ may be replaced by its value at $q = 0$ ($-\partial_q \vartheta_4(0|0) = 2$). Performing the remaining integration, we get

$$\sigma_{12}^2 \underset{\Delta t \gg L^2}{\sim} \frac{2\pi^4 \omega''(\gamma_c)}{3\gamma_c^3 L^3} \Delta t, \tag{5.41}$$

which is twice the second-order cumulant of the position of the front in a fixed impact-parameter model, see Eq. (4.66). For small Δt instead, say $L \ll \Delta t \ll L^2$, we use the expansion of $\partial_q \vartheta_4(0|q)$ for $q \to 1$, i.e. the first term in Eq. (5.36), which reads

$$\partial_q \vartheta_4(0|q) = -\frac{\sqrt{\pi}}{2} \frac{\pi^2 + 2\ln q}{q(-\ln q)^{5/2}} e^{\frac{\pi^2}{4 \ln q}}. \tag{5.42}$$

Equation (5.40) boils down to the following expression:

$$\sigma_{12}^2 \underset{\Delta t \ll L^2}{\sim} \frac{4}{3\gamma_c^3} \sqrt{\frac{2\pi^3}{\omega''(\gamma_c)\Delta t}} \exp\left(-\frac{L^2}{2\omega''(\gamma_c)\Delta t} \right). \tag{5.43}$$

So far, we have chosen the size of the front L constant, of the order of L_0. Another possible model for L would be to promote it to a function of δ at the level of Eq. (5.37), namely

$$L = L_0 + \delta + \text{const}, \tag{5.44}$$

where the constant has to be determined empirically. This choice takes maybe into account more accurately the extension of the front by δ generated by the fluctuations. The δ-integral cannot be performed analytically in Eq. (5.37) except in some limits, so a priori, there is no simpler

expression than Eq. (5.37). Thus we need to know the values of C_1 and C_2 individually. We can consider that $C_1 = \gamma_c$ is the natural normalization of the probability distribution $p(\delta)$. Then, we must set $C_2 = \pi^2 \omega''(\gamma_c)/\gamma_c$ in order to satisfy Eq. (4.65).

The above-mentioned two models, in which L is either constant or δ-dependent, differ by subleading terms in the large-L limit. Since the values of δ which dominate the δ-integral in Eq. (5.37) are of order $\frac{3}{\gamma_c} \ln L_0$, like the first correction to L_0 in the case of constant L, the models are not expected to differ significantly. We will check this statement numerically.

Scaling

Looking back at Eq. (5.40), we see that σ_{12}^2 has a nice scaling property. Indeed, we may rewrite the latter equation as

$$\sigma_{12}^2 = \frac{D}{\gamma_c(v_0 - v)} \int_{e^{-\gamma_c(v_0-v)\Delta t}}^{1} \frac{dq}{q} \left[-\partial_q \vartheta_4(0|q)\right] \tag{5.45}$$

in terms of the properties of a single front (its velocity v and the diffusion constant D whose analytical expressions were given in Eq. (4.52) and (4.66)), where v_0 can be read in Eq. (5.19). In particular, we have the following scaling:

$$\frac{\sigma_{12}^2}{D\Delta t} = \text{function}[(v_0 - v)\Delta t]. \tag{5.46}$$

From Eq. (5.43), we see that the function in the right-hand side is exponentially damped when its argument is smaller than 1, i.e. parametrically for $\Delta t \ll L^2$.

Once one knows the characteristics of the traveling waves in the FIP model (i.e. v and D), this scaling of the correlations is a pure prediction. Thus it will be interesting to check it in the numerical calculations.

Limits on the validity of the calculations

Let us try and evaluate the limits on the validity of our calculations. The latter were essentially based on the assumption that the eigenvalue $\gamma = \gamma_c$ of the kernel ω dominates. While this statement is clearly true at large times, when the traveling-wave front is well formed, it must break down at early times right after a fluctuation has occurred: Indeed, a fluctuation has an initial shape that is far from the one of the asymptotic front, see Fig. 4.10.

We wish to estimate the order of magnitude of the dispersion of the relevant eigenvalues about γ_c. To this aim, neglecting for the moment the boundary conditions and the prefactors, we write the solution of the general branching diffusion as

$$u(\Delta t, k) \sim \int d\gamma \, e^{-\gamma k + \omega(\gamma)\Delta t}. \tag{5.47}$$

The interesting values of k are the ones around the position of the wave front, therefore we write $k = v_0 \Delta t + \delta k$, where δk is of the order of the size L of the front. Expanding $\omega(\gamma)$ about γ_c, we write

$$u(\Delta t, v_0 \Delta t + \delta k) \sim e^{-\gamma_c \times \delta k} \int d(\delta\gamma) \, e^{-\delta\gamma \times \delta k + \frac{1}{2}\omega''(\gamma_c)(\delta\gamma)^2 \Delta t + \cdots}, \tag{5.48}$$

where $\delta\gamma = \gamma - \gamma_c$. It is clear from this equation that the relevant values of $\delta\gamma$ are of the order of $\delta k/(\omega''(\gamma_c)\Delta t)$. Since the order of magnitude of δk is the size L of the front, we would a priori conclude that the dispersion of γ around γ_c is small and hence that the calculation is valid as soon as $\Delta t \gg L$.

However, we have also expanded $\omega(\gamma)$ to second order. This means that for a generic kernel ω, we have neglected terms of the form $\frac{1}{6}\omega^{(3)}(\gamma_c)(\delta\gamma)^3 \Delta t \sim L^3/(\Delta t)^2$ (which would fit in the dots in Eq. (5.48)). The expansion is a good approximation if the latter term is small, i.e. if

$$\Delta t \gg L^{3/2}. \tag{5.49}$$

Back to impact-parameter space

So far, we have been working with the minimal model, consisting in two realizations of the FIP model which evolve in the same way until their common tip reaches $k_{\Delta b}$, and which decorrelate for $k > k_{\Delta b}$. The only relevant parameter which determined the decorrelation of the positions of the fronts of the realizations was the time $\Delta t = t - t_{\Delta b}$ after the tip had reached $k_{\Delta b}$. We now wish to discuss the transcription of the obtained results to impact-parameter space, which was our initial problem.

To this aim, we will of course make use of Eq. (5.21) to express $t_{\Delta b}$ with the help of the mean front velocity v. But we also need a length scale to which the distance in impact-parameter space Δb may be compared. The natural length is the dipole size at the position of the front, namely

$$l_s(t) = 2^{-X(t)} = l_s(t_{\Delta b}) 2^{-v\Delta t}. \tag{5.50}$$

On the other hand, according to Eq. (5.21) and disregarding the integer part operator, $-\log_2 \Delta b = k_{\Delta b}$ and the tip of the front $k_{\Delta b}$ is ahead of the bulk $X(t_{\Delta b})$ by L: $k_{\Delta b} = X(t_{\Delta b}) + L$. Using the previous equation, we may now express Δt as a function of Δb and of the length scale $l_s(t)$:

$$\Delta t = \frac{1}{v}\left[L + \log_2 \frac{\Delta b}{l_s(t)}\right]. \tag{5.51}$$

The scaling (5.46) reads

$$\sigma_{12}^2 \sim \frac{L + \log_2 \frac{\Delta b}{l_s(t)}}{L^3} \times \text{function}\left[\frac{L + \log_2 \frac{\Delta b}{l_s(t)}}{L^2}\right]. \tag{5.52}$$

This formula, together with the behavior of the scaling function (see Eq. (5.43)), shows that there is little b-dependence until $\log_2(\Delta b/l_s(t)) \sim L^2$, that is to say, until $\Delta b \sim l_s(t) e^{\text{const} \times L^2}$. In other terms, the size Δb of the domain around impact parameter b in which the fluctuations in the position of the fronts are negligible is, in notations more familiar to QCD experts,

$$\Delta b \sim \frac{e^{\text{const} \times \ln^2(1/\alpha_s^2)}}{Q_s(b)}, \tag{5.53}$$

where $Q_s(b)$ is the usual saturation momentum at impact parameter b. Note that since the fronts are statistically independent as soon as $\Delta b \times Q_s(b) > 1$, this result may seem a bit surprising: It says that the effective correlation length between different points in impact-parameter space is much larger than $1/Q_s(b)$ in the parametrical limit of small α_s.

5.2.4 Numerical simulations

In this section, we confront our analytical calculations to numerical simulations of the toy model. First, we consider the full model and test the validity of the assumption that the minimal model is a good approximation to the full model also for $\beta \sim 1$, i.e. when splittings to larger-size dipoles are authorized. Second, we compare the minimal model to the analytical results for the fluctuations between different positions in impact-parameter space (given essentially by Eqs. (5.37),(5.40)).

Full model

The model defined by Eqs. (5.14) and (5.15) is straightforward to implement numerically in the form of a Monte-Carlo event generator. The simplest is to store the number of dipoles in each bin in an array whose index i is related to k and j through $i = 2^{k-1} + j$. The splitting dynamics relates bin i to $2i$ (down left), $2i + 1$ (down right) and $[i/2]$ (up; the square brackets stand once again for the integer part).

We have to deal with an array whose size grows exponentially with time. It is thus very difficult to pick large values of t, and thus also large values of N. Indeed, the relevant time scale grows

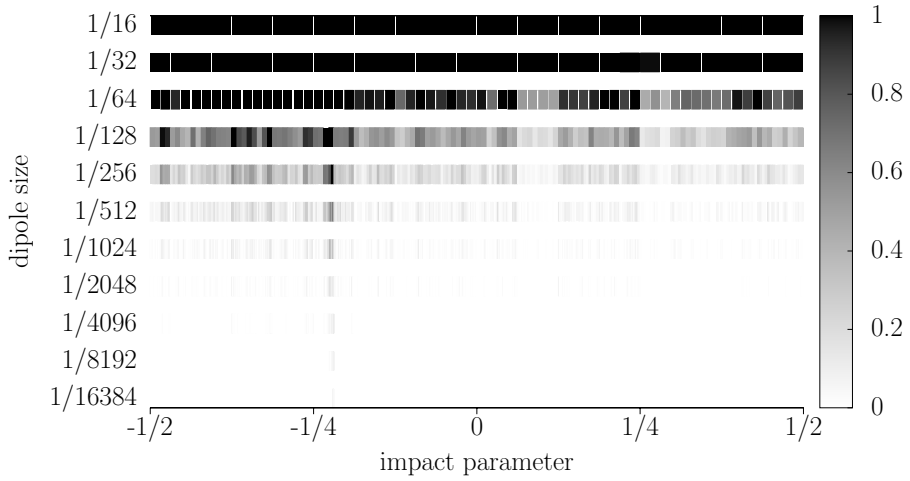

Figure 5.3: One event of the full model with $\alpha = \beta = 1$, $N = 100$ and $t - t_{\Delta b} = 4$. Only the bins $k \geq 5$ are represented. (The bins for $k < 5$ all contain N dipoles.) The number of dipoles in each bin is proportional to the blackness which is displayed. We see that in the transition region close to blackness, nearby bins are often of similar grey levels, which illustrates the statement that the density of gluons varies significantly only over scales which are larger than the relevant length scale $l_s(t)$ (see Eq. (5.50)).

with N like $\ln^2 N$, and consequently the minimum number of entries in the array one wants to consider grows like $e^{\ln^2 N}$. In practice, we limit ourselves to $t \leq 4$ and $N \leq 100$. As for the time step dt, the most convenient is to take it small but finite. We set $dt = 10^{-2}$.

We start with one particle and evolve it for a few hundred units of time using the FIP version of the model. We obtain a traveling wave front, whose tip we eventually label $k = 1$. (The complete front sits in the bins $k \leq 1$). From the initial condition built in this way, we evolve all bins for which $k < 1$ using the FIP model, and all bins for $k \geq 1$ using the full model. One event is shown in Fig. 5.3. Although N and t are small in this calculation, we see that the regions in impact-parameter space which have similar numbers of dipoles are larger than the local length scale $l_s(t)$ (see Eq. (5.50)).

After the evolution times $t = 3$ and $t = 4$ respectively, we measure the position of the front at various impact parameters on a uniform tight grid ranging from $-\frac{1}{2}$ to $+\frac{1}{2}$. We use the following definition of the position of the front:

$$X(\Delta b, t) = k_0 + \sum_{k=k_0+1}^{+\infty} \frac{n_{(k,[\Delta b \times 2^{k-1}])}(t)}{N} \tag{5.54}$$

where k_0 is the largest k for which $n_{(k,[\Delta b \times 2^{k-1}])} = N$. Note that in principle, we could have chosen $X(\Delta b, t) = k_0$. In practice however, because of the discreteness of k in our model, this choice would introduce artefacts which we do not expect in real QCD.

We compute the squared difference of the front positions between the impact parameters $-\frac{1}{2}$ and $-\frac{1}{2} + \Delta b$, and average over events. We plot the result as a function of $t + \log_2 \Delta b/v$, where v is the average front velocity measured at impact parameter $-\frac{1}{2}$.

We compare the results to the correlations obtained in the minimal model, i.e. when we consider two independent realizations of an initial front. We do not attempt to compare to our analytical

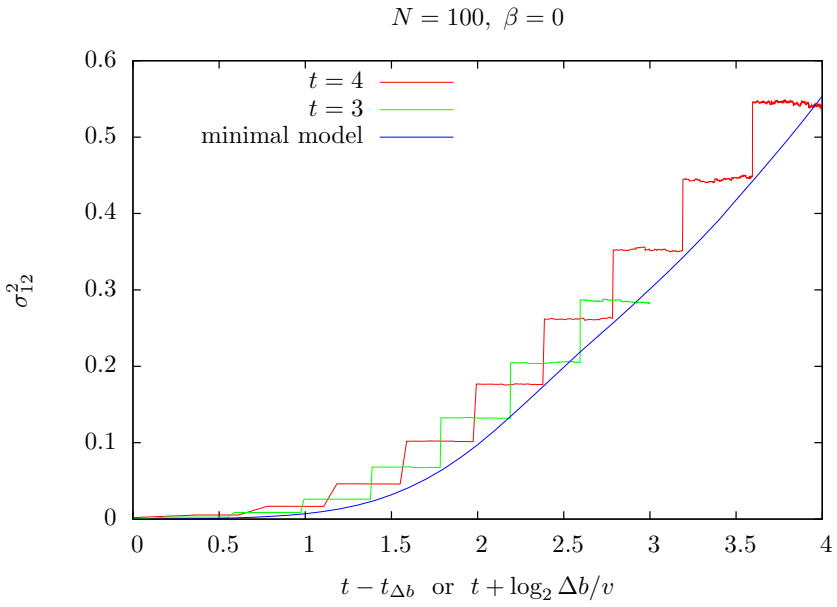

Figure 5.4: $\sigma_{12}^2 = \langle (X_1 - X_2)^2 \rangle$ as a function of $\Delta t = t - t_{\Delta b}$ in the full model with $\alpha = 1$ and $\beta = 0$ (lines with steps; one corresponds to an evolution time $t = 3$, the other one to $t = 4$) and in the minimal model. In the full model, $t_{\Delta b} = [-\log_2 \Delta b]/v$, where v is the measured velocity of the front at impact parameter $-\frac{1}{2}$. In the FIP model, $t_{\Delta b}$ is a fixed time, and corresponds to the time at which the tip of the front reaches $k_{\Delta b}$, the bin after which two uncorrelated evolutions take place.

formulas since the values of N that we are able to reach are too small for the approximations that we had to assume to be relevant.

The corresponding plot is displayed in Fig. 5.4 for $N = 100$, $\alpha = 1$, $\beta = 0$, and in Fig. 5.5 with the same parameters except $\beta = 2$. First, we see that in the full model, the graph of σ_{12}^2 exhibits steps, i.e. σ_{12}^2 is constant by parts. This is related to the hierarchical structure of the model: The correlations between $b = -\frac{1}{2}$ and any of the points at $b \geq 0$ are identical; The same is true for $-0.25 \leq b < 0$, $-0.375 \leq b < -0.25$ etc... The logarithmic b-scale on the t-axis makes the widths of the steps all equal. Next, we see that for small $t - t_{\Delta b}$ (i.e. impact parameters close to $-\frac{1}{2}$) there are very little fluctuations in the front positions.

Finally, we see that for $\beta = 0$, as anticipated, the full model and the minimal ones coincide almost perfectly (Fig. 5.4). For $\beta = 2$, i.e. when splittings towards larger dipole sizes are switched on and therefore new correlations appear beyond the ones taken into account in the minimal model, there are some quantitative differences for large t (Fig. 5.5). But we see that using the minimal model instead of the full model that keeps all impact parameters is a good approximation. This corroborates the conclusions of the work in Ref. [117].

Minimal model

We now set $\beta = 0$, in which case, as discussed earlier and as checked numerically, the model exactly reduces to a collection of one-dimensional FKPP-like models. Hence, in order to compute two-point correlation functions, it is enough to evolve two realizations of the corresponding FIP model with the constraint that all bins with $k \leq k_{\Delta b}$ be identical between the two realizations, and the bins $k > k_{\Delta b}$ be completely independent. Alternatively, we could also generate one single realization and evolve it for $t_{\Delta b}$ time steps, replicate it at time $t_{\Delta b}$, and then evolve the two replicas completely independently of each other. The difference between these two possible

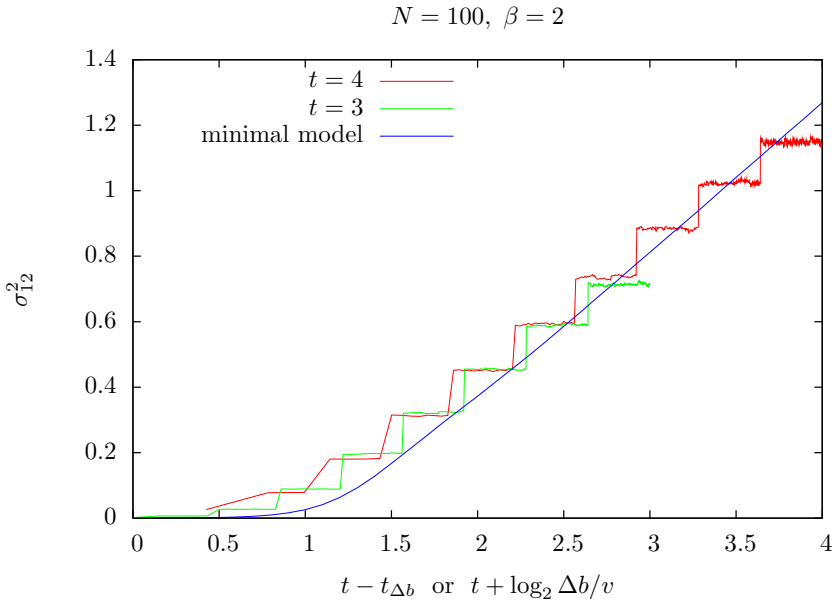

Figure 5.5: The same as in Fig. 5.4 but for $\beta = 2$.

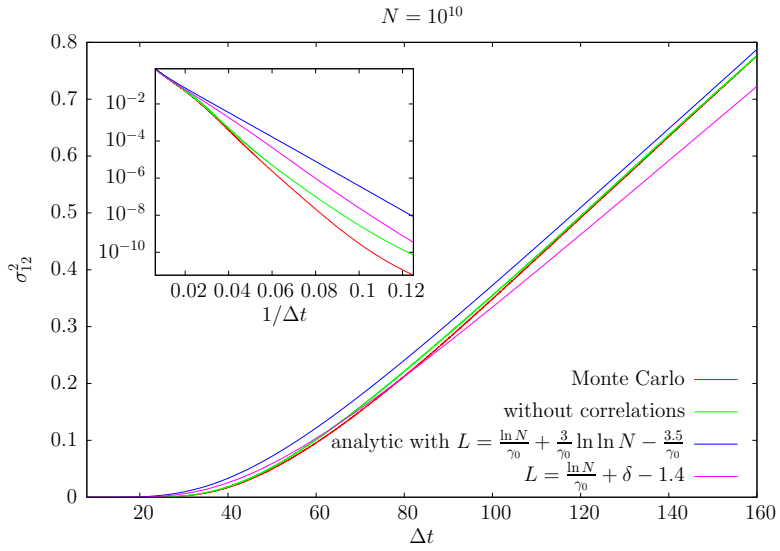

Figure 5.6: σ^2_{12} as a function of $\Delta t = t - t_{\Delta b}$ in the minimal model with $\beta = 0$ for $N = 10^{10}$. We display the results obtained within the model in which the realizations decorrelate in the bins $k > k_{\Delta b}$ (labelled "Monte Carlo"), and within the model in which the decorrelation is complete after time $t_{\Delta b}$ (labelled "without correlations"). The theoretical curves use Eq. (5.40) with the two possible choices for the front size L. *Inset:* The same, as a function of $1/\Delta t$ in order to highlight the small-Δt region where, as expected, important differences appear between the models.

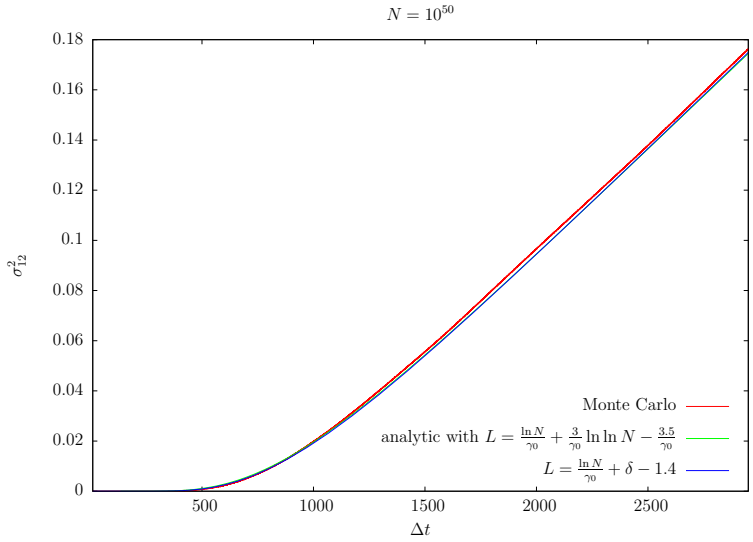

Figure 5.7: The same as in Fig. 5.6, for $N = 10^{50}$. All curves coincide almost perfectly.

implementations of the minimal model cannot be accounted for in our analytical calculations, thus the differences that we shall find numerically will give an indication of the model uncertainty. This time, our aim is essentially to check our analytical formulas, thus we will pick very large values of N, even if they appear to be unphysical in the QCD context since they would correspond to exponentially small values of the strong coupling constant α_s.

The parameters of the model are obtained from Eq. (5.20) with $\alpha = 1$, $\beta = 0$ and $dt = 10^{-2}$:

$$\gamma_c = 1.0136\cdots\ , \quad v_0 = 2.6817\cdots\ , \quad \omega''(\gamma_c) = 2.6098\cdots \tag{5.55}$$

These values are close to 1, e and e respectively, which would be the correct parameters if dt were infinitesimal, in which case $\omega(\gamma) = e^\gamma$ (see Eq. (5.20)).

The numerical results are shown in Fig. 5.6 for $N = 10^{10}$ with the two versions of the model (we generated about 10^5 realizations), and compared with the analytical predictions. We test the two possible choices for the size L of the front: Either L is a constant, which from our previous experience with FKPP traveling waves [114], we set to

$$L = \frac{1}{\gamma_c}\ln N + \frac{3}{\gamma_c}\ln\ln N - \frac{3.5}{\gamma_c} \tag{5.56}$$

(see e.g. Eq. (4.71)), or it is δ-dependent, namely

$$L = \frac{1}{\gamma_c}\ln N + \delta - 1.4. \tag{5.57}$$

The numerical constants, which are not determined in our theory, were chosen empirically so that they properly describe all numerical data for $N \geq 10^{10}$. In the first case, Eq. (5.40) is used. In the second case, Eq. (5.37) is integrated numerically over t and δ. We see that the agreement between the numerical calculation and the analytical predictions is good, except maybe for very small values of Δt where the calculations are not expected to be accurate. Indeed, for the same values of Δt, we also see in Fig. 5.6 a sizable discreapancy between the two versions of the minimal model. The calculations for $N = 10^{50}$ are shown in Fig. 5.7. The numerical results and the theoretical expectations (Eq. (5.40)) coincide almost perfectly.

For larger and more realistic values of α_s, the persistence of the correlations is still seen in the numerical simulations, but some parameters should be modified in the analytical expressions

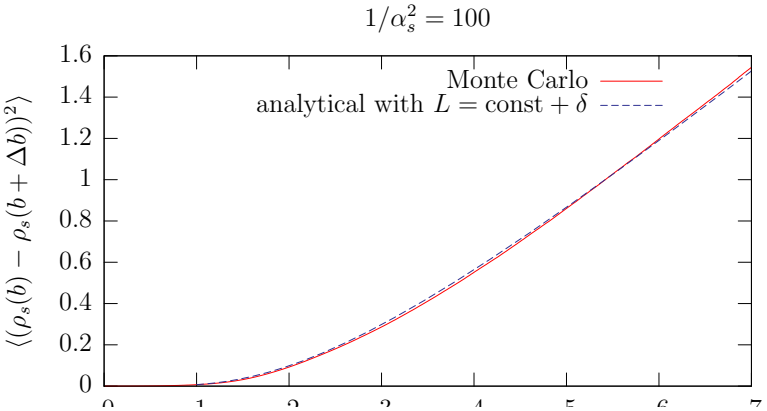

Figure 5.8: Comparison of a numerical Monte Carlo simulation and our analytical formula. The constant in the parameter L (see the text) which should be equal to $\ln(1/\alpha_s^2)/\gamma_0$ for very small α_s, has been shifted by a phenomenological constant. Once this is done, we get a very good agreement between the two calculations.

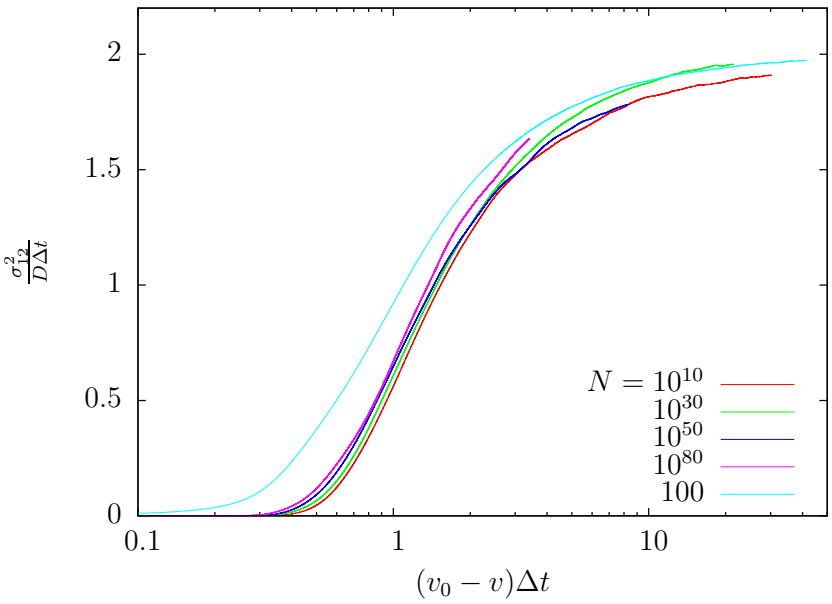

Figure 5.9: Numerical check of the scaling (5.46). The curves for the different values of N are very close together for $N \geq 10^{10}$, but the scaling seems to break down for low values of N (see the curve for $N = 100$), as expected.

and tuned to account for our lack of understanding of subleading corrections important for finite $\ln(1/\alpha_s^2)$. We show such a calculation for $\alpha_s = 0.1$ in Fig. 5.8, compared to a variant of Eq. (5.40).

Finally, we check that the scaling in Eq. (5.46) is well reproduced by the numerical data. The Monte-Carlo simulations are shown in Fig. 5.9, plotted in the appropriate scaling variables. The diffusion constant of a single wave front D as well as the velocity v are measured from the same data. We see that all curves nicely superimpose for $N \geq 10^{10}$ (we show data for values of N as large as 10^{80}), while there are clear deviations for smaller N (see the curve for $N = 100$), as expected.

Chapter 6

Phenomenological applications

In this chapter, we review the phenomenological consequences of the results obtained from the correspondence with statistical physics. We derive new properties of the QCD scattering amplitudes and discuss their impact on phenomenology.

Contents

As was stated in the Introduction, the initially unplanned opportunity to collect data in the high-energy regime of deep-inelastic scattering at HERA triggered a renewed interest in small-x physics among phenomenologists. The major discoveries in this regime is the (unexpected) important fraction of diffractive events, and a new scaling, *geometric scaling*, featured by total (and even semi-inclusive) cross-sections (see Fig. 1.1 in the Introduction).

In order to deal theoretically with the small-x regime, one needs new factorization theorems in order to single out the elements of the cross-sections that are computable in perturbation theory. High-energy, also called $k_\perp$-factorization [124–126], is the appropriate tool. A practical way to implement $k_\perp$-factorization is the color dipole model presented in Chap. 2.

6.1 Dipole models and geometric scaling

The main observable measured at HERA is the proton structure function F_2. It is proportional to the sum of the virtual photon-proton cross-section for a transversely and longitudinally polarized photon respectively.

A bare photon has no hadronic interactions, since it does not carry any color charge. However, it may easily fluctuate into a quark-antiquark pair, overall color-neutral, thus forming a color dipole. Subsequently, these dipoles interact with the target proton. This picture is represented by the following equations:

$$\begin{aligned} F_2(x,Q^2) &= \frac{Q^2}{4\pi^2\alpha_{\rm em}}\big(\sigma_T+\sigma_L\big), \\ \sigma_{T,L}(x,Q^2) &= \int dz d^2r\,|\Psi_{T,L}(z,r,Q^2)|^2\,\sigma_{\rm dipole}(x,r). \end{aligned} \tag{6.1}$$

Here, $\sigma_{T,L}$ are the photon-proton cross-sections for transversly and longitudinally polarized virtual photons. $\Psi_{T,L}$ are light-cone wavefunctions for γ^*, computable within QED (see, e.g., Ref. [28] for explicit expressions to lowest order in $\alpha_{\rm em}$). Furthermore, $\sigma_{\rm dipole}(x,r)$ is the cross-section for dipole–proton scattering (for a dipole of transverse size r), and encodes all the information about hadronic interactions (including unitarization effects). This cross-section is related to the

amplitude A discussed so far by an integration over the impact parameter. (Actually, A was the forward elastic amplitude; the optical theorem relates it to the total cross-section).

In Ref. [28, 29], the dipole cross-section was modeled as

$$\sigma_{\rm dipole}(x,r) \,=\, \sigma_0\Big(1-{\rm e}^{-r^2Q_s^2(x)/4}\Big), \tag{6.2}$$

where σ_0 is a hadronic cross-section: It stems from the integration over the impact parameter, when the impact parameter dependence is supposed to be uniform over a disk of radius $\sim\sqrt{\sigma_0}$. $Q_s(x)$ plays the role of the saturation momentum, parametrized as $Q_s^2(x)=(x_0/x)^\lambda\times 1\ {\rm GeV}^2$. Note that, by construction, this cross-section only depends on the combined variable $r^2Q_s^2(x)$ instead of r and x separately. This property is transmitted to the measured photon cross-sections $\sigma_{T,L}(x,Q^2)$, which then depend on $Q^2/Q_s^2(x)$ only (this scaling is slightly violated by the masses of the quarks). This is *geometric scaling*, predicted to be a feature of the solutions to the BK equation at large rapidity.

Historically, geometric scaling was discovered first in the data (see Ref. [30]), after Golec-Biernat and Wüsthoff (GBW) had written down their model: The latter happened to feature this scaling (up to small violations induced by the quark masses). There was no apparent need for finite rapidity scaling violations in the first HERA data. However, later analysis revealed that a significant amount of explicit scaling violations in the dipole cross-section, predicted by the BK equation, were actually required by more accurate data.

A now popular model that describes the HERA data in a way that takes a better account of the subasymptotics, beyond the GBW model, was formulated in Ref. [127]. The dipole scattering cross-section reads $\sigma_{\rm dipole}(x,r)=2\pi R^2\mathcal{N}(y,rQ_s)$, with

$$\mathcal{N}(y,rQ_s)=\begin{cases}\mathcal{N}_0\,\Big(\frac{r^2Q_s^2}{4}\Big)^{\gamma_c+\frac{\ln(2/rQ_s)}{\kappa\lambda Y}} & \text{for}\quad rQ_s\le 2,\\ 1-{\rm e}^{-a\ln^2(b\,rQ_s)} & \text{for}\quad rQ_s>2,\end{cases} \tag{6.3}$$

where $Q_s\equiv Q_s(x)=(x_0/x)^{\lambda/2}$ GeV. The expression for the cross-section for r small compared to $2/Q_s$ corresponds to the solution of the BK equation (compare to Eq. (4.22) with the help of Tab. 2.1), in which we substituted $\omega(\gamma_c)=\omega(\gamma_c)$ and $\omega''(\gamma_c)=\omega''(\gamma_c)$ by the parameters λ and κ that we subsequently fit to the data. The expression in the second line also has the correct functional form for $r\gg 2/Q_s$, as obtained by solving the BK equation [33]. This is strictly valid only to leading-order accuracy, but here it is used merely as a convenient interpolation towards the 'black disk' limit $\mathcal{N}=1$. (The details of this interpolation are unimportant for the calculation of σ_{γ^*p}.) The coefficients a and b are determined uniquely from the condition that $\mathcal{N}(rQ_s,Y)$ and its slope be continuous at $rQ_s=2$. The overall factor $\mathcal{N}_0$ in the first line of Eq. (6.3) is ambiguous, reflecting an ambiguity in the definition of Q_s. This model fits well all HERA data for structure functions, in the range $x\le 10^{-2}$. All details may be found in Ref. [127].

The model explicitely breaks geometric scaling. However, effectively, geometric scaling remains a fairly good symmetry of the model, as required by the data. The small finite-rapidity scaling violations are needed to describe accurately the high-precision HERA data.

The model may also accomodate less inclusive observables, such as diffraction [128]. It has been improved recently by including heavy quarks [129] (The crucial need for taking account of the charm quark was emphasized in Ref. [130]). An impact-parameter dependence was also introduced [131–133] that was already missing in the GBW model.

The range of validity of dipole models has been re-examined recently [134].

6.2 Diffusive scaling

At still higher energies, according to the discussion of Chap. 4, one expects the saturation scale to acquire a dispersion from event to event that scales with the rapidity like $\sqrt{\bar\alpha y}$ when rapidity increases. Although this dispersion is not an observable since there is no way to measure the

saturation scale of an individual event, it manifests itself in the total cross-section in the form of a new scaling, different from geometric scaling.

The physical amplitude for the scattering of a dipole of size r off some target is given by the average of all realizations of the evolution at a given y:

$$A(y,r) = \langle T(r) \rangle|_y. \tag{6.4}$$

For large enough rapidities and small enough α_s, these realizations are exponentially decaying fronts in the variable $\rho = \ln(1/r^2)$, fully characterized by a stochastic saturation scale, or rather its logarithm $\rho_s = \ln Q_s^2(y)$. For the purpose of the present discussion, it may be approximated in the same way as in Eq. (5.2), namely

$$T(\rho) = \theta(\rho_s - \rho) + \theta(\rho - \rho_s) e^{-\gamma_c(\rho - \rho_s)}. \tag{6.5}$$

The statistics of ρ_s is given by Eqs. (4.64),(4.66) (up to the replacements suggested in Tab. 2.1 to go from a generic reaction-diffusion to QCD). At ultrahigh energies (and very small α_s), it is essentially a Gaussian centered at

$$\langle \rho_s \rangle = \left(\frac{\omega(\gamma_c)}{\gamma_c} - \frac{\pi^2 \gamma_c \omega''(\gamma_c)}{2\left(\ln(1/\alpha_s^2) + 3\ln\ln(1/\alpha_s^2)\right)^2} \right) \bar{\alpha} y \tag{6.6}$$

and of variance

$$\sigma^2 = \langle \rho_s^2 \rangle - \langle \rho_s \rangle^2 = \frac{\pi^4 \omega''(\gamma_c)}{3\ln^3(1/\alpha_s^2)} \bar{\alpha} y. \tag{6.7}$$

The scattering amplitude may be expressed by the simple formula

$$A(y,\rho) = \frac{1}{\sigma\sqrt{2\pi}} \int d\rho_s \, T(\rho)|_y \exp\left(\frac{(\rho_s - \langle \rho_s \rangle)^2}{2\sigma^2} \right). \tag{6.8}$$

The most remarkable feature of this amplitude is the scaling form for A that it yields:

$$A(y,\rho) = A\left(\frac{\rho - \langle \rho_s(y) \rangle}{\sqrt{\bar{\alpha} y / \ln^3(1/\alpha_s^2)}} \right). \tag{6.9}$$

This equation may be obtained by performing the integration in Eq. (6.8) after the replacement of T by its approximation (6.5). This scaling obviously violates geometric scaling: If the latter scaling were satisfied, then A would be a function of $\rho - \langle \rho_s(y) \rangle$ only.

In Ref. [40], Mueller and Shoshi had already noted that geometric scaling had to be violated beyond the BK equation. However, the square root in the denominator of the scaling variable in Eq. (6.9) was missing because their approach was relying on mean field throughout, thus missing the stochastic nature of the evolution.

This new scaling is a firm prediction of the correspondence with statistical physics. However, it may not be tested at particle colliders in a simple way. Let us work out the order of magnitude of the rapidity needed for the different effects (saturation, geometric scaling, diffusive scaling) to show up. The rapidity that is needed to reach saturation is roughly

$$y_{\mathrm{BFKL}} \sim \frac{\ln(1/\alpha_s^2)}{\bar{\alpha}\omega(\frac{1}{2})}. \tag{6.10}$$

The BK picture is expected to be valid until the asymptotic exponential shape of the front has diffused down to the point where the amplitude becomes of the order of α_s^2. This additional rapidity needed to get to the regime of geometric scaling is thus given by Eq. (4.37) once the appropriate replacements have been done

$$y_{\mathrm{BK}} \sim \frac{1}{2\bar{\alpha}\omega''(\gamma_c)} \left[\frac{\ln(1/\alpha_s^2)}{\gamma_c} \right]^2, \tag{6.11}$$

and finally, the effect of the fluctuations of the saturation scale gets important at the rapidity

$$y_{\rm fluct} \sim \frac{3\ln^3(1/\alpha_s^2)}{\bar{\alpha}\pi^3\omega''(\gamma_c)}. \tag{6.12}$$

The relevant parameters in QCD are deduced from the BFKL kernel. They read

$$\gamma_c = 0.627549, \quad \omega(\gamma_c) = 3.0645, \quad \omega''(\gamma_c) = 48.5176. \tag{6.13}$$

For some realistic strong coupling constant, $\alpha_s \sim 0.2$, we get

$$y_{\rm BFKL} \sim 6.07879\ , \quad y_{\rm BK} \sim 1.41965\ , \quad y_{\rm fluct} \sim 0.348244. \tag{6.14}$$

Given that rapidities in the small-x regime at HERA were of the order of 10, and will be of the order of 15 at the LHC, these figures indicate that we may observe these effects. However, there are many criticism to these naive estimates.

First, the values of the rapidity that delimitate the different regimes are largely underestimated given that they rely on the leading-order BFKL kernel, which predicts a much too large growth of the cross-section with the rapidity and a too fast diffusion (see the large value of $\omega''(\gamma_c)$). Already the effect of the running coupling, which should be taken into account in any detailed phenomenological study, is expected to still reduce the effects of the fluctuations [135].

Next, one also has to keep in mind that the former estimates should only hold for very small values of α_s, such that $\ln 1/\alpha_s^2 \gg 1$ which is certainly not true in real-life QCD. Note that asymptotically, one should have $y_{\rm fluct} \gg y_{\rm BK} \gg y_{\rm BFKL}$. The fact that the order is inverted means that the quantitative results obtained within the phenomenological model for front propagation should not be trusted for values of α_s as "large" as 0.2.

Nevertheless, the effect of diffusive scaling (i.e. of the event-by-event fluctuations of the saturation scale) on observables has already been investigated in some detail by several groups. Diffractive amplitudes were studied in Ref. [136]. The ratio of the gluon distribution in a nucleus to the same quantity in a proton was computed in Ref. [137].

Chapter 7

Conclusion and outlook

We have reviewed a peculiar way of viewing high-energy scattering in QCD, based on the physics of the parton model, and its strong similarities with reaction-diffusion processes (Chap. 2). The correspondence is best summarized in the mapping of Tab. 2.1. We have seen that the equations that describe the dynamics of these processes are in the universality class of the stochastic FKPP equation, and admit traveling-wave solutions whose features are likely to be universal, in such a way that a study of simple reaction-diffusion-like models may lead to exact asymptotic results also for QCD scattering amplitudes. Understanding the very mechanism of traveling wave formation and front propagation was crucial to see how the universality may come about (see Chap. 4).

In zero-dimensional stochastic models, we could perform exact calculations and get analytical results within different formulations (Chap. 3). We understood that analyzing the structure of single events was technically much simpler if one wants to get leading orders at large N ($= 1/\alpha_s^2$), since in individual realizations, one may factorize the fluctuating part from the nonlinear effects. Thanks to this observation, in one-dimensional models which admit realizations in the form of stochastic traveling waves, we could also get precise analytical results on the form and shape of the traveling waves, which are presumably exact asymptotically (Chap. 4). Universality enables one to make statements on the form of the QCD scattering amplitudes at very high energies. Appropriate extensions of the relevant statistical models which incorporate an additional dimension lead to predictions for the correlations in the transverse plane (Chap. 5). Some of these results turn into firm phenomenological predictions (Chap. 6), which however do not seem to be testable at colliders in the near future. Nevertheless, getting new analytical results for QCD in some limit is always an interesting achievement, given the complexity of the theory. Furthermore, while our analytical results only apply for exponentially small α_s ($\ln(1/\alpha_s^2) \gg 1$), the picture itself should be valid in the whole perturbative range, namely for $\alpha_s^2 \ll 1$.

Prospects. There are still many open questions. On the statistical physics side, the statistics of the front position that we have found has not been derived rigorously, but rather guessed, and rely on many quite ad hoc conjectures. We got confidence on the validity of our conjectures on the basis of numerical simulations. Moreover, although we expect universality up to corrections of order $1/N$ (that is to say $\mathcal{O}(\alpha_s^2)$ in QCD), we could only get analytical expressions relative to the cumulants of the position of the front for the first terms in an expansion in powers of $1/\ln N$, which extremely large values of N (small α_s) to be valid. But on a more general footing, the sFKPP equation seems to describe many physical, chemical or biological problems (in particular population evolution with selection in evolutionary biology). We have also found recently an explicit analogy with the theory of spin glasses [138, 139]. This large universality is maybe the strongest incentive to try and find more accurate solutions to that kind of equations.

On the QCD side, the correspondence with reaction-diffusion processes strongly relies on the assumption that there is saturation of some form of the quark and gluon densities in the hadronic wave functions. While this is a reasonable guess that few experts would challenge, it is clear that we cannot consider that the problem is solved before the saturation mechanism at work in QCD

has been exhibited. QCD is formulated as a quantum field theory. To see the similarity with reaction-diffusion, we basically needed to translate it into the parton model first. It would be better to recover the results of Chap. 4 (and hopefully get more) directly from field theory [59], as one could do it in the zero-dimensional model introduced in Chap. 3. This requires to understand the strong field regime of field theory. This is an exciting challenge for both particle physicists and statistical physicists.

Let us finally state our personal prospects in the field. First, we wish to go back to the simple Balitsky-Kovchegov equation and study in more detail the properties of its solutions. It is important for phenomenology, since it seems that in the range of energy that may be reached at experiments, effects described by more advanced equations (incorporating genuine saturation effects, as discussed at length in previous chapters) are likely to be negligible. Interestingly, since the BK equation also represents the statistical properties of the tip of a random walk (see Chap. 4 and the recent paper [107]), some fine properties of scattering amplitudes may be inferred from the study of the latter. Work is in progress in this direction in collaboration with Al Mueller.

On the pure statistical physics side, we wish to pursue the study of simple models like the ones presented in Chap. 3, which could be of some interest in the interdisciplinary field of population evolution studies.

Last, if the formalism of the dipole model on which relies most our work in QCD seems well-suited for electron-proton or nucleus high-energy scattering, most of the experimental data which will become available in the next decade are about proton and nucleus interactions at the Large Hadron Collider (LHC). The new challenge to phenomenologists is to formulate and compute observables in this context. It seems that quadrupoles play an important role for all interesting observables, see e.g. Ref. [140]. Recently, we made a first step in the direction of computing the evolution of such objects with the energy [141] and we will pursue in this promising direction. An interesting theoretical question in the continuation of our work would be, for example, if the correlations computed in Chap. 5 would show up in the evolution of these quadrupoles and hence in the corresponding observables measured at the LHC.

Bibliography

[1] S. Munier, Phys. Rept. **473**, 1-49 (2009).

[2] T. Muta, Foundations of quantum chromodynamics. Second edition, World Sci. Lect. Notes Phys. 57 (1998) 1–409.

[3] V. N. Gribov, L. N. Lipatov, Deep inelastic e p scattering in perturbation theory, Sov. J. Nucl. Phys. 15 (1972) 438–450.

[4] Y. L. Dokshitzer, Calculation of the Structure Functions for Deep Inelastic Scattering and e+ e- Annihilation by Perturbation Theory in Quantum Chromodynamics. (In Russian), Sov. Phys. JETP 46 (1977) 641–653.

[5] G. Altarelli, G. Parisi, Asymptotic Freedom in Parton Language, Nucl. Phys. B126 (1977) 298.

[6] L. N. Lipatov, Reggeization of the Vector Meson and the Vacuum Singularity in Nonabelian Gauge Theories, Sov. J. Nucl. Phys. 23 (1976) 338–345.

[7] E. A. Kuraev, L. N. Lipatov, V. S. Fadin, The Pomeranchuk Singularity in Nonabelian Gauge Theories, Sov. Phys. JETP 45 (1977) 199–204.

[8] I. I. Balitsky, L. N. Lipatov, The Pomeranchuk Singularity in Quantum Chromodynamics, Sov. J. Nucl. Phys. 28 (1978) 822–829.

[9] M. Ciafaloni, G. Camici, Energy scale(s) and next-to-leading BFKL equation, Phys. Lett. B430 (1998) 349–354.

[10] V. S. Fadin, L. N. Lipatov, BFKL pomeron in the next-to-leading approximation, Phys. Lett. B429 (1998) 127–134.

[11] L. D. McLerran, The color glass condensate and small x physics: 4 lectures, Lect. Notes Phys. 583 (2002) 291–334.

[12] E. Iancu, R. Venugopalan, The color glass condensate and high energy scattering in QCD in: R.C. Hwa and X.-N. Wang, Editors, Quark-Gluon Plasma 3, World Scientific, Singapore (2003).

[13] L. V. Gribov, E. M. Levin, M. G. Ryskin, Singlet Structure Function at Small x: Unitarization of Gluon Ladders, Nucl. Phys. B188 (1981) 555–576.

[14] L. V. Gribov, E. M. Levin, M. G. Ryskin, Semihard Processes in QCD, Phys. Rept. 100 (1983) 1–150.

[15] A. H. Mueller, J.-w. Qiu, Gluon Recombination and Shadowing at Small Values of x, Nucl. Phys. B268 (1986) 427.

[16] L. D. McLerran, R. Venugopalan, Computing quark and gluon distribution functions for very large nuclei, Phys. Rev. D49 (1994) 2233–2241.

[17] L. D. McLerran, R. Venugopalan, Gluon distribution functions for very large nuclei at small transverse momentum, Phys. Rev. D49 (1994) 3352–3355.

[18] L. D. McLerran, R. Venugopalan, Green's functions in the color field of a large nucleus, Phys. Rev. D50 (1994) 2225–2233.

[19] I. Balitsky, Operator expansion for high-energy scattering, Nucl. Phys. B463 (1996) 99–160.

[20] J. Jalilian-Marian, A. Kovner, A. Leonidov, H. Weigert, The BFKL equation from the Wilson renormalization group, Nucl. Phys. B504 (1997) 415–431.

[21] J. Jalilian-Marian, A. Kovner, A. Leonidov, H. Weigert, The Wilson renormalization group for low x physics: Towards the high density regime, Phys. Rev. D59 (1998) 014014.

[22] E. Iancu, A. Leonidov, L. D. McLerran, The renormalization group equation for the color glass condensate, Phys. Lett. B510 (2001) 133–144.

[23] E. Iancu, A. Leonidov, L. D. McLerran, Nonlinear gluon evolution in the color glass condensate. I, Nucl. Phys. A692 (2001) 583–645.

[24] H. Weigert, Unitarity at small Bjorken x, Nucl. Phys. A703 (2002) 823–860.

[25] Y. V. Kovchegov, Small-x F2 structure function of a nucleus including multiple pomeron exchanges, Phys. Rev. D60 (1999) 034008.

[26] Y. V. Kovchegov, Unitarization of the BFKL pomeron on a nucleus, Phys. Rev. D61 (2000) 074018.

[27] A. H. Mueller, Soft gluons in the infinite momentum wave function and the BFKL pomeron, Nucl. Phys. B415 (1994) 373–385.

[28] K. J. Golec-Biernat, M. Wusthoff, Saturation effects in deep inelastic scattering at low Q**2 and its implications on diffraction, Phys. Rev. D59 (1999) 014017.

[29] K. J. Golec-Biernat, M. Wusthoff, Saturation in diffractive deep inelastic scattering, Phys. Rev. D60 (1999) 114023.

[30] A. M. Stasto, K. J. Golec-Biernat, J. Kwiecinski, Geometric scaling for the total gamma* p cross-section in the low x region, Phys. Rev. Lett. 86 (2001) 596–599.

[31] C. Marquet, L. Schoeffel, Geometric scaling in diffractive deep inelastic scattering, Phys. Lett. B639 (2006) 471–477.

[32] E. Levin, K. Tuchin, Solution to the evolution equation for high parton density QCD, Nucl. Phys. B573 (2000) 833–852.

[33] E. Levin, K. Tuchin, New scaling at high energy DIS, Nucl. Phys. A691 (2001) 779–790.

[34] N. Armesto, M. A. Braun, Parton densities and dipole cross-sections at small x in large nuclei, Eur. Phys. J. C20 (2001) 517–522.

[35] K. J. Golec-Biernat, L. Motyka, A. M. Stasto, Diffusion into infra-red and unitarization of the BFKL pomeron, Phys. Rev. D65 (2002) 074037.

[36] A. H. Mueller, D. N. Triantafyllopoulos, The energy dependence of the saturation momentum, Nucl. Phys. B640 (2002) 331–350.

[37] R. A. Fisher, Ann. Eugenics 7 (1937) 355.

[38] A. Kolmogorov, I. Petrovsky, N. Piscounov, Moscou Univ. Bull. Math. A1 (1937) 1.

[39] S. Munier, R. B. Peschanski, Geometric scaling as traveling waves, Phys. Rev. Lett. 91 (2003) 232001.

[40] A. H. Mueller, A. I. Shoshi, Small-x physics beyond the Kovchegov equation, Nucl. Phys. B692 (2004) 175–208.

[41] E. Iancu, A. H. Mueller, S. Munier, Universal behavior of QCD amplitudes at high energy from general tools of statistical physics, Phys. Lett. B606 (2005) 342–350.

[42] N. N. Nikolaev, B. G. Zakharov, Colour transparency and scaling properties of nuclear shadowing in deep inelastic scattering, Z. Phys. C49 (1991) 607–618.

[43] N. Nikolaev, B. G. Zakharov, Pomeron structure function and diffraction dissociation of virtual photons in perturbative QCD, Z. Phys. C53 (1992) 331–346.

[44] C. Ewerz, O. Nachtmann, Towards a Nonperturbative Foundation of the Dipole Picture: I. Functional Methods, Annals Phys. 322 (2007) 1635–1669.

[45] C. Ewerz, O. Nachtmann, Towards a Nonperturbative Foundation of the Dipole Picture: II. High Energy Limit, Annals Phys. 322 (2007) 1670–1726.

[46] L. N. Lipatov, The Bare Pomeron in Quantum Chromodynamics, Sov. Phys. JETP 63 (1986) 904–912.

[47] I. Balitsky, Factorization for high-energy scattering, Phys. Rev. Lett. 81 (1998) 2024–2027.

[48] I. Balitsky, Factorization and high-energy effective action, Phys. Rev. D60 (1999) 014020.

[49] E. Levin, M. Lublinsky, Balitsky's hierarchy from Mueller's dipole model and more about target correlations, Phys. Lett. B607 (2005) 131–138.

[50] K. Rummukainen, H. Weigert, Universal features of JIMWLK and BK evolution at small x, Nucl. Phys. A739 (2004) 183–226.

[51] Z. Chen, A. H. Mueller, The Dipole picture of high-energy scattering, the BFKL equation and many gluon compound states, Nucl. Phys. B451 (1995) 579–604.

[52] Y. V. Kovchegov, A. H. Mueller, S. Wallon, Unitarity corrections and high field strengths in high energy hard collisions, Nucl. Phys. B507 (1997) 367–378.

[53] A. H. Mueller, G. P. Salam, Large multiplicity fluctuations and saturation effects in onium collisions, Nucl. Phys. B475 (1996) 293–320.

[54] E. Avsar, G. Gustafson, L. Lonnblad, Energy conservation and saturation in small-x evolution, JHEP 07 (2005) 062.

[55] E. Avsar, G. Gustafson, L. Lonnblad, Small-x dipole evolution beyond the large-N(c) limit, JHEP 01 (2007) 012.

[56] A. H. Mueller, Parton saturation: An overview, in: QCD perspectives on hot and dense matter, edited by J.-P. Blaizot and E. Iancu. Dordrecht, The Netherlands, Kluwer, 2002. 522p. (NATO Science Series, II, Mathematics, Physics, and Chemistry, Vol. 87), `arxiv:hep-ph/0111244`.

[57] A. H. Mueller, Small x Behavior and Parton Saturation: A QCD Model, Nucl. Phys. B335 (1990) 115.

[58] A. H. Mueller, Parton saturation at small x and in large nuclei, Nucl. Phys. B558 (1999) 285–303.

[59] S. Munier, F. Schwennsen, Resummation of projectile-target multiple scatterings and parton saturation, Phys. Rev. D78 (2008) 034029.

[60] J. R. Forshaw, D. A. Ross, Quantum chromodynamics and the pomeron, Cambridge Lect. Notes Phys. 9 (1997) 1–248.

[61] R. Kirschner, L. N. Lipatov, L. Szymanowski, Effective action for multi - Regge processes in QCD, Nucl. Phys. B425 (1994) 579–594.

[62] R. Kirschner, L. N. Lipatov, L. Szymanowski, Symmetry properties of the effective action for high- energy scattering in QCD, Phys. Rev. D51 (1995) 838–855.

[63] L. N. Lipatov, Gauge invariant effective action for high-energy processes in QCD, Nucl. Phys. B452 (1995) 369–400.

[64] E. N. Antonov, L. N. Lipatov, E. A. Kuraev, I. O. Cherednikov, Feynman rules for effective Regge action, Nucl. Phys. B721 (2005) 111–135.

[65] J. P. Blaizot, E. Iancu, K. Itakura, D. N. Triantafyllopoulos, Duality and Pomeron effective theory for QCD at high energy and large N(c), Phys. Lett. B615 (2005) 221–230.

[66] Y. Hatta, E. Iancu, L. McLerran, A. Stasto, D. N. Triantafyllopoulos, Effective Hamiltonian for QCD evolution at high energy, Nucl. Phys. A764 (2006) 423–459.

[67] J. Bartels, Unitarity corrections to the Lipatov pomeron and the small x region in deep inelastic scattering in QCD, Phys. Lett. B298 (1993) 204–210.

[68] J. Bartels, Unitarity corrections to the Lipatov pomeron and the four gluon operator in deep inelastic scattering in QCD, Z. Phys. C60 (1993) 471–488.

[69] J. Bartels, C. Ewerz, Unitarity corrections in high-energy QCD, JHEP 09 (1999) 026.

[70] C. Ewerz, V. Schatz, How pomerons meet in coloured glass, Nucl. Phys. A736 (2004) 371–404.

[71] B. Derrida, H. Spohn, Polymers on disordered trees, spin glasses and traveling waves, J. Stat. Phys. 51 (1988) 817–840.

[72] W. van Saarloos, Front propagation into unstable states, Physics Reports 386 (2003) 29.

[73] R. Enberg, Traveling waves and the renormalization group improved Balitsky-Kovchegov equation, Phys. Rev. D75 (2007) 014012.

[74] R. Enberg, K. J. Golec-Biernat, S. Munier, The high energy asymptotics of scattering processes in QCD, Phys. Rev. D72 (2005) 074021.
URL `http://www.isv.uu.se/~enberg/BK/`

[75] D. Panja, Effects of fluctuations on propagating fronts, Physics Reports 393 (2004) 87.

[76] E. Iancu, D. N. Triantafyllopoulos, A Langevin equation for high energy evolution with pomeron loops, Nucl. Phys. A756 (2005) 419–467.

[77] A. H. Mueller, A. I. Shoshi, S. M. H. Wong, Extension of the JIMWLK equation in the low gluon density region, Nucl. Phys. B715 (2005) 440–460.

[78] E. Iancu, D. N. Triantafyllopoulos, Non-linear QCD evolution with improved triple-pomeron vertices, Phys. Lett. B610 (2005) 253–261.

[79] E. Iancu, G. Soyez, D. N. Triantafyllopoulos, On the probabilistic interpretation of the evolution equations with Pomeron loops in QCD, Nucl. Phys. A768 (2006) 194–221.

[80] G. P. Salam, Multiplicity distribution of color dipoles at small x, Nucl. Phys. B449 (1995) 589–604.

[81] G. P. Salam, Studies of Unitarity at Small-x Using the Dipole Formulation, Nucl. Phys. B461 (1996) 512–538.

[82] G. P. Salam, OEDIPUS: Onium evolution, dipole interaction and perturbative unitarisation simulation, Comput. Phys. Commun. 105 (1997) 62–76.

[83] M. Doi, J. Phys. A 9 (1976) 1479.

[84] L. Peliti, J. Phys. (Paris) 46 (1985) 1469.

[85] U. C. Tauber, Field theory approaches to nonequilibrium dynamics, Lect.Notes.Phys. 716 (2007) 295.

[86] L. Pechenik, H. Levine, Interfacial velocity corrections due to multiplicative noise, Phys. Rev. E 59 (4) (1999) 3893–3900.

[87] A. I. Shoshi, B.-W. Xiao, Pomeron loops in zero transverse dimensions, Phys. Rev. D73 (2006) 094014.

[88] A. I. Shoshi, B.-W. Xiao, Diffractive dissociation including pomeron loops in zero transverse dimensions, Phys. Rev. D75 (2007) 054002.

[89] E. Levin, A. Prygarin, The BFKL Pomeron Calculus in zero transverse dimensions: summation of Pomeron loops and generating functional for the multiparticle production processes, Eur. Phys. J. C53 (2008) 385–399.

[90] M. Kozlov, E. Levin, V. Khachatryan, J. Miller, The BFKL pomeron calculus in zero transverse dimensions: Diffractive processes and survival probability for central diffractive production, Nucl. Phys. A791 (2007) 382–405.

[91] M. Kozlov, E. Levin, A. Prygarin, The BFKL Pomeron Calculus in the dipole approach, Nucl. Phys. A792 (2007) 122–151.

[92] E. Levin, J. Miller, A. Prygarin, Summing Pomeron loops in the dipole approach, Nucl. Phys. A806 (2008) 245–286.

[93] C. W. Gardiner, Handbook of Stochastic Methods: for Physics, Chemistry and the Natural Sciences (Springer Series in Synergetics), 3rd Edition, Springer, 2004.

[94] S. Munier, Dense-dilute factorization for a class of stochastic processes and for high energy QCD, Phys. Rev. D75 (2007) 034009.

[95] J. P. Blaizot, E. Iancu, D. N. Triantafyllopoulos, A zero-dimensional model for high-energy scattering in QCD, Nucl. Phys. A784 (2007) 227–258.

[96] R. P. Feynman, "Negative Probability," in Quantum Implications : Essays in Honour of David Bohm, by F. David Peat (Editor), Basil Hiley (Editor) Routledge & Kegan Paul Ltd, London & New York, pp. 235âĂŞ248.

[97] S. Bondarenko, L. Motyka, A. H. Mueller, A. I. Shoshi, B. W. Xiao, On the equivalence of Reggeon field theory in zero transverse dimensions and reaction-diffusion processes, Eur. Phys. J. C50 (2007) 593–601.

[98] M. Bramson, Mem. Am. Math. Soc. 44 (1983) 285.

[99] J. L. Albacete, N. Armesto, J. G. Milhano, C. A. Salgado, U. A. Wiedemann, Nuclear size and rapidity dependence of the saturation scale from QCD evolution and experimental data, Eur. Phys. J. C43 (2005) 353–360.

[100] E. Levin, M. Lublinsky, Parton densities and saturation scale from non-linear evolution in DIS on nuclei, Nucl. Phys. A696 (2001) 833–850.

[101] J. L. Albacete, N. Armesto, A. Kovner, C. A. Salgado, U. A. Wiedemann, Energy dependence of the Cronin effect from non-linear QCD evolution, Phys. Rev. Lett. 92 (2004) 082001.

[102] E. Iancu, K. Itakura, L. McLerran, Geometric scaling above the saturation scale, Nucl. Phys. A708 (2002) 327–352.

[103] D. N. Triantafyllopoulos, The energy dependence of the saturation momentum from RG improved BFKL evolution, Nucl. Phys. B648 (2003) 293–316.

[104] U. Ebert, W. van Saarloos, Front propagation into unstable states: Universal algebraic convergence towards uniformly translating pulled fronts, Physica D 146 (2000) 1.

[105] S. Munier, R. B. Peschanski, Universality and tree structure of high energy QCD, Phys. Rev. D70 (2004) 077503.

[106] E. Brunet and B. Derrida, "Statistics at the tip of a branching random walk and the delay of traveling waves," EPL (Europhysics Letters), 87, 6, 60010, 2009.

[107] E. Brunet and B. Derrida, "A Branching Random Walk Seen from the Tip," Journal of Statistical Physics, 1-27, 2011.

[108] E. Brunet, B. Derrida, Shift in the velocity of a front due to a cut-off, Physical Review E 57 (1997) 2597.

[109] A. Kovner, M. Lublinsky, Remarks on high energy evolution, JHEP 03 (2005) 001.

[110] A. Kovner, M. Lublinsky, From target to projectile and back again: Selfduality of high energy evolution, Phys. Rev. Lett. 94 (2005) 181603.

[111] A. Kovner, M. Lublinsky, Dense-dilute duality at work: Dipoles of the target, Phys. Rev. D72 (2005) 074023.

[112] A. Kovner, M. Lublinsky, More remarks on high energy evolution, Nucl. Phys. A767 (2006) 171–188.

[113] A. Kovner, M. Lublinsky, U. Wiedemann, From bubbles to foam: Dilute to dense evolution of hadronic wave function at high energy, JHEP 06 (2007) 075.

[114] E. Brunet, B. Derrida, A. H. Mueller, S. Munier, A phenomenological theory giving the full statistics of the position of fluctuating pulled fronts, Phys. Rev. E73 (2006) 056126.

[115] C. Marquet, G. Soyez, B.-W. Xiao, On the probability distribution of the stochastic saturation scale in QCD, Phys. Lett. B639 (2006) 635–641.

[116] E. Moro, Numerical schemes for continuum models of reaction-diffusion systems subject to internal noise, Physical Review E 70 (2004) 045102.

[117] S. Munier, G. P. Salam, G. Soyez, Travelling waves and impact-parameter correlations, Phys. Rev. D78 (2008) 054009.

[118] D. Y. Ivanov, et al., The BFKL pomeron in 2+1 dimensional QCD, Phys. Rev. D58 (1998) 074010.

[119] M. Ciafaloni, D. Colferai, G. P. Salam, Renormalization group improved small-x equation, Phys. Rev. D60 (1999) 114036.

[120] A. H. Mueller and S. Munier, "Correlations in impact-parameter space in a hierarchical saturation model for QCD at high energy," Phys. Rev. D **81**, 105014 (2010) [arXiv:1002.4575 [hep-ph]].

[121] S. Munier, "Correlations in impact-parameter space in saturation models," PoS D **IS2010**, 083 (2010) [arXiv:1006.0425 [hep-ph]].

[122] G. Camici and M. Ciafaloni, "Model (in)dependent features of the hard pomeron," Phys. Lett. B **395**, 118 (1997).

[123] M. Abramowitz and I. A. Stegun, *Handbook of Mathematical Functions*, (1964) Dover Publications, New York. ISBN 0-486-61272-4.

[124] S. Catani, M. Ciafaloni, F. Hautmann, "Gluon contributions to small-x heavy flavor production," Phys. Lett. B242 (1990) 97.

[125] S. Catani, M. Ciafaloni, F. Hautmann, High-energy factorization and small x heavy flavor production, Nucl. Phys. B366 (1991) 135–188.

[126] J. C. Collins, R. K. Ellis, Heavy quark production in very high-energy hadron collisions, Nucl. Phys. B360 (1991) 3–30.

[127] E. Iancu, K. Itakura, S. Munier, Saturation and BFKL dynamics in the HERA data at small x, Phys. Lett. B590 (2004) 199–208.

[128] J. R. Forshaw, R. Sandapen, G. Shaw, Predicting F2(D(3)) from the colour glass condensate model, Phys. Lett. B594 (2004) 283–290.

[129] G. Soyez, Saturation QCD predictions with heavy quarks at HERA, Phys. Lett. B655 (2007) 32–38.

[130] R. S. Thorne, Gluon distributions and fits using dipole cross- sections, Phys. Rev. D71 (2005) 054024.

[131] H. Kowalski, D. Teaney, An impact parameter dipole saturation model, Phys. Rev. D68 (2003) 114005.

[132] G. Watt, H. Kowalski, Impact parameter dependent colour glass condensate dipole model, Phys. Rev. D78 (2008) 014016.

[133] S. Bondarenko, Gluon density and F_2 functions from BK equation with impact parameter dependence, Phys. Lett. B665 (2008) 72–78.

[134] C. Ewerz, A. von Manteuffel, O. Nachtmann, On the Range of Validity of the Dipole Picture, Phys. Rev. D77 (2008) 074022.

[135] A. Dumitru, E. Iancu, L. Portugal, G. Soyez, D. N. Triantafyllopoulos, Pomeron loop and running coupling effects in high energy QCD evolution, JHEP 08 (2007) 062.

[136] Y. Hatta, E. Iancu, C. Marquet, G. Soyez, D. N. Triantafyllopoulos, Diffusive scaling and the high-energy limit of deep inelastic scattering in QCD at large N(c), Nucl. Phys. A773 (2006) 95–155.

[137] M. Kozlov, A. I. Shoshi, B.-W. Xiao, Total gluon shadowing due to fluctuation effects, Nucl. Phys. A792 (2007) 170–186.

[138] E. Brunet, B. Derrida, A. H. Mueller, S. Munier, Noisy traveling waves: effect of selection on genealogies, Europhys. Lett. 76 (2006) 1–7.

[139] E. Brunet, B. Derrida, A. H. Mueller, S. Munier, Effect of selection on ancestry: an exactly soluble case and its phenomenological generalization Phys. Rev. E 76, 041104 (2007).

[140] F. Dominguez, B. -W. Xiao, F. Yuan, Phys. Rev. Lett. **106**, 022301 (2011). [arXiv:1009.2141 [hep-ph]].

[141] F. Dominguez, A. H. Mueller, S. Munier, B. -W. Xiao, "On the small-x evolution of the color quadrupole and the Weizsácker-Williams gluon distribution," [arXiv:1108.1752 [hep-ph]].